M.PHIL DISSERTATION

South-east Greenland Ice Sheet short term response to environmental conditions

Anthony Seale[1,2]

An automated method for tracking the calving margin positions of tidewater glaciers from MODIS imagery was developed, allowing for the recording of high temporal resolution change over 24 glaciers. Results compared well to those of other studies which have been limited in either temporal or spatial resolution by more labour intensive methods. Many glaciers exhibited a strong sensitivity to a seasonal forcing. Over 2002 to 2005, 14 of the glaciers retreated by over 0.5 km, the largest with a retreat of 5.0 km. Total recovery during 2005 to 2008 was 21% of previous retreat. During the study period both surrounding sea and air surface temperatures (SSTs and SATs) gradually increased by 2° and 1.5° C respectively until mid 2004, after which mean annual SAT dropped by 4° C and SSTs remained high, suggesting a dominant influence of SATs. Margin positions appeared to switch between stable bathymetric states, triggered by temperature changes. The rapid stepped retreats observed over short timescales indicate that future outlet glacier response to climate change is likely to be non-linear and that the findings of mass balance studies based upon comparisons between specific years may not be robust. Expanding this study over the whole ice sheet has been shown to be feasible and would depict margin changes in unprecedented spatio-temporal detail.

Supervised by Poul Christoffersen[1]

This dissertation is submitted for the degree of Master of Philosophy

Scott Polar Research Institute

[1]Scott Polar Research Institute
University of Cambridge
Lensfield Road
Cambridge
CB2 1ER

CLARE

[2]Clare College
Trinity Lane
Cambridge
CB2 1TL

Acknowledgements

I would like to thank my supervisor, Poul Christoffersen, for his advice and my parents for their enthusiasm and support.

Declaration

This dissertation is the result of my own work and includes nothing which is the outcome of work done in collaboration except where specifically indicated in the text.

The dissertation is no more than 20,000 words in length excluding the acknowledgements, declaration, list of references, tables, captions and appendices.

Contents

1 Introduction 4
1.1 Background 4
1.2 Recent changes 4
1.3 Explaining dynamic change 5
1.3.1 Basal lubrication 6
1.3.2 Control at the calving margin 6
1.3.3 Calving modulation 9
1.4 Research aims 10
2 Method 11
2.1 Margin position extraction 11
2.1.1 Use of MODIS data 11
2.1.2 Retrieval of MODIS data 14
2.1.3 Data preparation 14
2.1.4 Study area 16
2.1.5 Data importation 16
2.1.6 Cloud detection 16
2.1.7 Sensor quality assurance 20
2.1.8 Data Selection 22
2.1.9 Orthographic reprojection 23
2.1.10 Curved glacier handling 25
2.1.11 Active region selection 26
2.1.12 Edge detection 26
2.1.13 Noise reduction 36
2.1.14 Anomaly exclusion 37
2.1.15 Error 39
2.1.16 Validation 44
2.2 ERA-Interim data 47
2.3 MODIS SST data 47
3 Results 47
3.1 Data quality 47
3.2 Seasonality 51
3.3 Margin position trends 51
3.4 Environmental variables 56
3.4.1 SST/SAT forcing 59
3.4.2 Statistical testing 62
4 Analysis 69
4.1 Data quality 69
4.2 Seasonality 69
4.3 Margin position trends 70
4.4 SST/SAT forcing 71
5 Conclusion 73
6 References 76
7 Supplementary animations 82

1 Introduction

1.1 Background

For many years it was thought that the negative contribution to the Greenland Ice Sheet (GrIS) mass balance was determined largely by surface melt rates in response to air temperatures. Summarising the research of its time, the 2001 IPCC report (IPCC 2001) even suggested a contemporary and future positive mass balance, with snow accumulation outweighing melt rates. The magnitude (Krabill et al. 2004) and extent (Rignot & Kanagaratnam 2006) of rapid changes that have occurred on the GrIS in the last 10 years, taken with the speed of their onset (Howat et al. 2007) forced glaciologists to reconsider GrIS mass balance, recognising the role of dynamic change. The IPCC (2007) has since revised their position, stating that ice stream speeds can change rapidly, but that current understanding is insufficient to produce an adequate quantification. Increased knowledge of the changes that have occurred on the GrIS as well as their causes is therefore needed to produce realistic mass balance estimates of the future of the GrIS and its contribution to sea level rise.

1.2 Recent changes

Large scale changes on the GrIS are best observed using air or space-borne remote sensing techniques. Using repeat laser altimeter surveys Abdalati et al. (2001) found much thinning had occurred on the GrIS between 1993 and 1999 at elevations below 2000 m. Thinning was particularly large (in excess of 1 m yr^{-1}) near outlet glaciers, making the study one of the first to realise the role of glacier dynamics in GrIS mass balance and that such changes had started between 1993 and 1999. Extending the technique over the period 1997 to 2003, Krabill et al. (2004) estimated average ice loss from the GrIS to be 80 ± 12 km^3 yr^{-1}, up from 60 km^3 yr^{-1} for 1993 to 1999. The authors estimated that half of this increased ice loss was the result of dynamic flow. Flow accelerations have been tracked using satellite radar interferometry and were found to have increased from 28.5% to 57.0% between 1996-2000 and 2000-2005 for the largest 21 glaciers, whilst the domain of acceleration had spread northwards from below 60°N to 70°N (Rignot & Kanagaratnam 2006). A recent study (Rignot et al. 2008) found a strong relationship between ice discharge and surface mass balance anomalies on the GrIS, and used it to reconstruct an approximate continuous time series of

GrIS mass balance from 1958 to 2007. Ice loss rates were calculated as 110 ± 70 Gt yr^{-1} in the 1960s dropping to 30 ± 50 Gt yr^{-1} for the 1970s and 1980s. During the 1990s and early 2000s mass loss greatly increased to 97 ± 47 Gt yr^{-1} for 1996 before rising sharply to 267 ± 38 Gt yr^{-1} for 2007. Assuming such a reconstruction is valid, the study outlines the great size and rapid onset of mass loss possible by increased dynamic flow. The increase in mass loss rates appears to largely have been caused by marine terminating outlet glaciers. An altimetry based study (Sole et al. 2008) of the GrIS has shown that marine outlet glacier thinning rates over 1993-1998 compared to those of 1998-2006 exhibited a fourfold increase, whilst land terminating glaciers remained statistically unchanged. Another study of 203 glaciers found retreat rates to have accelerated between 1992-2000 and 2000-2006 for tidewater glaciers, whilst land terminating glaciers showed almost no change (Moon & Joughin 2008).

1.3 Explaining dynamic change

The observed changes have occurred synchronously across much of the ice sheet in a short time scale (Rignot & Kanagaratnam 2006). This suggests a single forcing mechanism with a large effective area. On higher resolution timescales, Luckman et al. (2006) found that both annual velocities and ice front positions of Helheim and Kangerdlugssuaq Glaciers varied simultaneously over 1992-2005, despite being over 300 km apart. Two possible explanations exist for this, either internal connections through the ice mass exist, or a single external forcing is in operation. Force-based teleconnections within the ice appear unlikely to have caused such behaviour as relief of a centralised driving stress is unlikely to induce accelerations elsewhere. This suggests an environmental forcing mechanism. Further evidence for this may be found in seismological records. Identification of the glacial earthquakes signals (Ekstrom et al. 2003) allows for the monitoring of discrete glacier sliding events. Seasonality, analogous to temperature forcing, can be seen in the frequency of earthquakes detected from GrIS outlet glaciers (Ekstrom et al. 2006). Seasonality has also been observed in the frontal positions and velocities of south-eastern outlet glaciers (Howat et al. 2008), whilst the difference between summer and winter velocities on Jacobshaven Isbrae differ by a factor of 6 (Sohn et al. 1998), further exemplifying the widespread sensitivity of the GrIS to environmental forcings.

1.3.1 Basal lubrication

Two theories have been suggested by which GrIS outlet glaciers may be coupled to environmental conditions. One of these was first observed on Greenland by Joughin et al. (1996) and popularised by the findings of Zwally et al. (2002). The theory is that surface meltwater may propagate to the bed of the GrIS, enhancing flow rates through bed decoupling, warming and lubrication (Paterson 1994). The level of flow enhancement would be dependent on surface air temperatures and absorption of solar radiation by ice. Although observations that meltwater could penetrate through over a kilometre of ice were surprising to the glaciological community, further observations have shown both the magnitude and duration of the effect to be limited. Das et al. (2008) detected ice sheet uplift, transient acceleration and horizontal displacement during a surface drainage event, although the effects were limited to a duration of under 24 hours. Similar observations at the start of melt seasons lasted only a few days (van de Wal et al. 2008), whilst another study found the velocity increases to be under 15% for fast flowing ice streams (Joughin et al. 2008a). It has been postulated (Bamber et al. 2007) that the high ice velocities of GrIS outlet glaciers show that the bed is already well lubricated, which is why additional water input has little effect. The most recent study of the effect (Shepherd et al. 2009) suggested that it is important in determining the slower response of land terminating glaciers, but that the response of marine-terminating glaciers will also depend on other factors. These factors (see below) appear to have a significantly larger influence on dynamic flow than surface melt induced accelerations.

1.3.2 Control at the calving margin

A second, and perhaps more likely control theory, is that changes at the calving margin are controlling flow dynamics. Evidence can be found in the discrepancy between responses of land and marine terminating glaciers (Sole et al. 2008; Moon & Joughin 2008), previously described, as well as more detailed observations from individual glaciers and theoretical considerations. The loss of 2 km from the floating tongue of Jakobshavn Isbræ in 1997 and 1998 (Luckman & Murray 2005) preceded thinning and acceleration, repeated after further losses in 2002 and 2003 (Joughin et al. 2004; Alley et al. 2005). Holland (2008) also noted changes in elevation and velocity of the glacier followed significant calving events, continuing into 2007. This responsive draw-down process suggests the glacier is responding

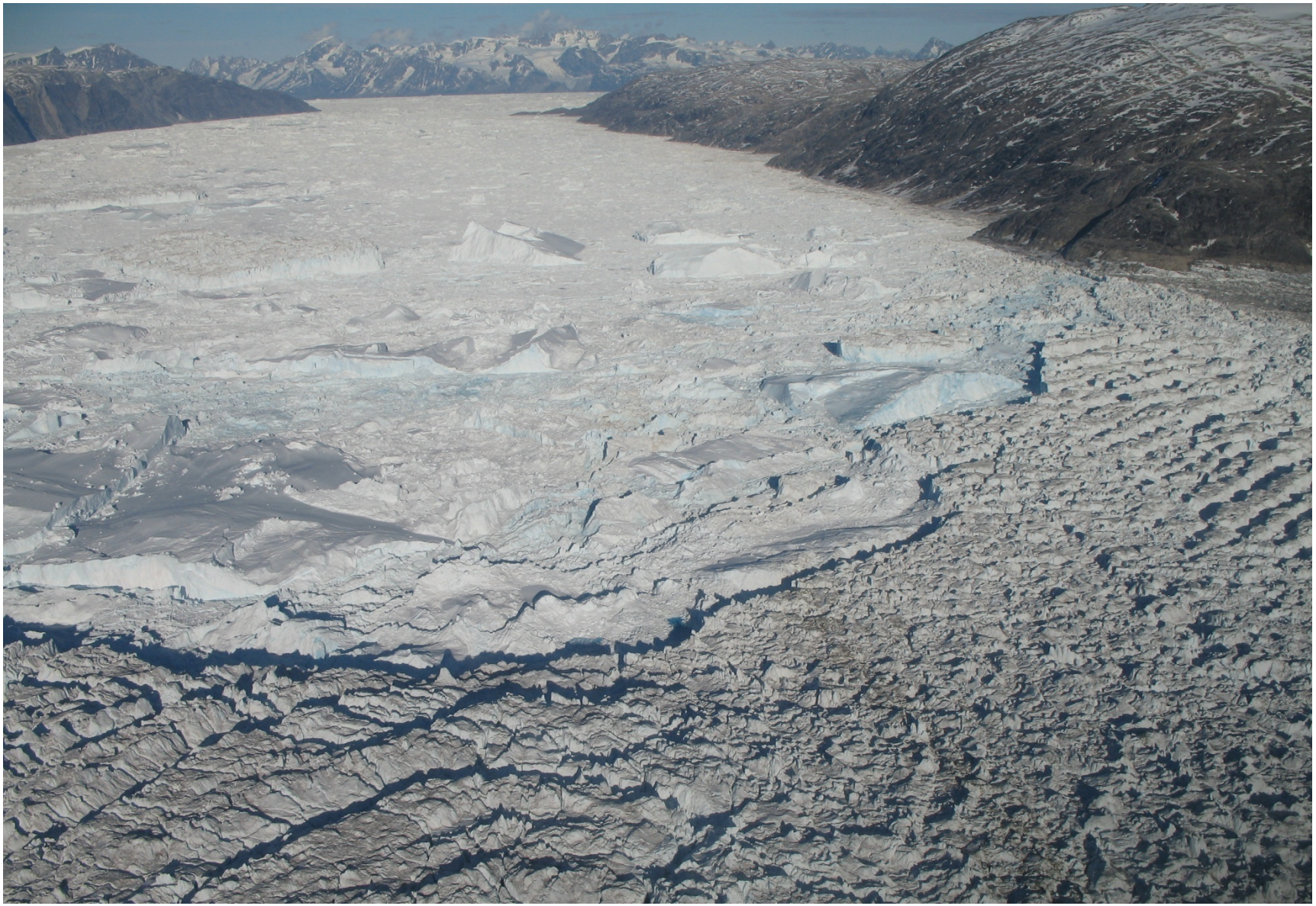

Figure 1 Calving margin of Helheim Glacier from the fieldwork of Nettles et al. (2008). A difference in surface brightness may be seen between the glacier and floating fjord ice. It may also be seen that the calving front is not straight.

to a change in frontal resistive stress. This has been considered for Jakobshavn Isbræ in a force perturbation analysis (Thomas 2004), which found that velocity changes were likely to be initiated by calving and sustained by rapid thinning of the remaining ice tongue.

Helheim Glacier (**Figure 1**), on the opposite coast to Jakobshavn Isbræ, has also experienced similar retreats followed by accelerations and thinning. Howat et al. (2005) noted that between 2000 and 2005 Helheim Glacier experienced two major speed-ups from 8 to 11 km yr^{-1} following retreats of the calving margin totalling more than 7.5 km. Nettles et al. (2008) found that step-wise changes in Helheim Glacier ice velocities corresponded to seismically detected events consisting of ice rolling off the terminus. Without a significant floating tongue (Rignot et al. 2004), calving margin retreat corresponds to a loss of grounding line position, concentrating gravitational driving force over a smaller area and reducing resistive forces (Howat et al. 2005). Observations of Helheim show that increases in speed are the result of an instantaneous loss of driving stress followed by thinning and draw-down of ice propagating upstream (ibid.). A numerical model of Helheim Glacier (Nick et al. 2009) also demonstrated that ice velocities respond very rapidly to calving margin perturbations, again propagating upstream. Kangerdlugssuaq Glacier has been shown to follow a remarkably similar pattern (Luckman et al. 2006), leading research to the same conclusions (Howat et al. 2007).

Feedbacks exist which operate to increase the rate of ice loss after a retreat in floating tongue length or grounding line position. Pfeffer (2007) noted that the relationship between bed traction, which provides resistance to flow, and ice thickness is nonlinear, whilst gravitational driving stress resulting is approximately proportional to ice thickness. Given the appropriate glacier geometry, a loss of ice thickness can have the effect of reducing flow resistance more than the driving stress, leading to further ice flow (Meier & Post 1987). Pfeffer (2007) notes that this can cause thinning to propagate upstream, further enhancing the process.

For tidewater glaciers, thinning may be initiated at the glacier front by an increase in melt or calving rates above that of glacier flow. The described instability could then continue, reducing basal friction and increasing velocity. This would eventually cause the ice to reach its floatation point, where it may be unstable and continue to retreat until shallower water

was reached (Vieli et al. 2001). Weertman (1974) first recognised this phenomenon, hypothesising that under idealised conditions marine terminating glaciers are unstable on reverse bed slopes. It has been suggested that this behaviour has been observed in the recent retreats of Helheim (Howat et al. 2007) and Kangerdlugssuaq Glaciers (Joughin et al. 2008b) as well as considered in models (Vieli et al. 2001).

1.3.3 Calving modulation

The mechanism by which the calving rate is modulated by environmental conditions is unknown. Considering the glacier terminus environment, there are three physical controls which may exert an influence: air temperatures, sea temperatures (at many depths) and sea ice. Each of these may in turn be controlled by wider phenomena, such as ocean currents, for example the Irminger Current, or climatic trends, like the North Atlantic Oscillation.

Although meltwater propagation to the bed may be considered a limited contribution to marginal dynamic GrIS change (see 1.3.1 Basal lubrication) it is still possible that surface air temperatures could control margin positions through crevasse hydrofracturing. This process involves the supply of heat to the glacier surface by warm air masses which causes melt. Meltwater then flows into crevasses providing a heat source within the glacier, precisely at a likely fracturing point. The heat provided by this water may further deepen the crevasses until calving occurs. Moon and Joughin (2008) have suggested that the decrease in glacier speeds observed on Greenland since 2006 corresponds with reduced air temperatures. Further research on Helheim Glacier has also suggested that velocity decreased during the onset of cooler temperatures measured from a nearby weather station (Joughin et al. 2008b). Both of these postulations are based on a very short data period, preventing confident conclusions from being drawn. Such a process has however been observed with a greater degree of certainty during the break-up of the Larsen B ice shelf in Antarctica, which was caused in part by a persistent atmospheric circulation pattern providing warm air to the region (van den Broeke 2005) .

Ocean temperatures may control calving rates through basal melt, which can extend basal crevasses, thin ice tongues and cause retreat of the grounding line. Water within the fjords of tidewater glaciers has the potential to directly change the position of the grounding line and consequently the level of frictional resistance provided by the glacier. Theoretically,

glacier flow speeds may therefore be very sensitive to the temperature of the surrounding ocean. Melting of grounded ice may also move glaciers off pinning points, leading them into unstable bed configurations, which may initiate further retreat (see section 1.3.2 Control at the calving margin). Subsurface temperature observations from fishing vessels around Jakobshavn Isbræ suggest that an inflow of warm Atlantic water from the Irminger Current caused the rapid disintegration of its floating tongue (Holland 2008), which was followed by accelerations.

Air temperatures may also modulate dynamic change through their control on the formation and decay of sea ice. The presence of sea ice is largely controlled by surface air temperatures and to a lesser degree sea surface temperatures (McPhee 2008 chap. 6). Reeh et al. (2001) have suggested four ways in which sea ice may control the rate of calving on tidewater glaciers. The first is a reduction in crevasse formation due the back pressure of sea ice, which may also stop crevasses already in place from propagating. The second suggestion was that long ocean waves may be dampened, and thus their potential to cause flexure and weakening of ice tongues (Legresy et al. 2004) is diminished. The third suggested mechanism is the reduction of mixing within the water column which may be caused by shorter wind induced waves. This allows a cooler body of water to remain stratified close to the floating tongue ice, reducing melt rates. The fourth mechanism is that of a buttressing effect, whereby the sea ice forms a frozen wedge within the fjord, providing a resistive stress to glacier flow.

1.4 Research aims

The present study seeks to further investigate and understand the short term dynamic change that has occurred on the GrIS over the past 10 years. This will be achieved through the monitoring of glacier frontal position change, signifying periods where there is an imbalance between glacier flow and the rate of calving. Monitoring will be enabled through the development of a new method for processing satellite data to allow for high temporal resolution information to be gained for a large number of glaciers. The study will be confined to the south-east, serving as a pilot for expansion of the project across the whole ice sheet. Environmental data describing air and sea surface temperatures around the glaciers will then be used in an attempt to explain the causes of observed changes. Understanding the response of the GrIS to environmental conditions would give us an idea

of how the ice sheet may respond to climate change and how we might go about improving our models of such processes.

2 Method

2.1 Margin position extraction

The method used in this study was designed to gain high temporal resolution margin positions for a large number of GrIS outlet glaciers. Previous studies (Howat et al. 2008) using manual edge tracing techniques require high researcher input levels, limiting the number of satellite images that may be processed in a given time frame. Semi-automatic edge detection, as implemented by Joughin et al. (2008b), uses a combination of automatic edge detection and manual checking. Although few methodological details are given, it is presumed that selection of high quality cloud-free data and the visual interpretation of every image is laborious. This may be the reason that studies to date of glacier margin position have either been restricted to a sampling frequency of bi-annually (Howat et al. 2008) or a number of years (Moon & Joughin 2008) or to a small number of glaciers (Joughin et al. 2008b). The method developed for the present study maximises levels of automation to allow for the processing of daily images of 24 glaciers for the duration of MODIS operation (27/02/2000 to 09/03/2009), totalling 79,152 images, each with multiple spectral bands. As this is a novel method, the description of it contained herein is given in detail to allow for reproducibility and subsequent application to other scenarios. This method may also be applied to other regions, such as Svalbard, and other sensors, potentially to include those which operate at different wavelengths. The application of edge detection techniques is also not limited to glaciological inquiry; for example the method could be adapted to study problems such as tree line migration.

2.1.1 Use of MODIS data

The primary data source used for this study was the MOD09GQ L2G daily surface reflectance product. The product is produced by the MODIS (Moderate Resolution Imaging Spectroradiometer) sensor on board the NASA EOS (Earth Observation System) Terra satellite which follows a Sun-synchronous near polar orbit (Ahmad et al. 2002). It was launched on December 18th 1999 with data available data spanning 27th February 2000 to

the present (April 2009). The data was chosen for use in this study due to its high temporal resolution (almost daily) and satisfactory spatial resolution (250 m). This allows for a more continuous tracking of small changes over short timescales which may be linked to changes in environmental conditions occurring over similar scales. Detection of margin position through analysis of visible wavelength radiation is subject to interference from cloud and thus high frequency repeat passes increase the probability of returning cloud-free data within a given time frame.

Another advantage of the MODIS data is that they are provided in a tiled form. Swath data are compiled into geographically consistent tiles with each pixel representing the same location across all images. This simplifies high volume application of space dependent algorithms, alleviating the requirement for image geolocation. Where swaths overlap during a daily period the data with the lowest cloud cover level are chosen for inclusion within a tile.

MODIS data are freely available, a requirement of this study. It is possible that radar data, such as that of RADARSAT-1 could have provided an alternative methodology for this study, had it been available without charge. RADAR imagery is not subject to cloud cover, giving an evenly spaced sampling interval and may operate at high spatial resolutions. The frequency at which RADARSAT-1 observations could be obtained would however have been limited to its 24 day repeat pass period.

The MOD09GQ data product contains the band 1 (0.659 µm) and band 2 (0.865 µm) imagery as well as some data quality information layers. Band 1 imagery was used for this study. The MOD09GA data product contains data covering bands 1-7 at 500 m resolution as well as additional quality information at 1 km resolution. MOD09GQ data are intended as supplementary high resolution data to the more comprehensive MOD09GA dataset. The MOD09GA data product was used for quality control and cloud cover determination. This used information from the quality information layers as well as bands 4 (0.555 µm) and 6 (1.640 µm), for the calculation of NDSI (Normalised Difference Snow Index, see Cloud Detection).

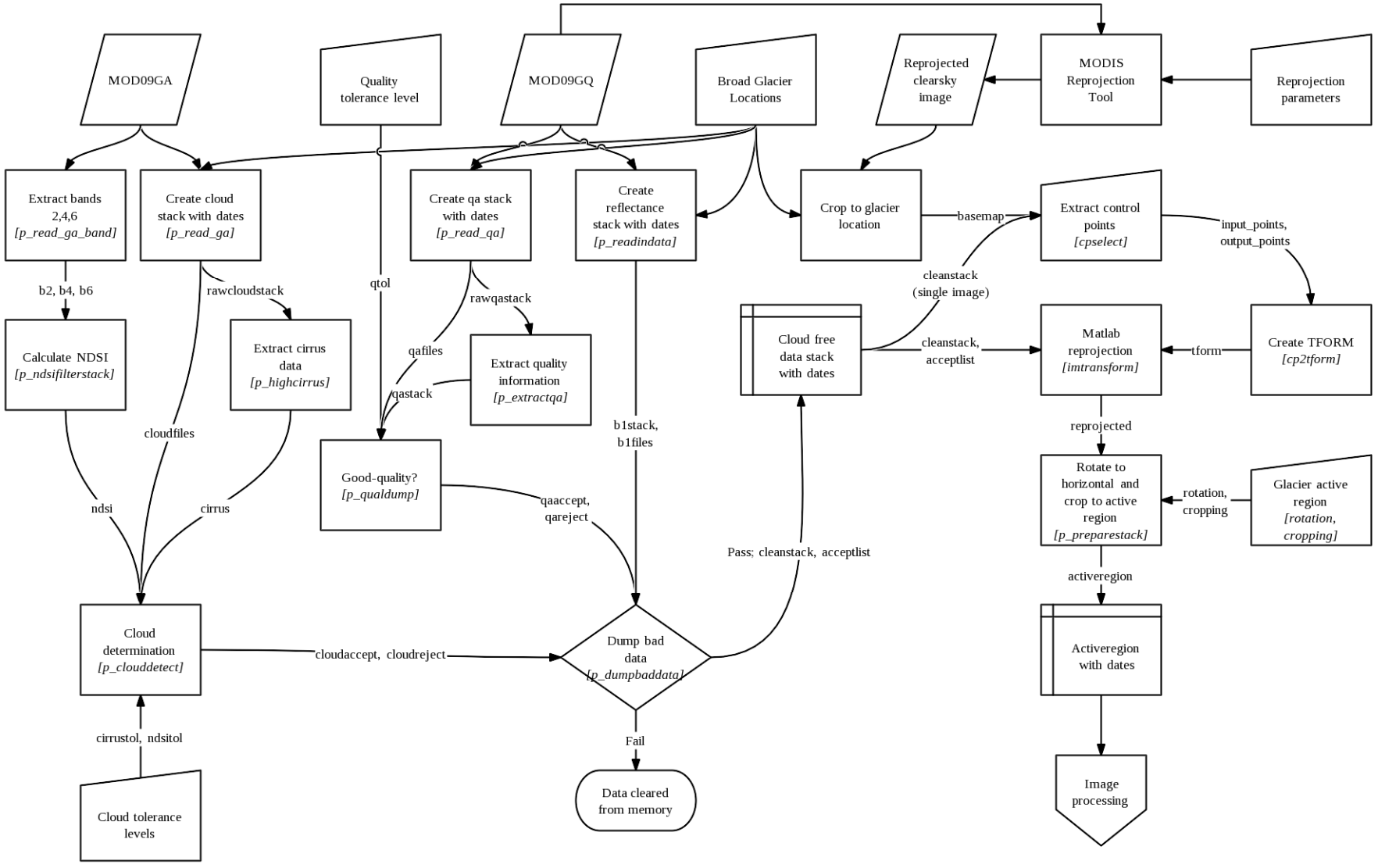

Figure 2 Flowchart depicting image pre-processing routines. Component module descriptions are given, followed by their names in square brackets.

2.1.2 Retrieval of MODIS data

Although the downloading and handling of some satellite data is familiar to many geoscientists, the techniques used within the present study were developed from the need to handle unusually large data quantities. MODIS data are provided by NASA for use in research without charge. Data retrieval is through the use of WIST (the NASA warehouse inventory search tool) and an associated FTP server. WIST allows for the searching of up to 1000 data granules (image files). Multiple requests were therefore made to download the entire dataset, consisting of 6,596 granules. The default search method is through the selection of an aerial domain, a dataset and a time period. Searches were instead conducted by data granule ID, which forms the unique file names of image files. This attempted to reduce search times and allowed for simpler tracking of the files contained within each request. The retrieval of data was monitored by importing search requests and directory listings into Microsoft Excel for comparison using the MATCH function. This allowed for easy re-requesting of missing files due to failed file transfers.

File transfer speeds were important as the total dataset had a large size of 1.19 TB (terabytes). File transfers were conducted using the FileZilla open source FTP client [http://filezilla-project.org/], which has the ability to operate simultaneous file transfers. NASA appeared to allow for 8 simultaneous FTP connections, which provided the greatest transfer speeds. Data were stored on a network fileserver and copied to a local external hard drive when being used for analysis. Internal transfers were conducted using FastCopy [http://www.ipmsg.org/tools/fastcopy.html.en] which represents a speed improvement over built-in windows file copying procedures.

2.1.3 Data preparation

Before edge detection could take place, the data had to be imported into the system memory and put through a number of quality control routines. These served to eliminate images which were cloud covered or were labelled as having poor sensor data.

All data processing routines were written as a number of functions in MATLAB. This modular programming structure allowed for efficient programming of routines without repetition, improved tracing of coding errors, flexibility during the development of algorithms and an intuitive structure. A representation of the data preparation structure can be seen in **Figure**

2. The preparation routine may be divided into six phases: data importation, cloud detection, sensor quality assurance, data selection, orthographic reprojection and 'active region' selection, each of which is described. All modules created for this study were analysed using the MATLAB code profiling tool to identify processing time bottlenecks and, where possible, re-written in the most efficient manner by implementing vector arithmetic, memory pre-allocation and other module specific techniques.

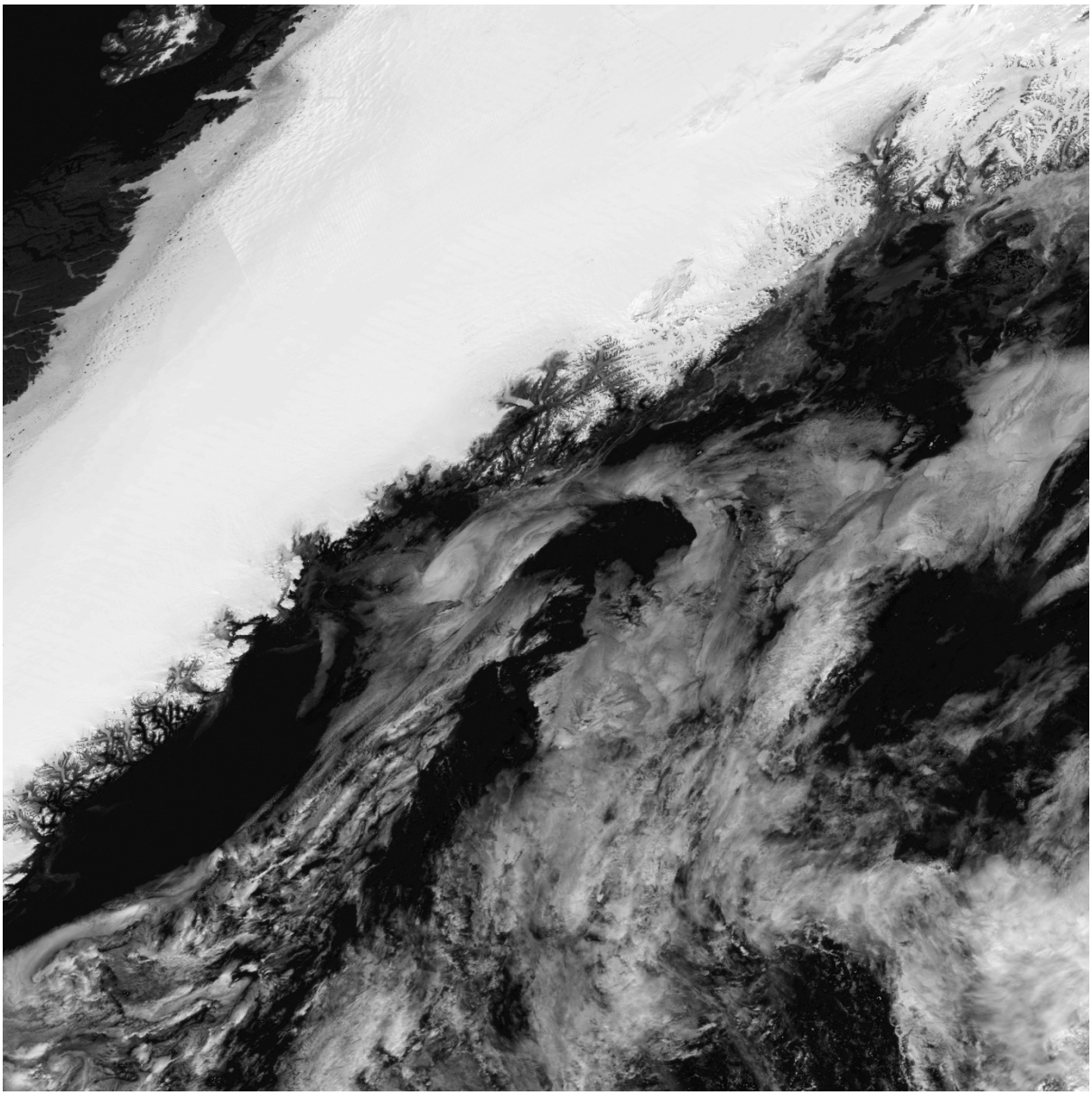

Figure 3 MODIS Terra band 1 image of eastern Greenland (tile H17, V2) acquired on 02/08/2001. This image tile shows the limits of the study area. The image is notable for its low cloud cover over land and, taken in summer, the image shows little sea ice.

2.1.4 Study area

The study area is that of a single MODIS tile, as may be seen in **Figure 3**. Due to the large data storage requirements, only a single tile could be handled using the resources available. This is sufficient to develop the edge detection method and investigate the south-east of the GrIS. Jakobshavn Isbræ is also included on the MODIS tile, results for which are presented in this study, but not included in regional averages or conclusions drawn about south-eastern Greenland. The study area includes Kangerdlugssuaq and Helheim glaciers, which taken together with Jakobshavn Isbræ, represent the three glaciers with the fastest drainage rates on the ice sheet (Rignot & Kanagaratnam 2006). The sampled glaciers within the south-east are labelled in **Figure 4**. This study serves as a developmental and pilot study for expansion of the investigation across the whole of the GrIS (see section **5 Conclusion**).

2.1.5 Data importation

For band 1 data, the visible wavelength data used for edge detection, each MODIS image (**Figure 3**) has dimensions of 4800 × 4800 pixels, with pixels stored as a 16-bit integers. Each image has an operational memory requirement of 4.608×10^7 bytes making the simultaneous handling of all images is impossible on a desktop computer. A spatial subsection of the image was therefore taken by the data input modules around each glacier to be analysed, allowing for the handling of a whole time series across multiple bands. Due to the considerable amount of time taken to open a data file, seek to the correct location, transfer the data to the memory and close the file for a large number of images, the reading in of all required data bands for a single subsection took approximately 12 hours. A system performance analysis (**Figure 5**) conducted during this task showed that the process was held up most by memory access times, which have not developed as quickly as CPU speeds or hard drive access times. Where possible, proximal glaciers were read in together and then divided to save time. Multiple computers were also used in parallel to accelerate the task.

2.1.6 Cloud detection

Cloud detection is not possible from visible band data alone due to the similarly high albedos of cloud and snow. The Normalised Difference Snow Index (NDSI) was therefore used to determine low level clouds which may be identified by their shortwave infra-red

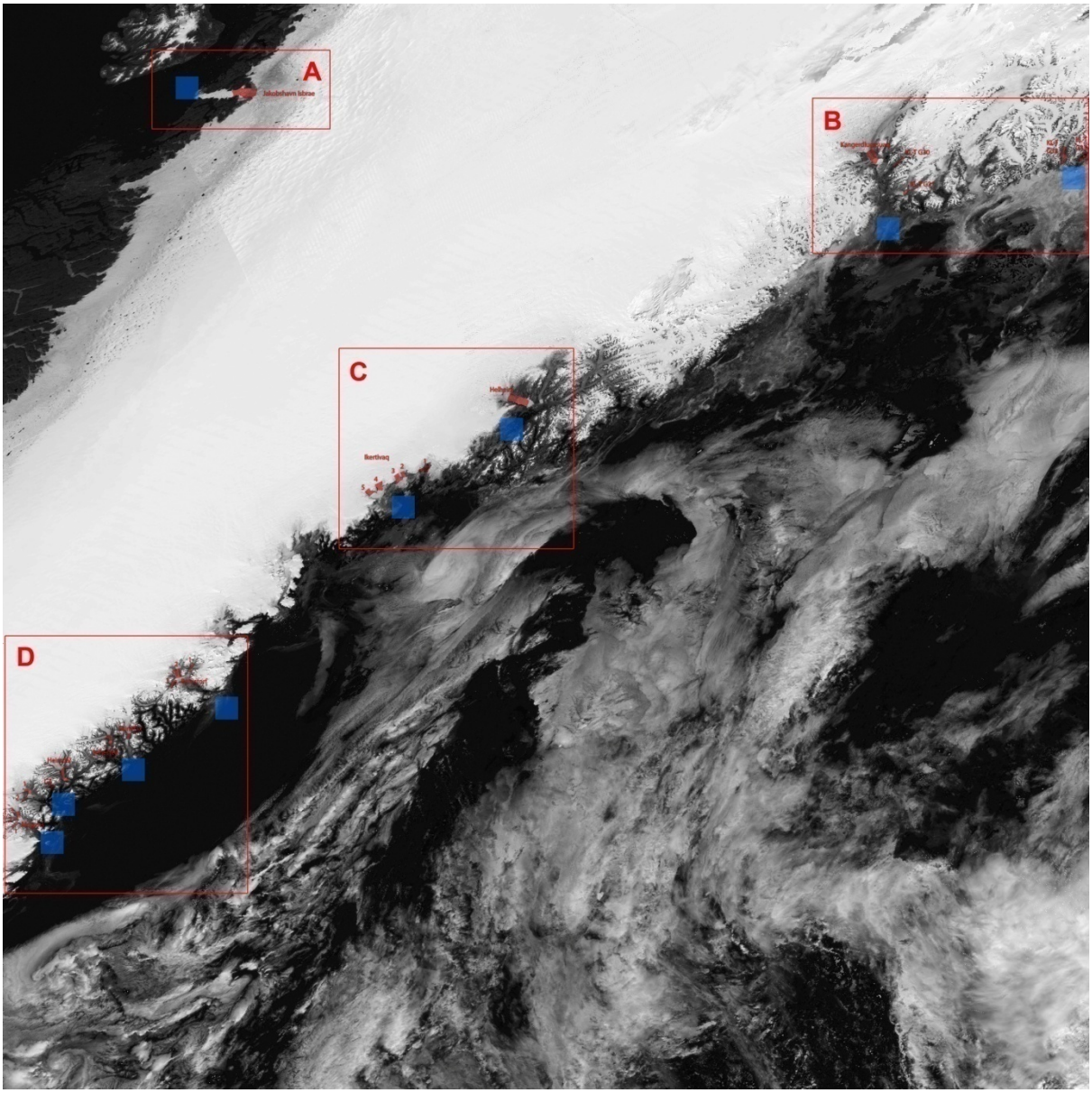

Figure 4 MODIS image showing locations of sampled glaciers (coloured red) and locations of sea surface temperature sampling boxes (blue). Regions marked A, B, C and D are enlarged below.

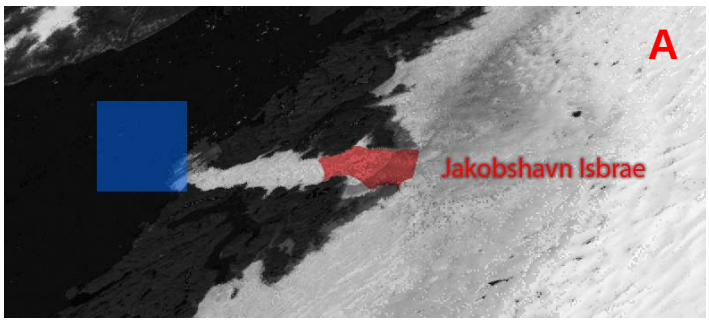

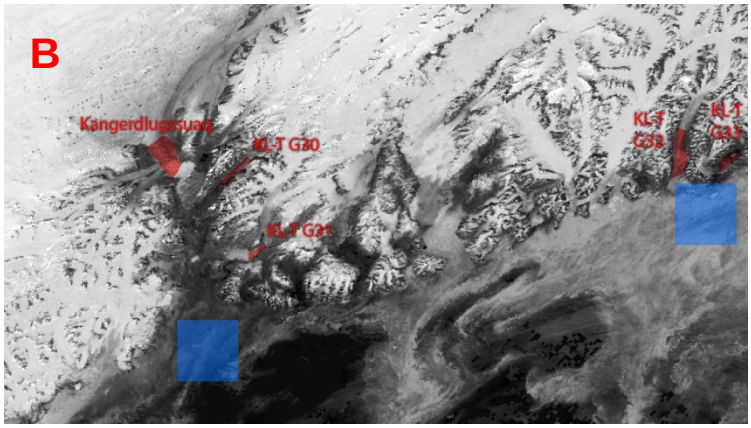
B
Kangerdlugssuaq
KL-T G20
KL-T G21
KL-T G33
KL-T G33

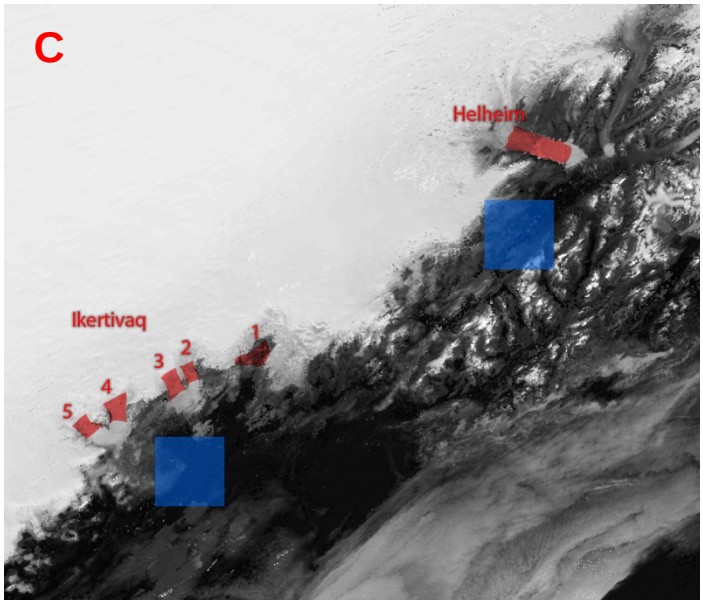
C
Helheim
Ikertivaq
1
2
3
4
5

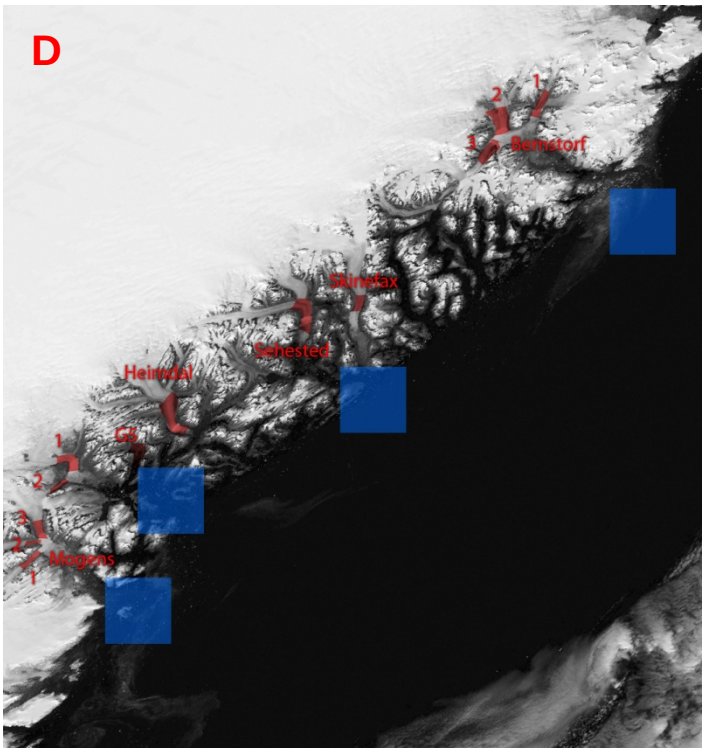
D
1
2
3
Bernstorf
Skinnefax
Schested
Heimdal
G5
1
2
3
2
1
Mogens

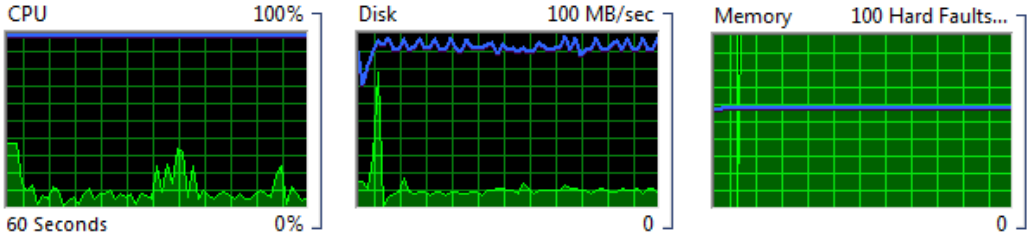

Figure 5 Windows Vista Resource Monitor charts showing CPU usage, disk data transfer rates and memory hard faults per second during the reading in of image files to MATLAB. It appears that the process is limited by memory access rates.

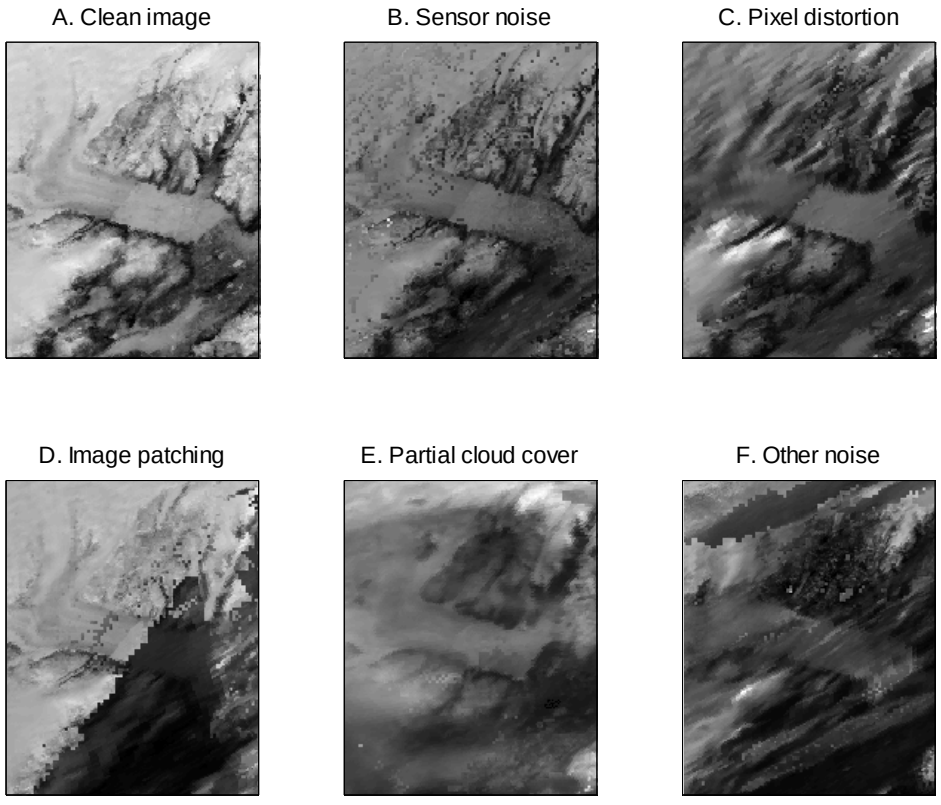

Figure 6 Sample of six MOD09GQ images of Helheim glacier showing different types of noise. All these images passed the quality control algorithms. Images acquisition dates are: A 24/05/2000, B 29/05/2000, C 07/06/2000, D 16/05/2001, E 12/10/2000 and F 14/07/2000.

(1.6 µm) response which is higher than that of snow (Riggs & Hall 2004). The NDSI is calculated using the following formula, after Klein et al. (1998):

$$NDSI = \frac{Band\ 4 - Band\ 6}{Band\ 4 + Band\ 6}$$

NDSI pixel values above 0.4 are denoted as snow. Further following Klein et al. (1998), pixels must also have an absolute band 2 reflectance of over 11% to prevent water, which can produce high NDSI values, being incorrectly identified as snow, as well as a band 4 reflectance of over 10% to prevent dark objects being misclassified as snow.

Due to their high position in the atmosphere, cirrus clouds have a different temperature profile and are not accurately detected by the NDSI measure. To identify scenes overlain by cirrus cloud the MOD06 cloud identification product output was used, obtained from a bitflag provided in the quality assurance layer of the MOD09GA dataset. This identifies cirrus cloud based on their spectral response in many bands. The algorithm and processing details may be found in Vermote and Kotchenova (2008).

Cloud cover can be highly variable across Greenland and thus subsections of the images were taken, containing each glacier to be investigated, with a surrounding region extending approximately 8 km in all directions. The proportion of pixels classified as cloud by the NDSI and cirrus measures was then calculated for each subsection. This avoids classification of a whole scene as cloud covered, when a single glacier may be cloud-free.

2.1.7 Sensor quality assurance

During operation, data obtained by the MODIS sensors may be subject to a number of environmental and internal influences, leading to poor quality data. This is usually exhibited as random speckle noise, as can be seen in **Figure 6**. When identified as erroneous data, a corresponding quality assurance value is assigned to a bitflag within a quality assurance bitfield layer of the MODIS data products. As the data products used were geographically tiled datasets constructed from swath passes, there were also areas of image tiles for which no data were collected. These no-data pixels were assigned appropriate bitflag values. A measure of data usability was produced by an analogous procedure to the NDSI and cirrus measures, with each subsection assigned a value based on the proportion of pixels identified as containing sufficient quality data.

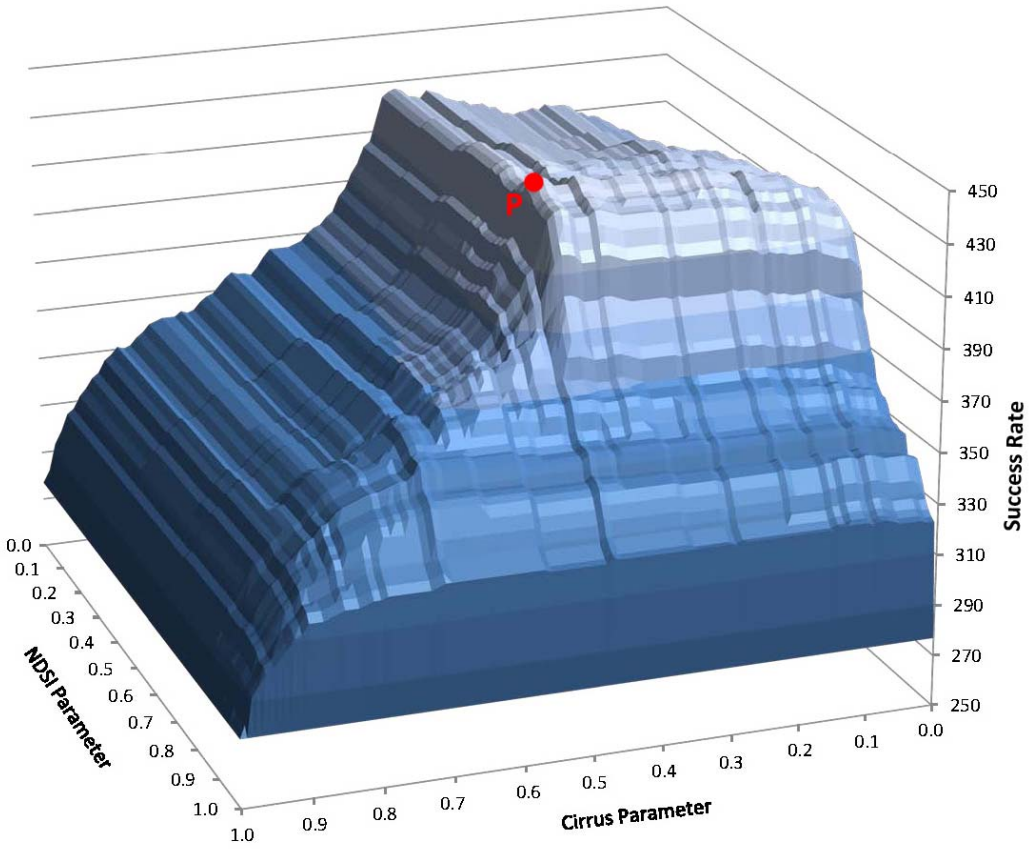

Figure 7 Cloud detection algorithm parameter space showing the image classification success rate achieved with the use of a range of NDSI and cirrus parameter values. The success rate is the number of images successfully classified out of the sample of 500 images. It can be seen that the peak success rate (P) occurs near a region of steeply declining success rates.

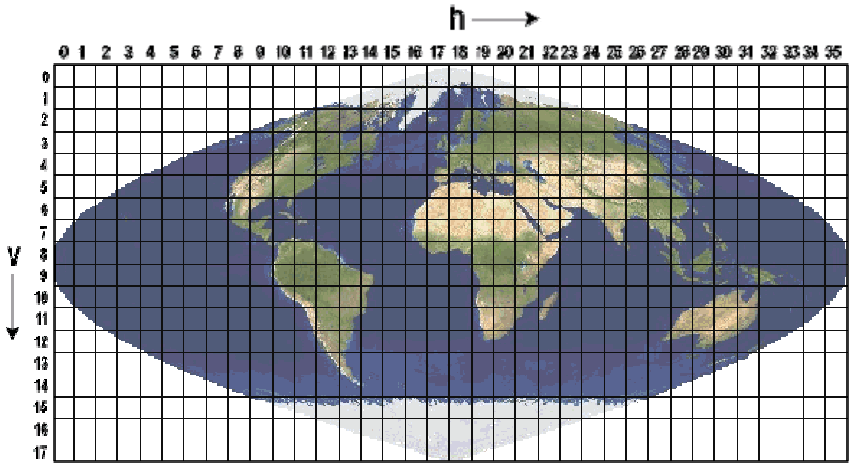

Figure 8 The Earth projected on to a MODIS sinusoidal grid. Tile H 17, V 2 was used for the present study. Image reproduced from the MODIS Land Surface Product User Guide (Vermote & Kotchenova 2008).

2.1.8 Data Selection

Image subsections were removed from the dataset if they had high NDSI or cirrus measures, or low data usability measures. This ensured that the edge detection algorithm operated only on images where it was possible to correctly identify an edge, reducing the amount of noise in the extracted margin position data caused by incorrect identifications. Cut-off thresholds were defined for each of the quality control criteria.

A sample of 500 image subsections containing Helheim Glacier were taken and manually examined for edge visibility. They were tagged as to whether they were suitable input for the edge detection procedure. It was found that no images had sufficiently high levels of error speckle to prevent an edge from being identified and thus the data usability measure was found to be almost entirely an indicator of missing data. As the image subsections were relatively small, data tended to be either present or missing for the entire subsections, making the usability measure close to a binary index. A threshold requiring 90% of the image to be visible was chosen.

The NDSI and cirrus measures contained a full range of values between 0 and 1. To determine the most effective cut-off thresholds to use, a 10,000 point parameter space was created using each measure at increments of 0.01. For each point the number images successfully classified as acceptable was calculated, using the input cut-off thresholds. The result was plotted as a three dimensional surface, shown in **Figure 7**. The figure shows the peak success rate (marked P) to use values of 0.62 and 0.38 for NDSI and cirrus levels respectively. It can be seen that these values lie close to a 'cliff edge', where the success rate rapidly decreases with only small increases in cut-off thresholds. Reductions in the thresholds (moving towards the far side of the **Figure 7**) have only slightly reduced success rates, a relative 'plateau'. As the parameter space output is likely to vary due to the particularities of the selected sample images, 'safe' thresholds were chosen, on the plateau side of peak success point. These were 0.42 for cirrus and 0.58 for NDSI. Although this represented a small reduction in image classification success rates using this sample, selection of the peak parameter value too close to the cliff edge could mean that the success rate rapidly declines, 'falling off the cliff', with only a small change in location of the steep success rate gradient.

Using all three cut-off values a classification success rate of 87.4% was achieved. Examination of animations of accepted and rejected images from multiple glaciers found this procedure considerably more likely to misclassify an acceptable image as unacceptable than vice versa (see Supplementary Animations S1 and S2). This meant that the images passed to the edge detection modules contained very little cloud covered or unusable data. For each glacier subsection the described image selection procedure rejected approximately two thirds of the daily images.

2.1.9 Orthographic reprojection

Tiled MODIS imagery is supplied projected on a sinusoidal grid (**Figure 8**). This results in severe distortion over Greenland. As the margin positions required for the present study are calculated using image distances, the images had to be reprojected into a form that minimised distance errors. A Lambert-Azimuthal projection centred about Greenland was used, which maintains areas at the expense of angles, and allowed for more accurate relative margin position calculation.

Originally it was planned to reproject all images before parsing by the data preparation modules. This was attempted through the use of the MODIS reprojection tool [Department of Mathematics and Computer Science, South Dakota School of Mines and Technology; https://lpdaac.usgs.gov/lpdaac/tools/modis_reprojection_tool]. Reprojection took approximately 12 minutes per image and thus for one tile, consisting of two imagery products, each containing 3250 images, the total computation time was 1300 hours. This was attempted through the use of multi-threaded parallel computing on 6 dual-core and 3 quad-core computers. A piece of software was written in the Microsoft VB.net language to manage the distribution and calling of the command line version of the MODIS reprojection tool. The interface of the software can be seen in **Figure 9**. Three centrally located lists of files were maintained on a fileserver, containing the file names of images yet to be processed, in processing and those for which processing had been completed. The software 'picked up' an image, by moving the filename from the to-be-processed to the in-processing list, before generating an image specific input parameter file for the MODIS Reprojection Tool. The reprojection was then performed and the file added to the completed list. At first, all data were read and written to a network fileserver. This presented problems for the fileserver which had to cope with 24 simultaneous input/output (IO) tasks, eventually

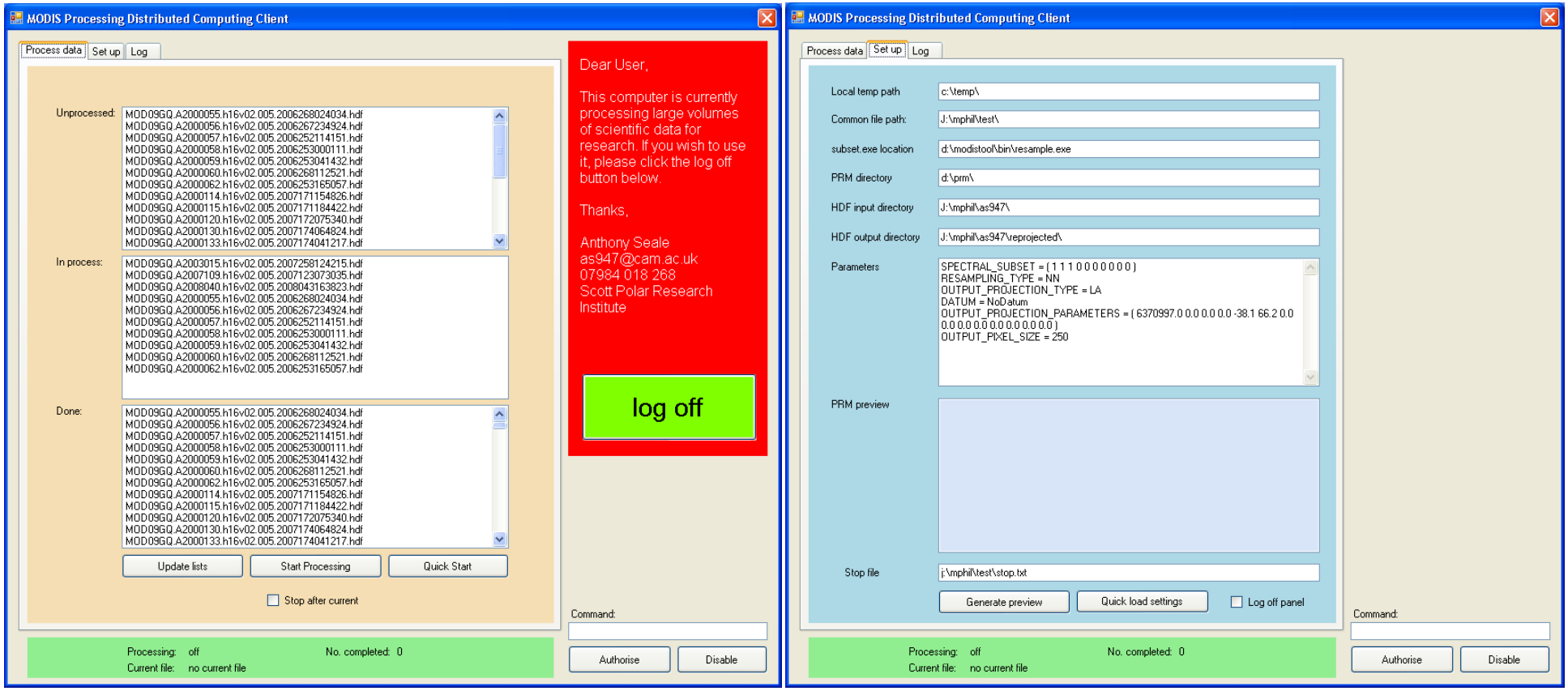

Figure 9 User interface of MODIS image reprojection distributed computing client written for this study. The process data tab (left) shows the central image list of images yet to be processed, being processed by clients and those for which processing has been completed. The program was designed to be run on public shared use workstations, and thus contains a message to the user which allows them to suspend processing and log the computer off. The 'set up' tab (right) shows the processing parameters in use. The software also maintains an event log, detailing any errors encountered.

causing it to fail. To attempt to remedy this, files were automatically copied from the fileserver, processed and then returned, rather than read and written live. Although this reduced the number of active IO requests and data fragmentation levels, the fileserver still failed on multiple occasions, likely due to the high workload. Network transfer speeds also limited the rate at which data could be processed, altogether resulting in an unsatisfactory solution.

To remedy the issues presented by processing of the entire dataset using the MODIS Reprojection Tool, reprojection was instead performed on image subsections using a faster reprojection routine built into the MATLAB Image Processing Toolbox. This performed an image transformation inferred from the location of multiple 'control points' across two images of the same area, one of which had previously been reprojected. A single image was reprojected using the MODIS Reprojection Tool to be used as a 'base image'. The same image in its original form was used as the input image. Control point selection was performed using pixels which could be precisely identified in both images, such as corners of features and pixels containing noisy data. These points were then processed to infer the distortion and saved as a variable set termed a 'TFORM' by MathWorks. The TFORM was then used to transform the whole time series of each image subsection (a small area containing a glacier, as in the cloud detection routine). To acquire local TFORMs, avoiding processing of the entire dataset, the task had to be completed for each subsection. This was automated as far as possible, but still required the manual inputting of subsection control points. To save inputting time, some proximal glaciers were processed in a single subsection.

2.1.10 Curved glacier handling

Curved glaciers were put through a distortion procedure to allow the edge detection algorithm to operate on them. A clear image of the glacier was selected and marked with three lines, two which followed its lateral margins and one which followed its centre line along the direction of flow. Each line was 'dotted', consisting of superimposed white pixels at 2 pixel intervals upon the image. A grid consisting of three similarly spaced and dotted straight lines was also produced and used a base projection image (see **Figure 10**). Using the MATLAB Reprojection Tool, a number of control points were selected across both images, aligned with the white pixels. A TFORM map, which contains the parameters of the

distortion from one image to the other, was then created and used to reproject all images of the glacier. This resulted in a distortion of distance in the final extracted margin positions, which can only be taken as indicative and relative responses.

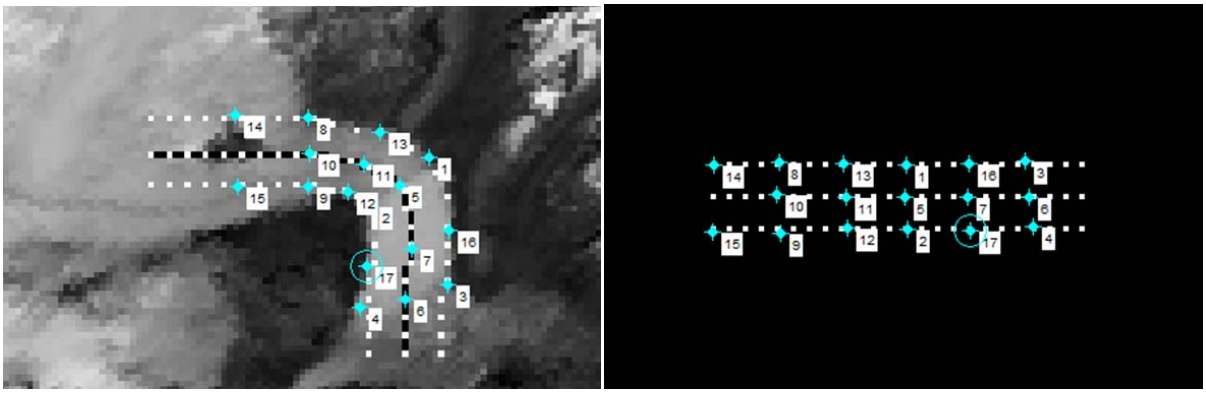

Figure 10 Control point selection for distortion of a curved glacier to a straight form. A curved grid is drawn upon the glacier (left) and mapped on to a regular grid (right). 17 control points were used.

2.1.11 Active region selection

The edge detection algorithm required an input of an 'active region'. This was defined as an area within which the margin position could vary, excluding surrounding pixels. The pixels contained within the area were those which were useful for margin position detection; those outside it did not contain useful information. An example of such an area may be seen for Helheim Glacier in **Figure 11** A. The width of the area was maximised in the direction perpendicular to glacier flow to provide as many edge pixels as possible, without the inclusion of surrounding rock, which may have caused false and static margin position locations. The length of the area was made sufficient to contain the full variation in edge position, approximated through the viewing of a high frame rate animation of the images (**Supplementary Animations S1** and **S2**). Active regions were rotated to produce images of horizontal glacier flow from left to right, with approximately vertical margins, allowing analysis procedures to maintain their orientation.

2.1.12 Edge detection

Once the active region was prepared it was passed to the edge detection modules for extraction of glacier margin position. A flowchart of the edge detection operations may be seen in **Figure 12**. Two edge detection methods were used to increase the probability of

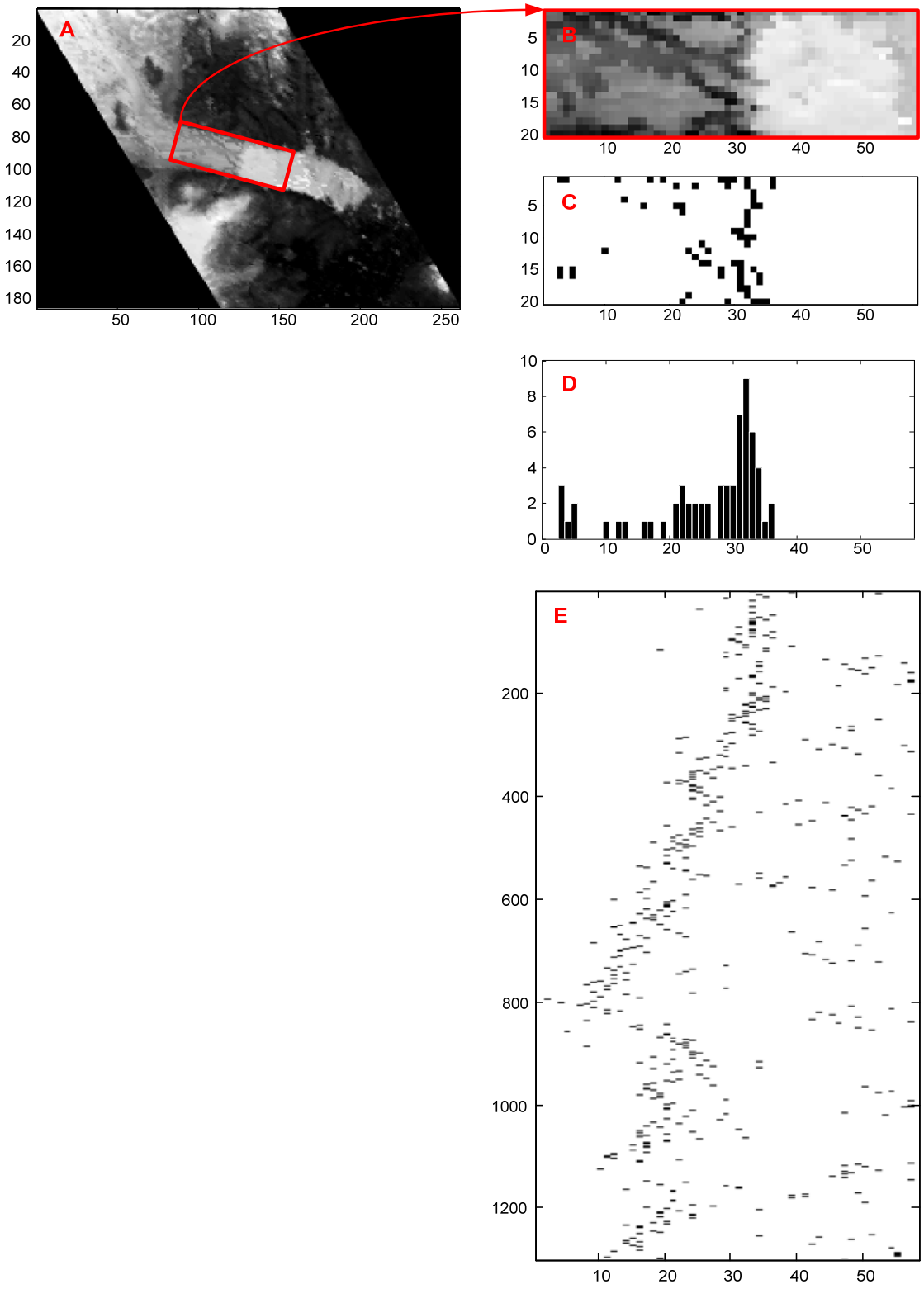

Figure 11 Schematic depicting simplified extraction of margin positions on Helheim Glacier by the Sobel edge detection method. The active region (red box) is manually defined on the glacier (A), selected and rotated by pre-processing modules to give the active region (B). Sobel edge detection is then performed on the active region using automatically defined thresholds. Axes for A and B show numbers of pixels. Histogram C displays the frequency (y-axis) of edge detections along each column of pixels. The process is repeated for every cloud-free image and the maximum edge detection frequency marked to give D (y-axis is index of cloud-free days, x-axis is horizontal pixel location), which starts to show progression of glacier margin position through time.

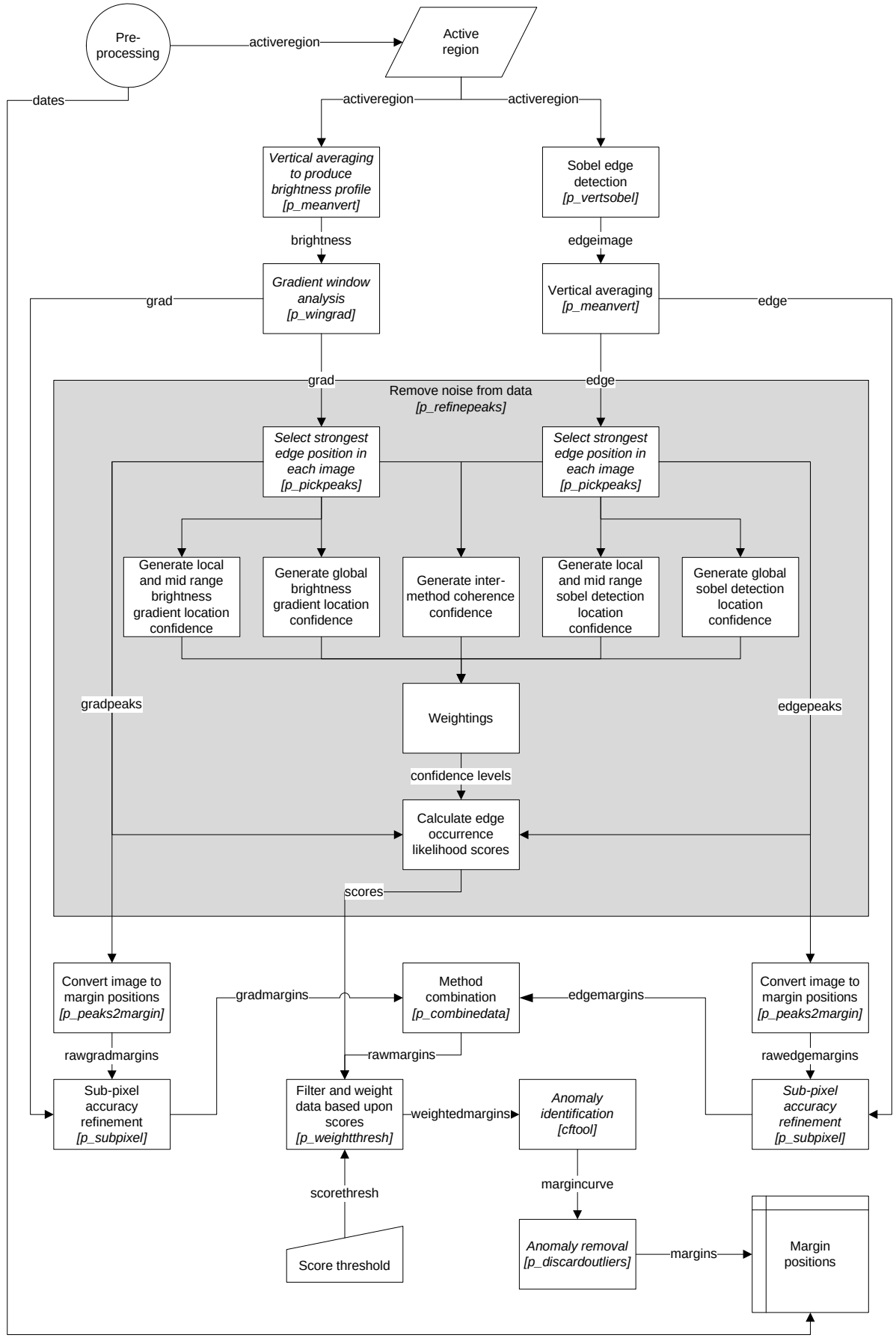

Figure 12 Edge detection algorithm program modules. Module names are given in square brackets whilst the names of variables passed between them interrupt arrows.

successfully detecting an edge and to provide cross-validation, which subsequently informed noise removal procedures.

2.1.12.1 Sobel Method

A great number of edge detection algorithms have been developed (Canny 1986; Heath 1997; Hassan et al. 2008) which operate in a variety of ways (Costa & Cesar 2000). To determine the most suitable edge detection method for use in this study a test image was put through all available algorithms. The results can be seen in **Figure 13**. The Prewitt and Sobel methods produced the highest ratios of correctly detected edge pixels to incorrectly identified pixels. The results obtained by the Prewitt and Sobel methods were very similar over a number of images. The Sobel method was chosen for use in the study due to its widespread use in computer vision procedures. It is possible to operate Sobel edge detection in a single direction, where only vertical edges are identified.

Vertical Sobel detection was then carried out for each active region image (**Figure 11** B) to produce a new stack of images depicting the vertical edges found. A binary edge image was thereby calculated, where pixels containing an edge were given the value of 1 and those where no edge was found were given a value of 0 (**Figure 11** C). Each column of pixels was then summed to give the number of edge pixels detected across the glacier active region (**Figure 11** D). Columns containing high values were those most likely to contain a coherent vertical edge. A version of these figures animated through time may be seen in **Supplementary Animation S1** for Kangerdlugssuaq Glacier and **S2** for Helheim Glacier. The vertically averaged data are shown in **Figure 14**, where it can be seen that a coherent margin position across time emerges. The spatio-temporal coherence exhibited in the figure shows that a glacier margin is being successfully identified. It can also be seen that there is a high level of noise in the data. This arises from the detection of features that are not the glacier margin, such as iceberg edges, crevasses, small clouds, moraines and fjord shadows as well as sensor error. Picking out the pixels containing the peak number of edges in each image helps remove some of this noise (**Figure 11** E and **Figure 15**).

2.1.12.2 Brightness Profiling Method

The second way in which the glacier margin was located was through brightness profiling. Inspection of a number of images found that the area beyond the glacier margin usually

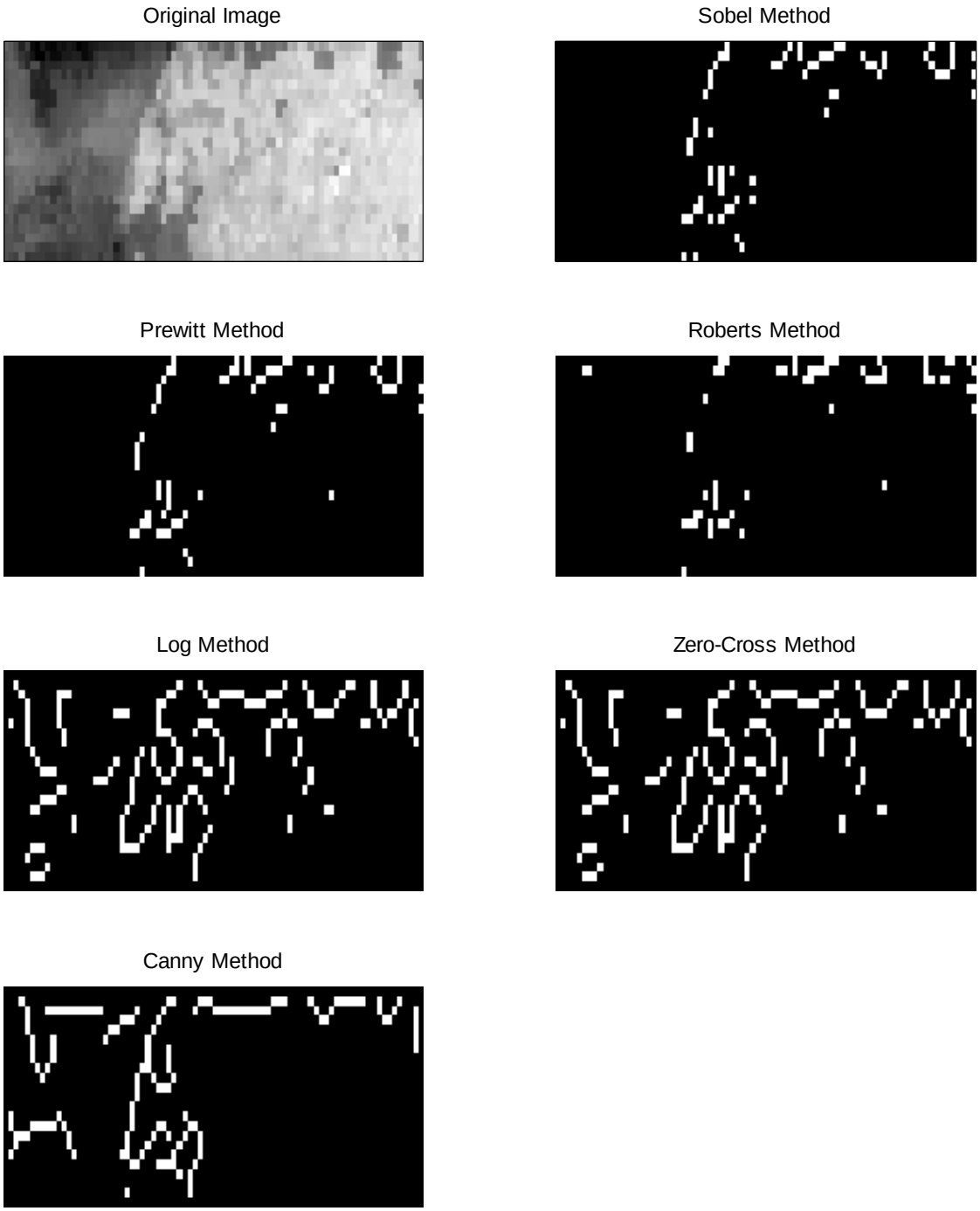

Figure 13 Test image of glacier margin processed using multiple edge detection algorithms. Similarly good results are obtained from the Prewitt and Sobel methods. An image with a partially ambiguous margin was used for this test to assess the response of different detection algorithms.

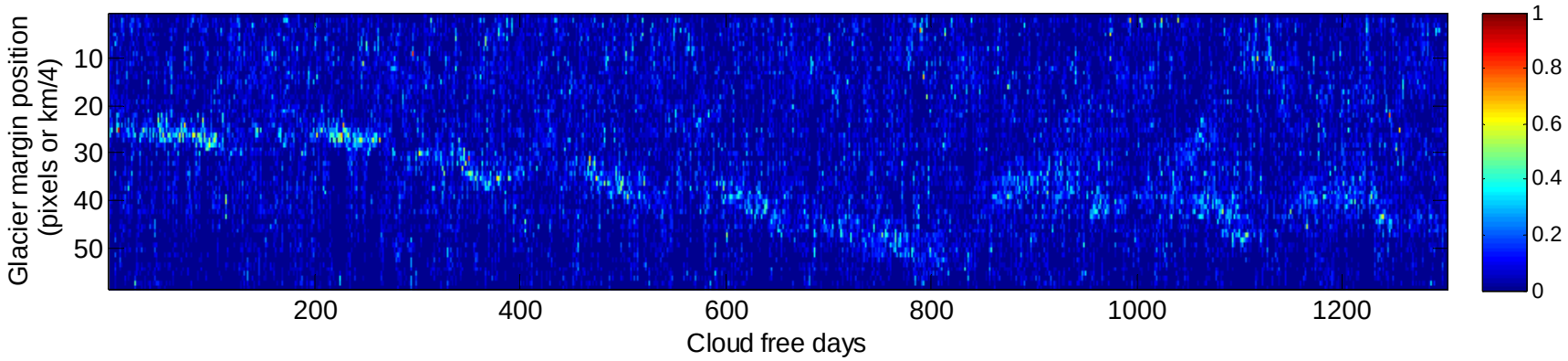

Figure 14 Spatially distributed number of daily detected edge pixels, perpendicular to the flow line of Helheim Glacier, by the Sobel method. Amongst much noise, the glacier calving margin position emerges as a coherent line.

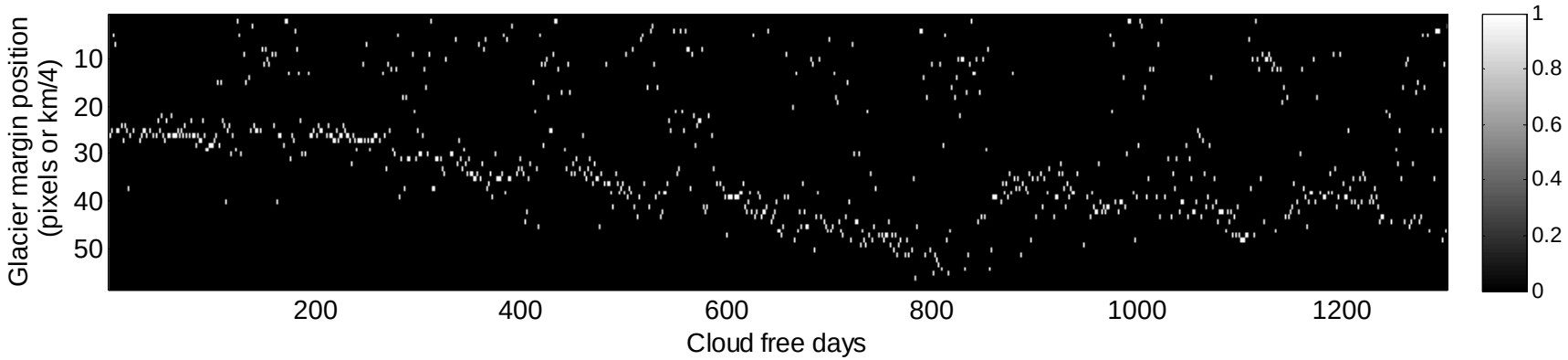

Figure 15 Location of peak number of edges for each image of Helheim Glacier, detected daily by the Sobel method. This removes much of the noise from the margins observable in **Figure 14**

contained broken up sea ice (sikussak) and occasionally consisted of open water. Both of these surfaces have albedos different from that of glacier ice. **Figure 11** A shows the high albedo of sikussak relative to glacier ice and the low albedo of open water from a satellite image, whilst **Figure 1** shows the same in an aerial photograph.

To identify this change in albedo, the brightness levels of each glacier active region were vertically averaged in a similar manner to the vertical averaging for the Sobel method detected edges described above. This created a brightness profile parallel to the direction of flow for each image. Profiles for 11 images of Helheim Glacier are plotted in **Figure 16** B. It can be seen that there is a large increase in mean brightness at the glacier margin. Identifying the position of this increase allowed for location of the glacier margin position. Similar to taking the first derivative, a moving window of width 3 pixels was applied across each profile, outputting the difference in brightness levels across it. For each image, this produced an approximate gradient from the pixel brightness data (**Figure 16** C). This plot is animated through time for two glaciers in **Supplementary Animations S1** and **S2**. Stacking the gradients of each image produces **Figure 16** E and **Figure 17**, which shows how this gradient varies through time. A coherent margin position can be seen in this data, again amongst background noise. Picking the greatest value of gradient from the modulus of each image removes much of this noise, as can be seen in **Figure 18**.

2.1.12.3 Sub-pixel accuracy refinement

The Sobel detection and brightness profiling methods identified the single pixel columns that appeared most likely to contain a glacier edge. A time series of edge positions derived from these methods alone may therefore only take up discrete values, based upon the location of pixels. This results in edge positions artificially constrained to pixel boundaries, 250 m apart.

The glacier margin edge was rarely contained within a single pixel column. This was due to it often not being exactly orientated in the same direction as the edge detection algorithms, lying at a diagonal or varying in orientation across the fjord. It was therefore possible to interpolate the exact position of the edge, within the identified pixel, using information from the surrounding pixels. To achieve this, five pixel width sections of the vertically

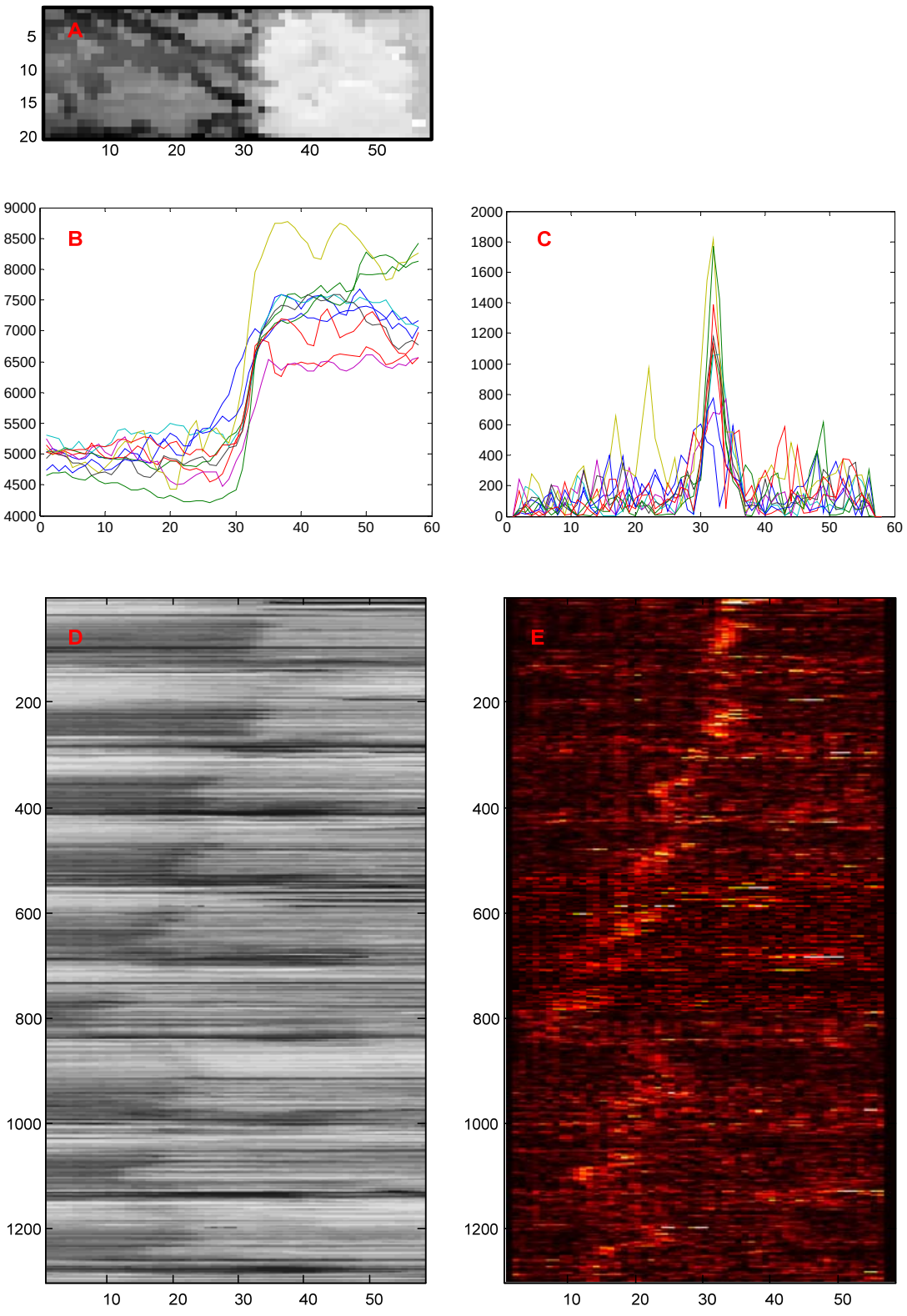

Figure 16 Schematic showing workings of gradient window edge detection technique. The intensity values of the active region (image A) are averaged across the glacier to give intensity gradient profiles, a sample of 11 of which are shown in B (y-axis is surface reflectance; x-axis is position in direction of glacier flow). The across glacier averaged intensity levels for each cloud free day are shown in D, where the x-axis shows position in direction of glacier flow and the y-axis shows an index of cloud free days. Results of applying the 3 pixel moving window across the glacier profile are shown in C, the values of which, plotted over an index of cloud free days, are shown as E.

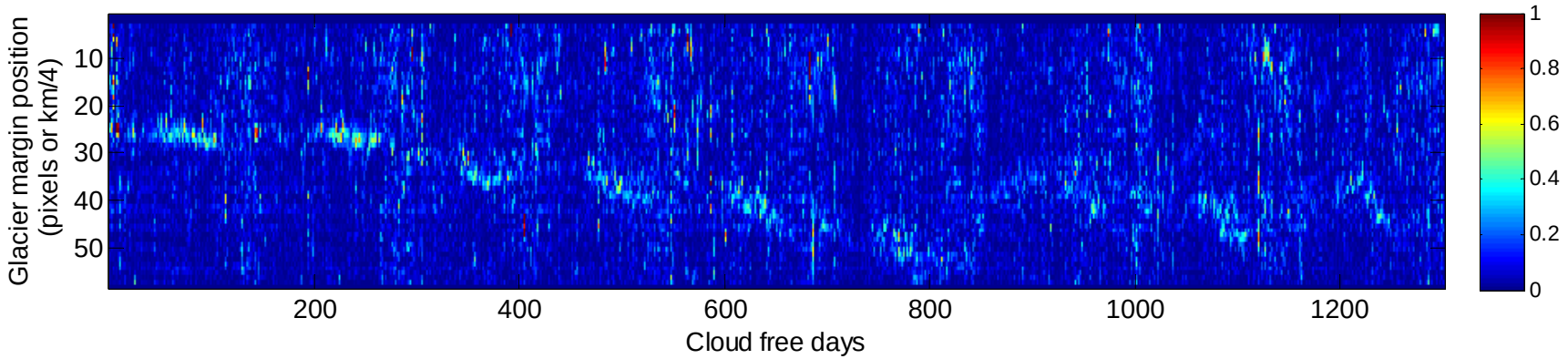

Figure 17 Edges detected using a moving window gradient approach. Values show modulus of gradient detected across the width of Helheim Glacier for each cloud free day.

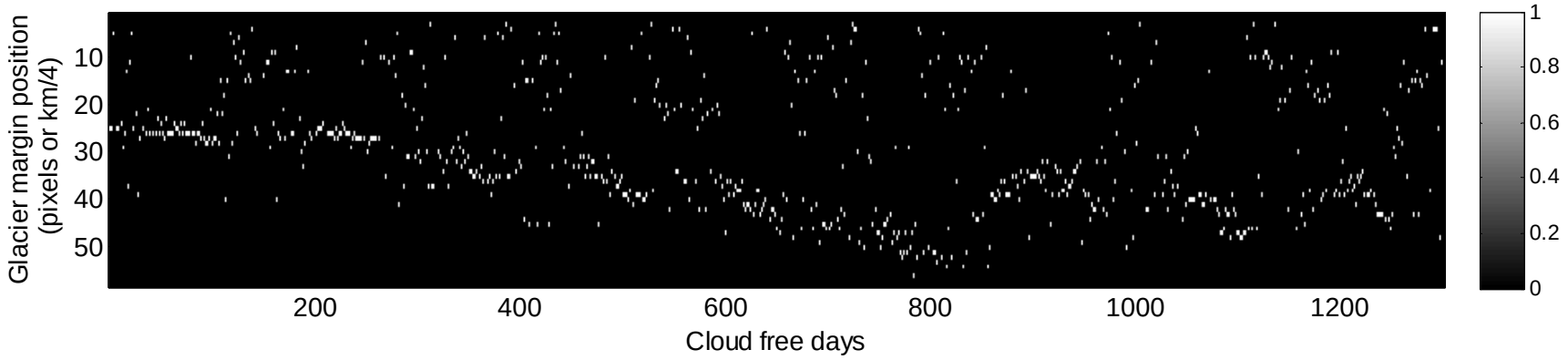

Figure 18 Positions of the largest absolute value of calculated gradient for each cloud free day on Helheim Glacier. This removes much of the noise present in **Figure 17**.

averaged gradients and edge detection columnular totals were taken for each image, centred about the pixel column initially identified as containing the edge. A Gaussian distribution (ideal for identifying peaks) was then fitted to the data (as in **Figure 19**) and the coefficient corresponding to the location of the peak returned. This interpolated a precise margin position, used to create a continuous and more accurate margin position time series. Data before and after sub-pixel accuracy refinement can be seen in **Figure 20**. This procedure improves upon the method of Joughin et al. (2008b), who used averaging to attempt to identify sub-pixel margin locations. The method could be further improved with the implementation of the Orthogonal Fourier-Mellin Moment algorithm, which uses radial orders and rotation invariance of moments to assess images (Zunfeng et al. 2008), although this would require much coding to implement and would not have been possible in the time period allowed for this study.

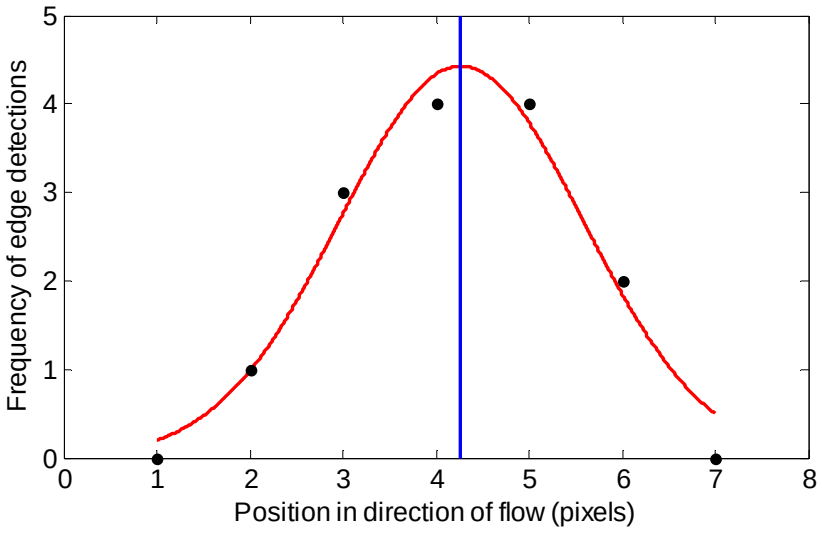

Figure 19 Fit of Gaussian curve to a detected margin position range (red line). Blue line indicates the location of the curve maximum, which represents the estimated sub-pixel margin position.

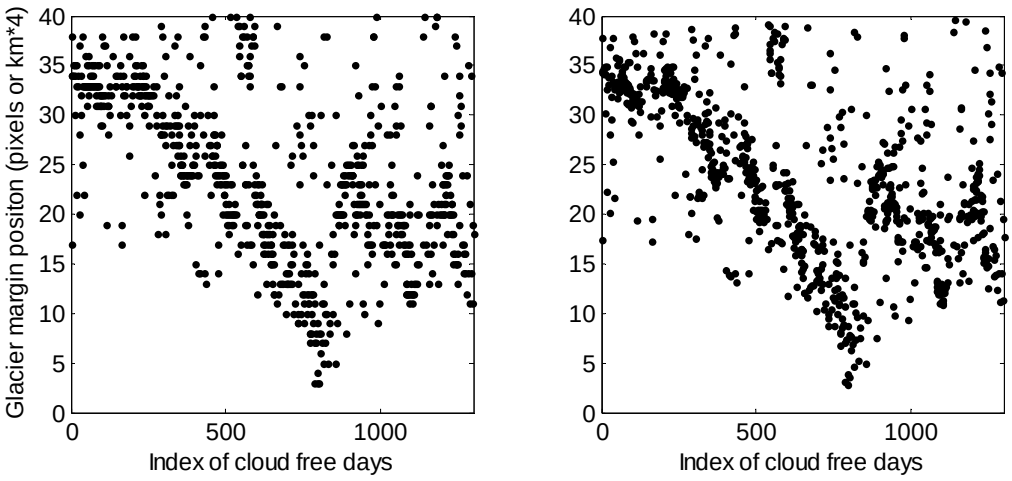

Figure 20 Data before (left) and after (right) sub-pixel accuracy refinement procedure. Data were produced by gradient edge detection algorithm for Helheim Glacier and has not had noise removal algorithms applied.

2.1.13 Noise reduction

The identified peak gradient locations from the brightness profiling method the high edge detection frequency locations of the Sobel method were the data sources used to ascertain glacier margin position. Both datasets contained an indication of margin position plus a large degree of noise. A number of methods were used to produce noise likelihood scores for every discrete pixel location of the active region space over the image acquisition period. These were then weighted and combined to give a single noise likelihood score; an indicator of the degree of confidence with which a detected edge can taken to be correct. The scoring methods are described below.

2.1.13.1 Time independent margin position zone scoring

A limited spatial zone across all time was defined in order to eliminate isolated noise points, far from the body of identified potential glacier margin positions. This was achieved by averaging the potential position data across time to produce an indication of the spatial domain of variation. The technique was applied to both the Sobel and brightness profiling derived potential margin positions. This may have had the negative effect of introducing an artificial limit on particularly extreme but correctly identified margin positions. To help reduce the probability of this occurring the scores were smoothed and slightly widened.

2.1.13.2 Spatio-temporal coherence scoring

Confidence that margin positions had successfully been identified was also gained through their proximal occurrence in space and time. This helped remove incorrectly identified pixels which were not located near other detected margin positions. Spatio-temporal zones of likely occurrence were identified using moving averages of pixel brightness gradients and Sobel edge detection frequencies across time and space. This was conducted over both short and long timescales (7 days and 3 months and spatial scales of 1.75 km and 2.5 km to produce indicators of both long and short term spatio-temporal coherence. Observations conforming to a slowly changing margin position were therefore scored as more likely to be correct than those which were isolated in time or space.

2.1.13.3 Inter-method coherence scoring

The final way in which levels of confidence in the potential margins positions were ascribed was the degree of coherence between the pixels identified by both the brightness profiling and Sobel methods. The maximal gradient change location was used to create a dataset of most likely edge position within each image. A similar dataset was created using the peak number of detected edge pixels across a glacier from the Sobel detection dataset. These two datasets were then combined using a logical AND filter to produce scores describing the margin positions detected in the same place and time by both methods.

2.1.13.4 Score masking

The confidence scores generated by the above techniques were normalised, weighted and then summed to give an overall score matrix spanning glacier margin position and time (**Figure 21**). This score matrix was taken to be the probability that a particular detected edge was correct. A cut-off threshold was defined for each glacier based upon a visual inspection of scored data. This mask was then applied to the most likely margin position detected by both detection algorithms, removing noise from the data. The threshold was selected conservatively to preserve variability and large abrupt changes in margin position.

2.1.14 Anomaly exclusion

To further exclude outliers from the dataset, a spline curve was fitted to the masked margin position data using the MATLAB Curve Fitting Toolbox. This allowed data points to be

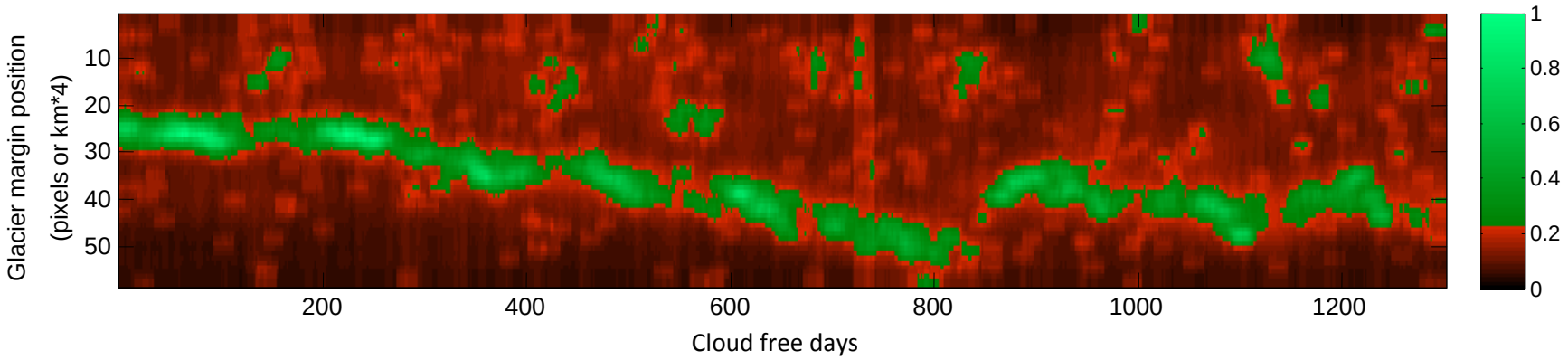

Figure 21 Validity score matrix of all possible margin positions for each cloud free day. Higher scores indicate greater confidence in margin positions occurring in their location. A threshold is defined to create a mask. Green areas indicate regions in which margin positions are acceptable, red areas indicate regions in which margin positions are masked out to reduce noise levels.

manually and rapidly excluded from the fit by selecting them individually, or as part of an exclusion zone. The remaining points were then weighted by their confidence score and fitted with a robust spline curve (**Figure 22**). The smoothing parameter of the spline curve function was chosen to preserve variability in the margin positions, although it is possible that very rapid large scale changes were not accurately represented by it. Points far away from the curve were then excluded from the final margin position product and those close to the curve became the margin position dataset. It is possible that noise pixels which were not accurate representations of margin position but which lay near to the fitted spline curve were included in the dataset.

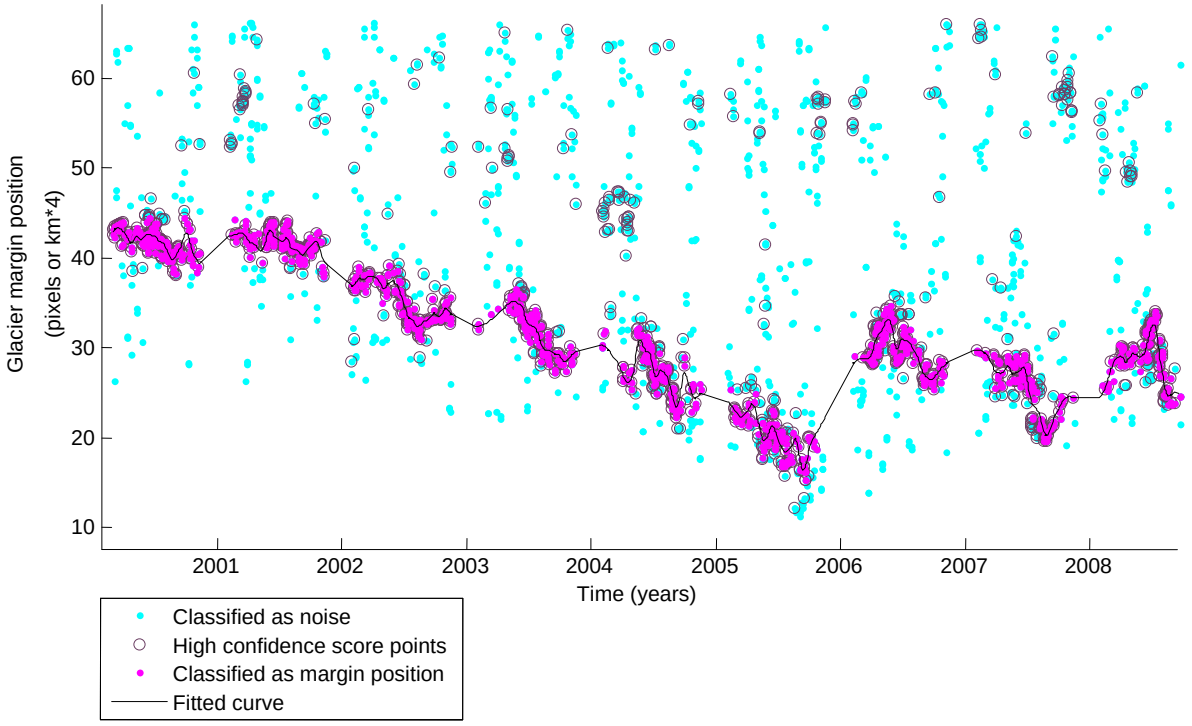

Figure 22 Margin positions selected by progressive noise elimination procedures. Points classified as having high confidence levels by the automated scoring system are circled, whilst those selected by the weighted spline curve (black line) are highlighted magenta and form the final margin position dataset for Helheim Glacier.

2.1.15 Error

Error in the detected margin positions may be derived from many sources some of which are difficult to quantify. Identified sources of error include sensor and image registration variation, sensor noise, image distortion, incorrect edge detection location, sub-pixel estimation errors and noise classification error. An assessment of typical error within the

data may be found in the Validation section (2.1.16), where margin positions for two glaciers are compared to manually checked data from another study. This section considers likely error sources and their potential influence upon the data.

It was noted when viewing animations of sequential MODIS images that the occasional image was incorrectly geolocated. This was observed as a 'jump' of all features in the image for the duration of a frame. This error could have originated from incorrect orbit location information, which may have errors of up to 200 m (Rojas et al. 2002) or have been introduced dfuring the conversion of swath raw sensor data to tiled daily images. It is estimated that this was present for less than one in 1000 images and the displacement was not larger than one pixel. Image geolocation displacement was therefore close to an insignificant source of error.

Sensor noise can have a variety of origins including interference from energetic protons or solar radio emissions. It often manifests itself as image speckle (**Figure 6** B) which was present to some degree on the majority of images. This may result in an incorrectly identified edge location due to the detection of high contrast sensor noise as edge pixels. Poor quality images may also be gained from distorted pixels, those which are taken at high magnitude zenith viewing angles and projected onto a grid. An example of this effect may be seen in **Figure 6** C). This decreases the effective resolution of the image and could have the effect of displacing the observed glacier margin position by a few pixels. Another source of error can derive from the amalgamation of multiple swath images, with overlapping pixels chosen upon their image quality, to form a single MODIS product tile. Images taken under different sunlight conditions, or with different correction parameters applied can produce contrast stripes in an image. Changes in contrast, as observed in **Figure 6** D, particularly when near and parallel to the glacier terminus, are likely to be incorrectly identified as the glacier margin position. **Figure 6** E shows the effect of light cloud cover, which is allowed through the cloud exclusion algorithms. It is still possible to discern a glacier edge in this image, but the contrast has been reduced, making the task more difficult. Other noise of unknown origin or a combination of sources is also present in the images, as can be seen in **Figure 6** F.

The stated 250 m resolution of the MODIS tiled imagery can vary across the sinusoidal grid it is supplied on and may therefore not represent a continuous 1:4 pixel to kilometre scaling factor across the globe. The scaling factor would also have changed when the data were reprojected to a Lambert Azimuthal grid, which was performed to give more consistent distance measurements across the images, but potentially with a different scale. Data gained during the validation process (see below) suggests that this may produce a scaling error of up to 15% of the data range.

There are many features that appear in the images that could cause false glacier edge detections. High contrast features such as icebergs, moraines and shadows may disturb the algorithm. Features that do not extend across the glacier, perpendicular to the defined long axis of margin position variation are less likely to be misclassified. Longitudinal moraines should therefore not present a large problem, however features such as shadows, which may be cast by the fjord walls across the glacier (**Figure 23**) could easily be detected as the glacier margin position.

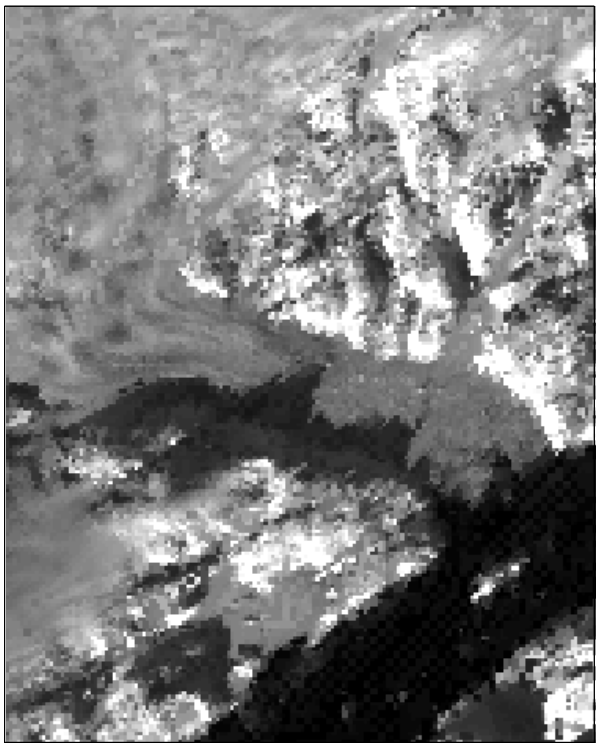

Figure 23 MOD09GQ image of Helheim Glacier (acquired on 7/2/2001) showing the long shadows that cast across it in early February. These shadows may be incorrectly detected as a glacier margin position.

Sub-pixel accuracies are interpolated and could contain errors of up to one pixel. The sub-pixel refinement calculates a likely position within a pixel but has no way of validating its output. Sub-pixel accuracy refinement is likely to produce the best results when the edge is not perpendicular to the pixel grid, as the position within a pixel may be calculated as a function of the rate of margin position variation across the surrounding pixels (as in the data of **Figure 24** A) . If the edge is aligned with the pixel grid there is no surrounding pixel information to determine the margin position within a column of pixels and the true margin position may lie at any point within the pixel (**Figure 24** B).

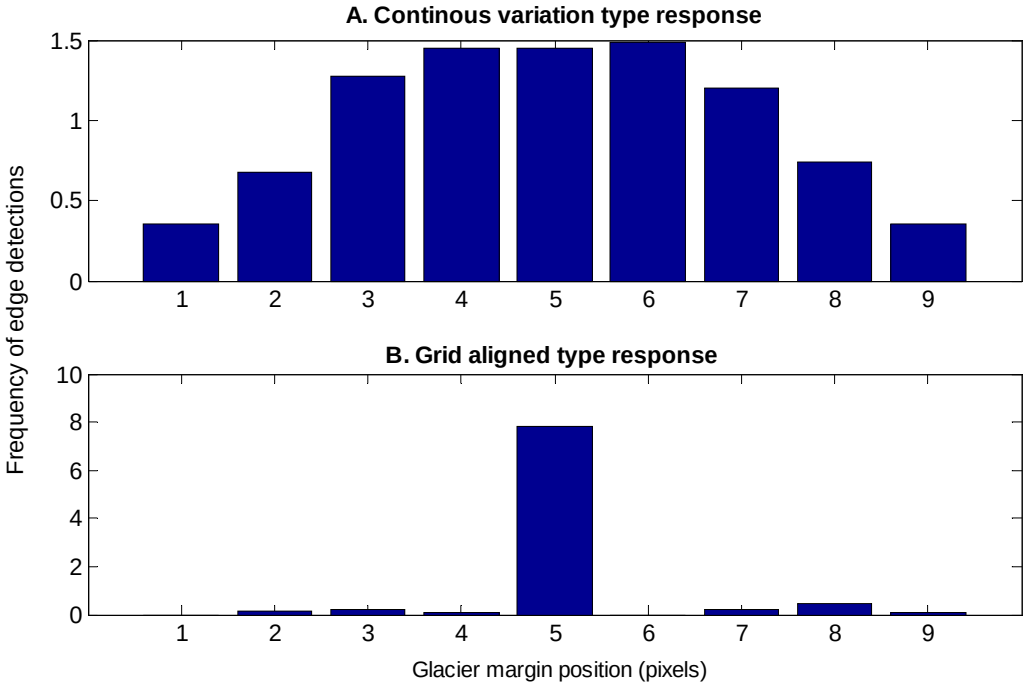

Figure 24 Bar chart showing examples of the type of edge detection responses that may be obtained in situation A, (above) where the glacier has a margin position lying across the vertical axis, and B, where a precise margin position lies within a pixel, in line with the axis of detection.

Additional error is likely to have been introduced into the calculated margin positions by the noise detection algorithms. The noise probability score masking system (see 2.1.13.4 Score masking) may limit the speed at which large abrupt changes can be made. If a large change is detected with low confidence (for example the margin is detected only part way across the glacier, and the contrast over the margin is low) it will be classified as noise. Conversely a pixel which may be noise, but is in line with surrounding margin position observations is likely to be included in the final margin position dataset. The calculated margin positions are therefore more likely to vary slowly and continuously than the actual glacier margin. Large

calving events may therefore not be adequately depicted over short timescales. Erroneous manual exclusion of data during the curve fitting process may also remove valid margin positions, although care was taken only to remove points which could confidently be recognised as noise.

An estimation of short term stochastic noise was derived by taking likely margin position spline smoothing curves of all glaciers and calculating the residuals. An example of such a curve may be seen in **Figure 25**. A histogram of the residuals for all glaciers may be seen in **Figure 26**. The RMSE (Root Mean Squared Error) of the residuals is 0.186. Almost all short term stochastic variation may be seen to lie between -1 and 1. It is important to note that the definition of short term stochastic noise in this calculation is a function of the smoothing parameter used.

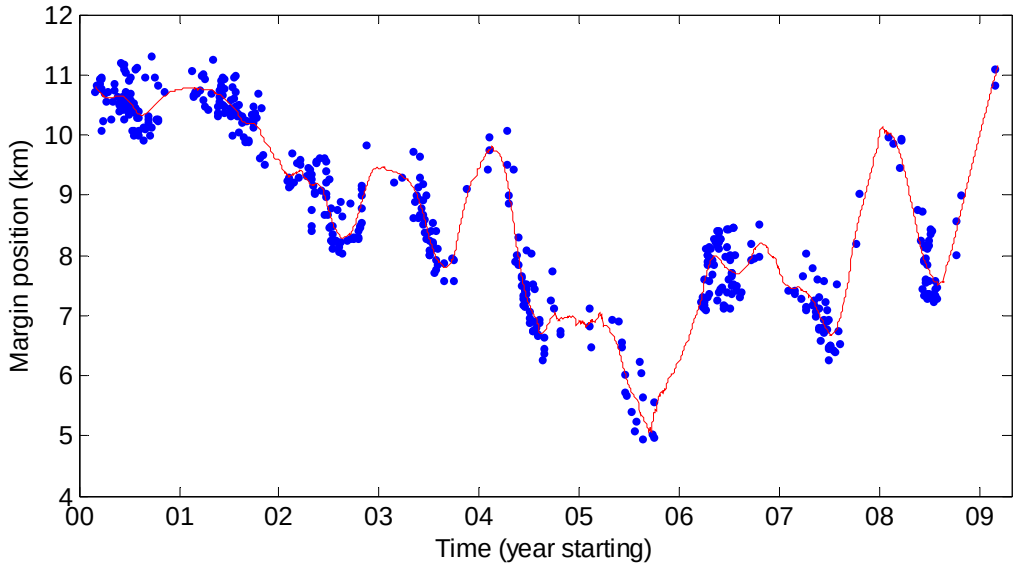

Figure 25 Spline curve with smoothing parameter set to an approximately seasonal time-scale, fitted to Helheim Glacier margin positions for stochastic error analysis.

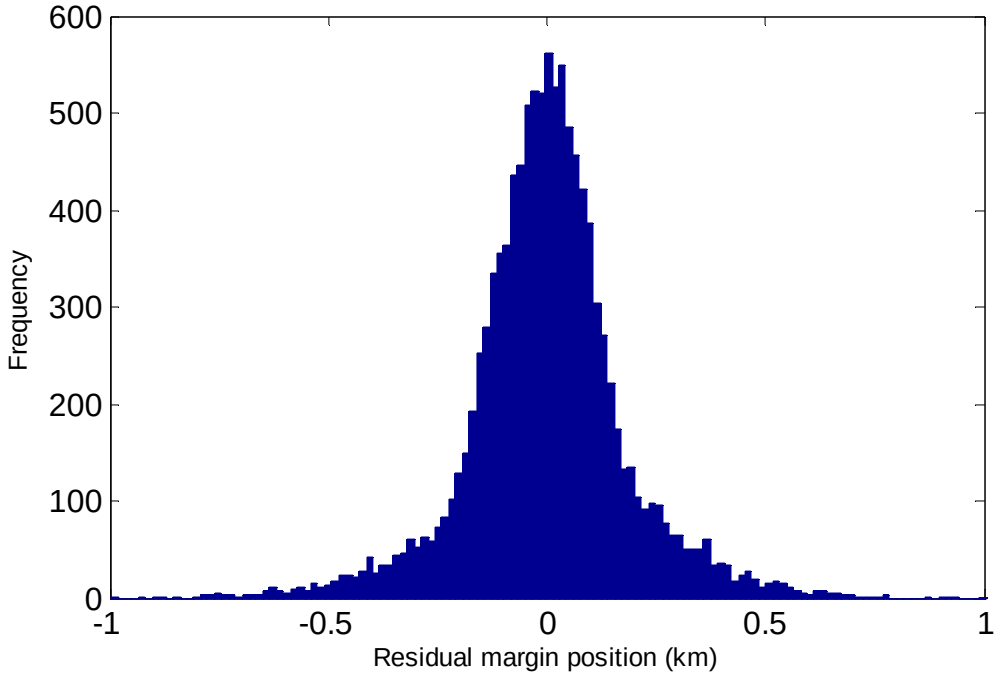

Figure 26 Histogram of residuals for all glaciers after fitting seasonal-scale varying spline smoothing curves to the margin positions.

2.1.16 Validation

Validation of the methodology was performed against the data of Joughin et al. (2008b). Joughin et al. used a semi-automatic method, in which automatically detected edges were visually inspected for inclusion. **Figure 27** shows a comparative plot of the two datasets for Helheim Glacier, whilst **Figure 28** shows the same for Kangerdlugssuaq. The margin positions of the present study were adjusted by the difference in means to have similar margin position origins to those of the Joughin et al. (2008b) data. When interpreting the graphs it is important to note that lines drawn between points are linear interpolations and, over longer periods of data absence, do not represent the margin position data. Meaningful validation comparisons should therefore be restricted to regions at, or proximal to, data points.

For both Helheim and Kangerdlugssuaq, the overall trend captured by both the data of the present study and Joughin et al. (2008b) appears the same. For Helheim glacier there appears to be a scaling difference between the two datasets, with the Joughin et al. margin positions showing a greater range of variation. This could be due an incorrect pixel-to-

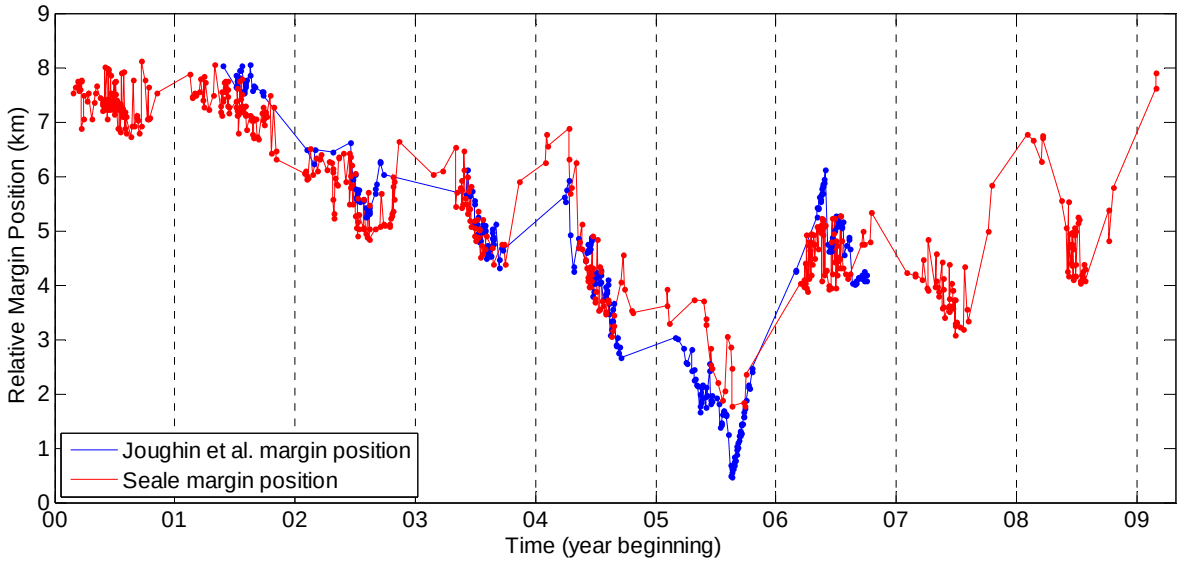

Figure 27 Comparison of the margin positions of Joughin et al. (2008b) and the present study for Helheim glacier. Straight lines are drawn between points but should not be taken as valid comparisons over low data density regions.

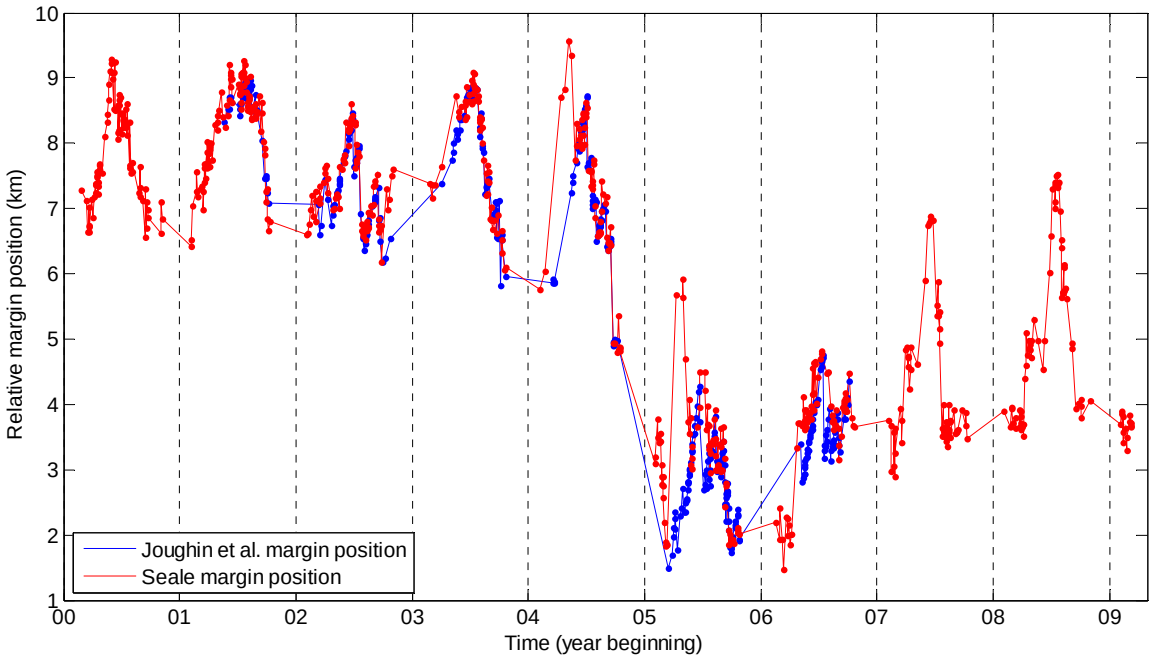

Figure 28 Comparison of margin positions produced by automated method of present study and visually checked semi-automatic method of Joughin et al. (2008b).

distance scaling factor used to transform the data of the present study, or a distortion resulting from the reprojection of data (see 2.1.9 Orthographic reprojection). It is also possible that the validation dataset was subject to similar distortions during its production. A degree of care should therefore be taken when interpreting inter-annual absolute margin changes from the data.

On sub-annual timescales, the data of the present study appears to capture the large scale changes within a season. For example, the retreat and advance during 2002 for Helheim Glacier or the approximately linear decline in margin position during the summer of 2003 and 2004, again for Helheim, is shown in both datasets. The seasonal cycle of Kangerdlugssuaq is reproduced well in both datasets. There are a number of anomalous points found in the Kangerdlugssuaq data of the present study, not reflected in the Joughin et al. data. These appear at the start of 2004 and 2005, where an artificial peak due to poor noise removal has been left in the data. There is a moderate degree of short term variability exhibited in the data of the present study which not in the Joughin et al. data. This is particularly prevalent for Helheim Glacier where daily to weekly changes in margin position appear somewhat stochastic. This is likely due to the size of changes being similar to the resolution of the MODIS sensor and limits our ability to establish causality between margin positions and environmental variables over short time scales (see section 4.4 SST/SAT forcing).

A quantification of typical error may be produced from the absolute differences between the datasets. As the sampling intervals were not equal, comparisons are made between interpolated artificial points. This is likely to increase the size of the error, making it an overestimate. The calculated root mean squared errors (RMSE) for the Helheim and Kangerdlussuaq datasets were 0.548 and 0.367 km respectively. The higher error for Helheim than Kangerdlussuaq is likely to be due to the scaling distortion present on Helheim. Helheim may thus adequately represent trends on a relative or short term scale, but have an elevated RMSE. These errors reduce to 0.193 and 0.193 km (these figures happen to be the same to 3 decimal places) when only days containing data across both studies are used (n = 176 and 220). These RMSEs show a good degree of agreement between the datasets, being less than one pixel (250 m).

2.2 ERA-Interim data

There are a very limited number of air temperature monitoring stations situated in Greenland which do not adequately represent the study area. The ERA-Interim reanalysis product (Simmons et al. 2007), produced by the European Centre for Medium-Range Weather Forecasts (ECMWF) was therefore used to gain surface air temperature (SAT) data. The product is the output of a weather model, which assimilates data from weather stations, satellites, ocean buoys, aircraft, ships, radiosonde and other sources. It is based upon the ERA-40 reanalysis product (Uppala et al. 2005), with a number of added datasets and model improvements, such an increased number of calculated pressure levels, higher spatial resolution and better model physics. Data were interpolated between grid calculation locations (spaced 1.5° apart) using a two dimensional interpolation function to give SATs for each glacier.

2.3 MODIS SST data

Sea surface temperatures (SSTs) were gained from the same MODIS sensor as collected the visible imagery used for glacier margin position tracking. As pass times were the same for both datasets the probability of obtaining simultaneously cloud free margin position and proximal SST data was increased, allowing for greater comparisons to be drawn. The MOD28 SST data product has a spatial resolution of 4 km and is produced daily. It is calculated from calibrated mid and far IR radiances (bands 20, 22, 23, 31 and 32) and is corrected for atmospheric effects using knowledge of the different transmissivities of IR bands (Parkinson & Greenstone 2000).

Sea surface temperatures were sampled from and averaged over a number of 25 km square boxes defined just off the coast of each glacier terminus. Their locations may be seen in **Figure 4**. Some glaciers share the same sampling box, due to their close proximity and thus have the same SST data series.

3 Results

3.1 Data quality

During application of the cloud detection method (see section 2.1.8 Data Selection) one glacier subsection containing Jakobshavn Isbræ was found to produce high misclassification

rates whilst using the normal tolerance values derived from the parameter space sensitivity testing. It is unknown why this was the case, and was presumed to be a function of the particular images produced by its local setting. A sample of 300 images was taken for this glacier to produce a new parameter space. The result showed a similar shaped success surface but with a large shift in the location of the 'cliff'. Glacier specific threshold values of 0.27 and 0.62 for NDSI and cirrus respectively were instead used in this case.

The raw extracted margin position data are presented for all 24 glaciers in **Figure 29**. A number of key measures for each glacier are shown in **Table 1**. The mean number of data points obtained for each glacier was 468.3. This corresponds to an average sampling frequency of 6.78 days. Data frequencies are higher during summer than winter due to winter snow cover of the glacier and surrounding sea ice making the margin position more difficult to detect. The lack of surface reflectance disparity across the calving margin during winter may be seen as periodic white bands with little contrast in **Figure 16**. The plot of Jakobsahvn Isbræ margin position (contained in **Figure 29**) clearly shows a lack of winter data points, although some other glaciers such as Tingmjarmiut 1 have more continuous data. Winter sampling could be possible on some glaciers due to the orientation of the calving edge, which may cast an observable shadow under certain illumination angles. One may assume a linear interpolation between summers as it is likely that the glacier flow rate remains relatively constant over winter and calving rates are low. It is possible that some of the data points present over the winter periods were the result of data reintroduction (see 2.1.14 Anomaly exclusion), whereby noise lying along a fitted spline curve had been included as a margin position point.

A number of glaciers did not produce coherent margin positions. This can be detected when a margin position appears stochastic within the imposed restrictions on variability, due to the selection of margin position data points from a range around a spline curve (see 2.1.14 Anomaly exclusion). The restrictions on variability were intended to exclude noise points far from the main body of detected margin positions. Where the data appears to vary randomly within these boundaries it is likely that a coherent margin position has not been detected and that the given margin position data largely consists of noise. It is still possible that the data represents an approximation of margin position, but high levels of caution should be

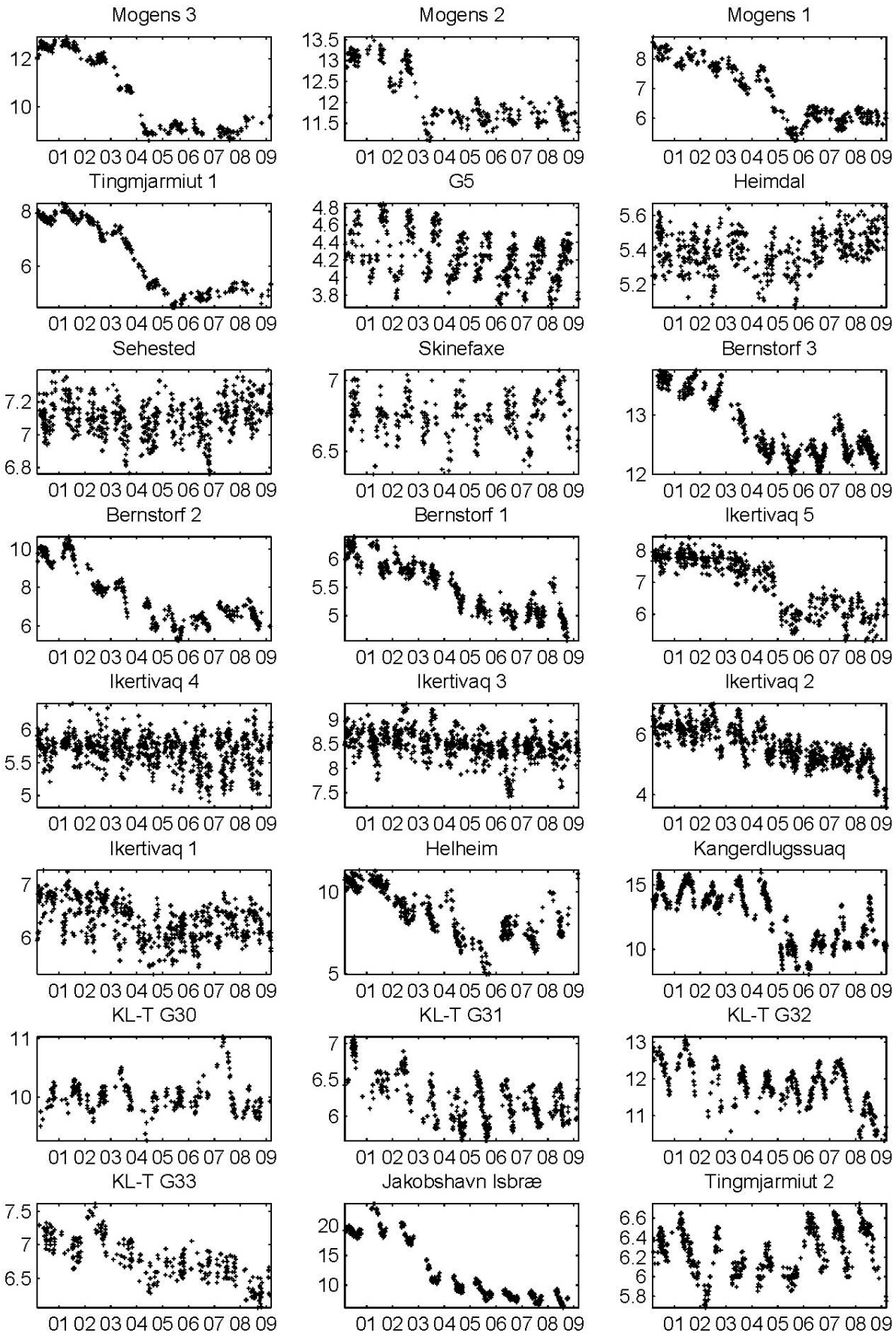

Figure 29 Extracted margin position data points for entire sample of 24 glaciers. x-axes denote year start points, y-axes show relative margin positions in kilometres.

Glacier	Data points	Margin Coherence	Quality	Mean residual (km)	Seasonality	Seasonal Range (km)	Margin level change 1/7/2001-1/7/2005 (km)	Margin level change 1/7/2005-1/7/2008 (km)	Glacier width (km)
Mogens 3	272	Good	Good	0.08	Weak	0.2729	-3.42	0.25	1.65
Mogens 2	268	Good	Good	0.09	Moderate	0.5273	-1.42	0.07	1.27
Mogens 1	318	Good	Good	0.11	Moderate	0.4199	-2.38	0.53	2.90
Tingmjarmiut 1	267	Good	Good	0.08	Moderate	0.3848	-3.17	0.36	3.07
G5	526	Good	Good	0.06	Strong	0.5912	-0.22	-0.11	2.84
Heimdal	474	Unknown	Unknown	0.06	None	0.1516	-0.08	0.18	3.30
Sehested	549	Unknown	Unknown	0.07	Weak/None	0.1777	-0.06	0.07	3.54
Skinefaxe	291	Good	Unknown	0.06	Moderate	0.2795	-0.02	0.16	2.58
Bernstorf 3	544	Good	Good	0.13	Strong	0.5413	-1.21	0.13	2.15
Bernstorf 2	343	Good	Good	0.06	Strong	1.1926	-4.03	0.61	4.65
Bernstorf 1	481	Good	Good	0.17	Moderate	0.5362	-0.81	-0.14	3.14
Ikertivaq 5	491	Poor	Unknown	0.14	Unknown	0.4469	-1.92	0.02	4.67
Ikertivaq 4	776	Poor	Poor	0.14	Unknown	0.3491	-0.13	-0.03	5.37
Ikertivaq 3	762	Poor	Poor	0.19	Unknown	0.4829	-0.17	-0.02	5.46
Ikertivaq 2	715	Poor	Poor	0.18	Unknown	0.7847	-0.75	-0.46	4.62
Ikertivaq 1	554	Poor	Poor	0.25	Unknown	0.5063	-0.51	0.20	2.87
Helheim	503	Good	Good	0.27	Weak	1.7587	-4.52	2.17	7.28
Kangerdlugssuaq	670	Good	Good	0.08	Strong	2.5625	-5.00	1.93	6.60
KL-T G30	278	Good	Unknown	0.08	Moderate	0.4907	-0.12	-0.16	1.86
KL-T G31	428	Good	Good	0.10	Strong	0.5222	-0.38	0.07	1.51
KL-T G32	420	Good	Good	0.11	Strong	1.1668	-0.78	-0.70	4.69
KL-T G33	294	Poor	Unknown	0.27	Unknown	0.2428	-0.25	-0.39	3.51
Jakobshavn Isbræ	486	Good	Good	0.05	Strong	2.9207	-11.32	-1.35	9.33
Tingmjarmiut 2	529	Good	Good	0.08	Strong	0.3833	-0.33	0.43	0.80

Table 1 Summary of margin position extraction results showing the number of extracted data points per glacier, the degree of coherence exhibited by the margin position data, a rating of extracted data quality, short term variability levels represented as the mean residual found by subtraction of a fitted smoothed spline curve, the degree of seasonality exhibited by the glacier margin position, the average annual seasonal range of the seasonal component data, margin position level change over July 2001 to July 2005, margin position level change over July 2005 to July 2008 and glacier width. Background shading colour scales are used to assist with rapid interpretation of the data.

exercised in the interpretation of data from these glaciers. Glaciers which appear to have produced such data are Ikertivaq 1, Ikertivaq 2, Ikertivaq 3, Ikertivaq 4, Ikertivaq 5 and KL-T G33. They have been denoted as exhibiting 'poor' margin coherence in **Table 1**. Two glaciers, Heimdal and Sehested, also appear to have produced such data but have a very small range of margin position variability, preventing accurate identification of the phenomenon. They have been labelled as having 'unknown' margin coherence in **Table 1**. The 'quality' column of **Table 1** reflects for each glacier the degree of confidence which may be had in the margin position data. Labels are assigned to glaciers based upon a consideration of margin coherence, the number of data points included and the plausibility of the extracted calving margin positions.

3.2 Seasonality

Many of the calving margins of the sampled glaciers display seasonal fluctuations. The approximate degree to which a regular seasonal pattern may be found in the data is described in the 'seasonality' column of **Table 1**. The seasonal range of each glacier was calculated from margin positions, smoothed to remove stochastic variation but with sufficient temporal independence to retain monthly scale trends. The 'level' component (a 365-day centred moving average) of each glacier margin position time series was subtracted from the data, to remove long term trends. For each glacier, each year of smoothed detrended data was then split midway through the winter advance. The maximum and minimum annual values were taken to give a range of variation and then averaged across years to give the mean seasonal variability. The results may be seen in the 'seasonal range' column of **Table 1**. The calculation may not be valid for those glaciers which do not follow a regular seasonal pattern as denoted in the 'seasonality' column of **Table 1**. The glaciers with the largest seasonal ranges were Jakobshavn Isbræ (2.9 km), Kangerdlugssuaq (2.6 km), Helheim (1.8 km), Bernstorf 2 (1.2 km) and KL-T G32 (1.2 km).

3.3 Margin position trends

To examine the next order of trend, inter-annual changes were investigated. To isolate change on this scale, a 365-day centred moving average of the glacier margin position time series was calculated and is **hitherto referred to as the 'level' component of the data**. The moving average calculation produces invalid results for the first and last 182 days of data

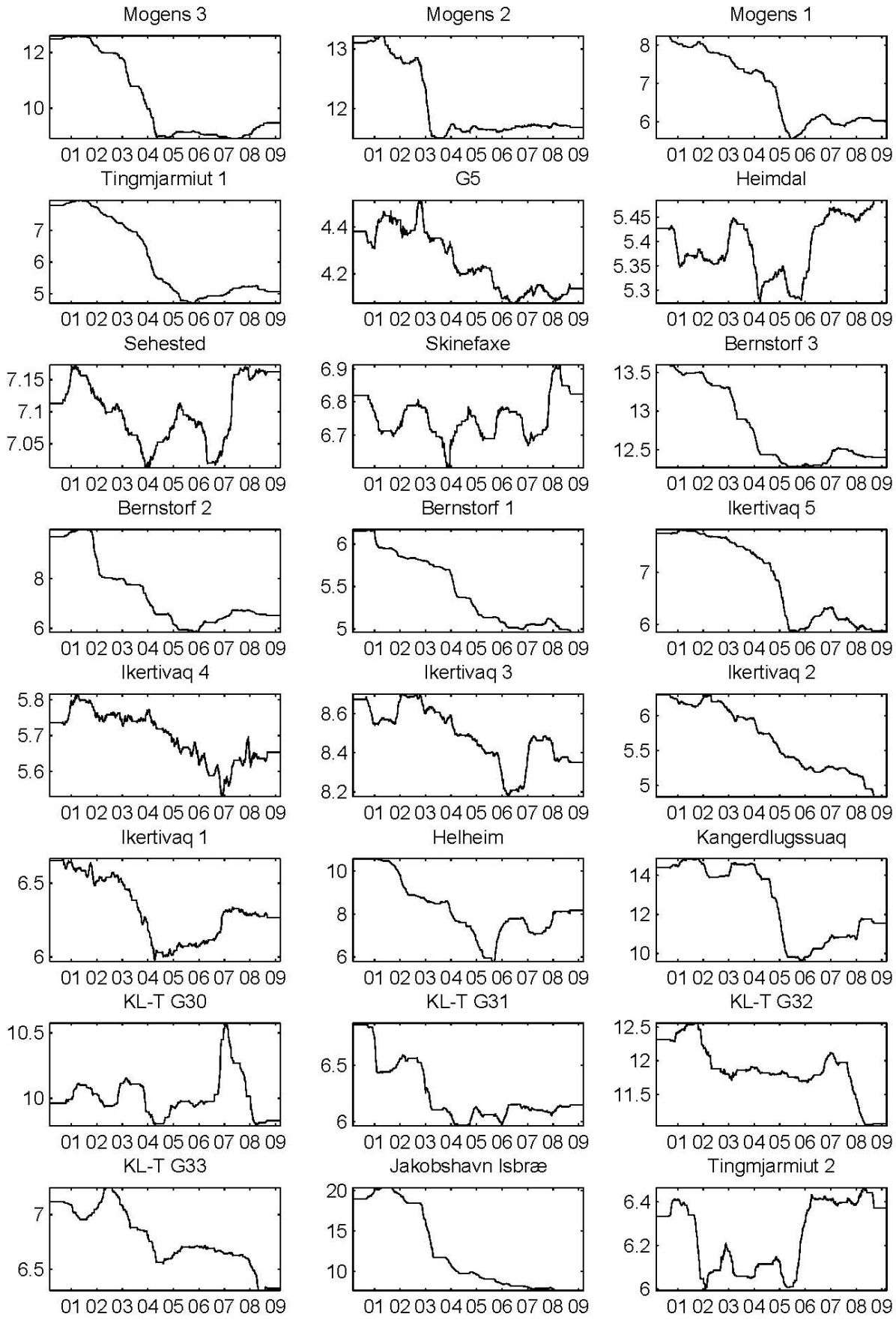

Figure 30 Margin position levels (365 day centred moving average) for complete sample of 24 glaciers. Data for the first and last 182 days of each series are unlikely to be valid due to data insufficiencies in the moving average calculation.

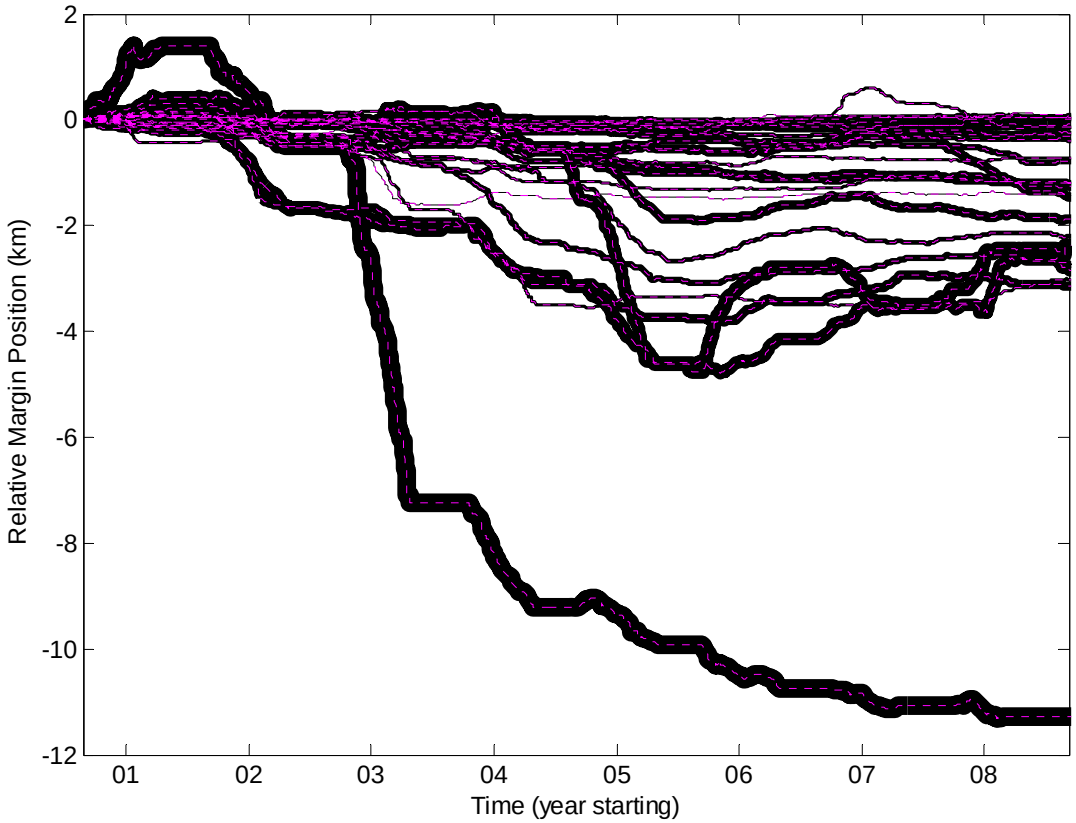

Figure 31 Relative margin positions of all sampled south-eastern GrIS glaciers (Jakobshavn Isbræ excluded). Dotted magenta line indicates glacier margin position, whilst black line behind has a thickness proportional to glacier width. The largest glacier width (thickest line) is 7.3 km, whilst the smallest is 0.8 km.

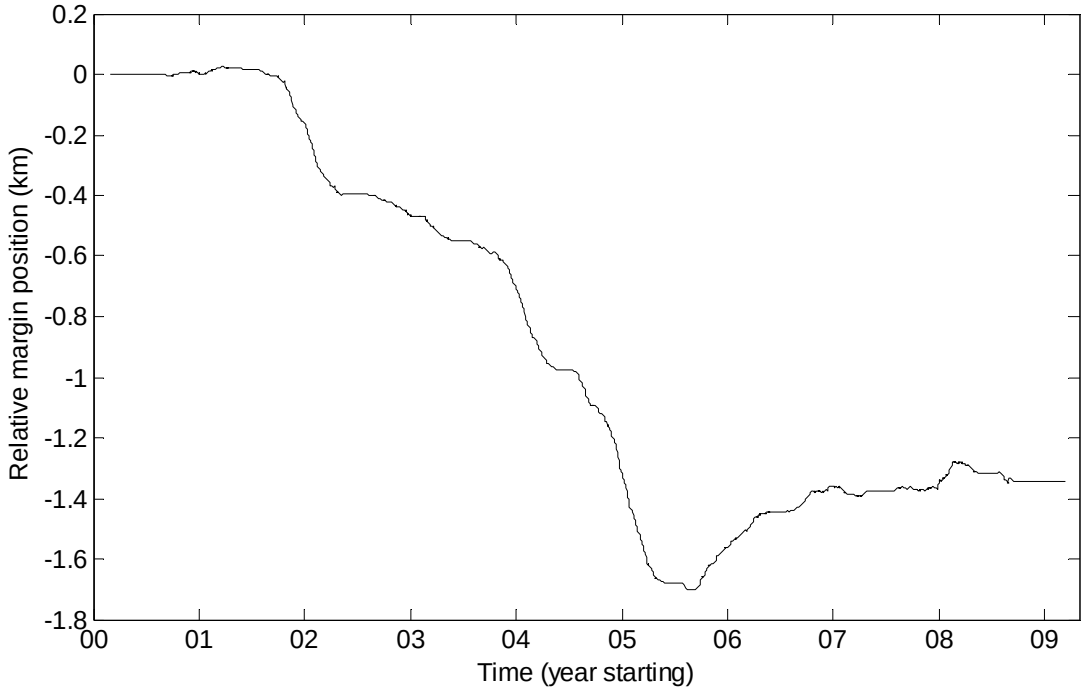

Figure 32 Averaged glacier margin positions for all south-eastern GrIS glaciers (Jakobshavn Isbræ excluded), with glacier weightings by glacier widths.

due to insufficient boundary information. The results may be seen in detail for each glacier in **Figure 30** and for all glaciers in **Figure 31**. **Figure 31** shows that over the course of observation many glaciers have experienced significant levels of retreat. Retreat appears to occur in steps, starting in 2002 and continuing to mid 2005. After this period many of the glaciers stay at the same level or experience some advance, but do not recover to 2001 levels. The level position change between July 2001 and July 2005 may be seen for each glacier in **Table 1**. Over this period all changes are negative with the largest retreats (over 2 km) occurring on Jakobshavn Isbræ (-11.3 km), Kangerdlugssuaq (5.0 km), Helheim (4.5 km), Bernstorf 2 (4.0 km), Mogens 3 (3.4 km), Tingmjarmiut 1 (3.2 km) and Mogens 1 (2.4 km). Significant partial recovery (over 0.5 km) from July 2005 to July 2008 is limited to Helheim (2.2 km), Kangerdlugssuaq (1.9 km), Bernstorf 2 (0.61) and Mogens 1 (0.5 km), whilst two glaciers, Jakobshavn Isbræ and KL-T G32 showed continued significant retreats of 1.4 and 0.7 km respectively. Weighting each glacier by its width, the average response of the sampled glaciers in the south east of the ice sheet (excluding Jakobshavn Isbræ) is presented in **Figure 32**. It can be seen that retreat occurs from late 2001 to mid 2005, followed by a small advance which continues until the end of 2006, after which there is little change.

To allow for continued analysis, the rate of margin position change (first derivative of margin position) was calculated to show periods of advance and retreat. In order to achieve this, the margin positions were smoothed and interpolated using a spline curve to remove short term variability and noise. The spline curve function was then differentiated to give the rate of margin position change and scaled to units of m day^{-1}. The results can be seen in **Figure 33**. Glaciers with high levels of stochastic variation, which are generally those with low data quality labels (**Table 1**) such as the Ikertivaq glaciers, produce margin progression rates which vary from highly positive to highly negative over short periods of time. This data appears physically unlikely and is probably invalid. Many of the other glaciers produce seasonal patterns with stable frequencies, advancing in winter followed by summer retreat. This pattern can be seen in the mean margin position rate of change for all south-eastern glaciers; **Figure 34**. Years of retreat appear to have longer calving seasons, as opposed to higher calving rates.

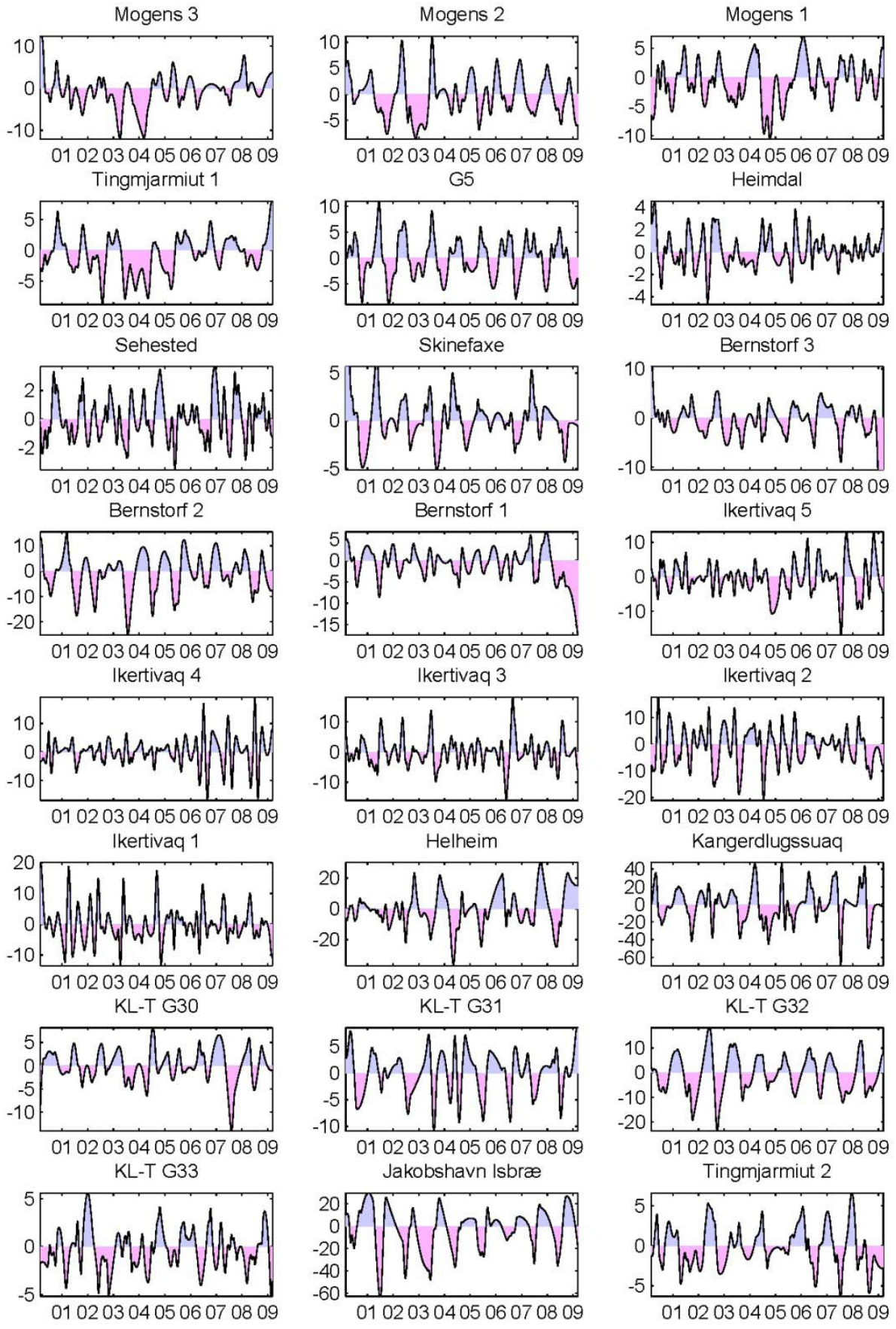

Figure 33 First derivative of margin positions (rate of margin position change) for all glaciers studied, showing periods of advance (blue) and retreat (pink). y-axis is rate of change in m day^{-1}, x-axis units show starts of years.

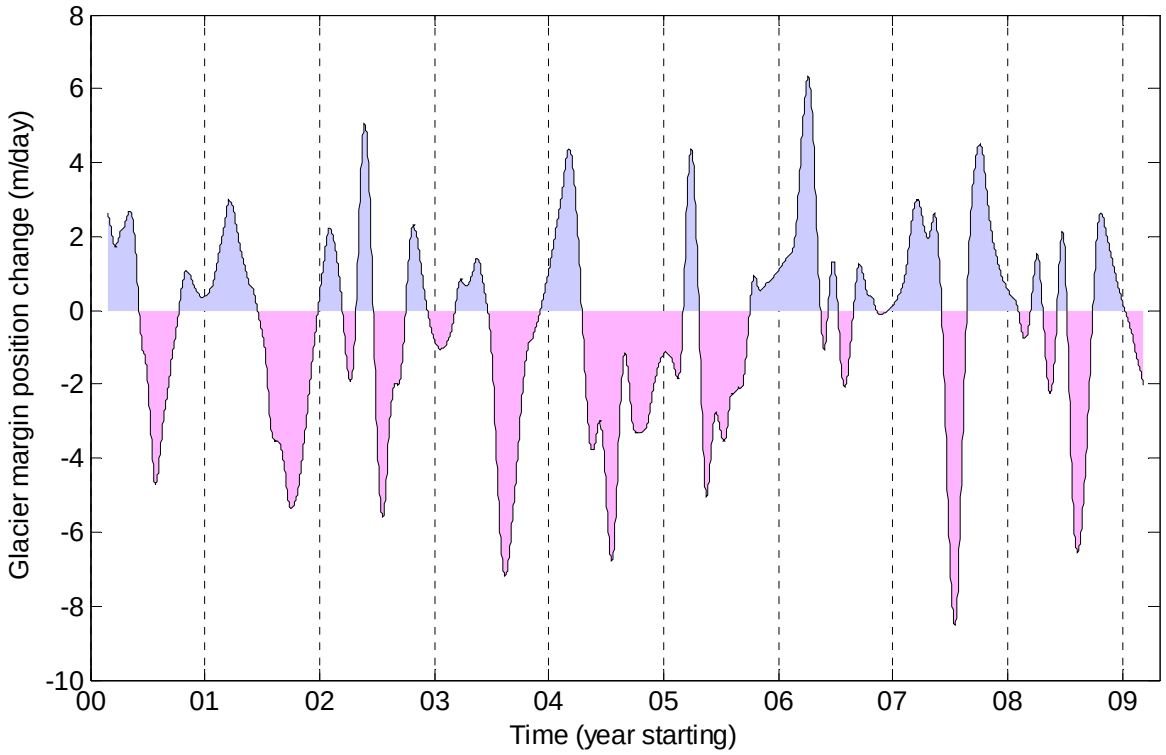

Figure 34 Mean rate of margin position change for all south-eastern glaciers (n = 23), with averaging weighted by glacier width. Retreat is marked in pink for values below 0, whilst advance is marked in blue for those above.

3.4 Environmental variables

Air and sea surface temperatures (SAT and SST) were studied in an attempt to determine their possible role in the modulation of calving margin position. The data levels were extracted using the same 365-day moving average technique as for the margin positions and are presented in **Figure 35** (SAT) and **Figure 36** (SST). Surface air temperatures levels follow a very similar pattern across all sampled sites, but with different mean temperatures. SAT levels rise steadily from early 2001 to a peak in mid 2002. Averaged across all glaciers this rise is 3.8° C. This peak is then largely sustained for many southern glaciers, such as the Mogens and Bernstorf glaciers until mid 2004, whist in northerly areas such as those around Helheim, Kangerlugssuaq and the KL-T glaciers the peak lasts for only a year, before dropping to by approximately 1.5° C to a new constant level. At the start of 2004 the SAT around all glaciers drops sharply, on average by 4.9° C by the start of 2006. Temperatures then increase by 1.2° C during 2006, before falling again to levels on average 0.6° C lower than at the start of 2006.

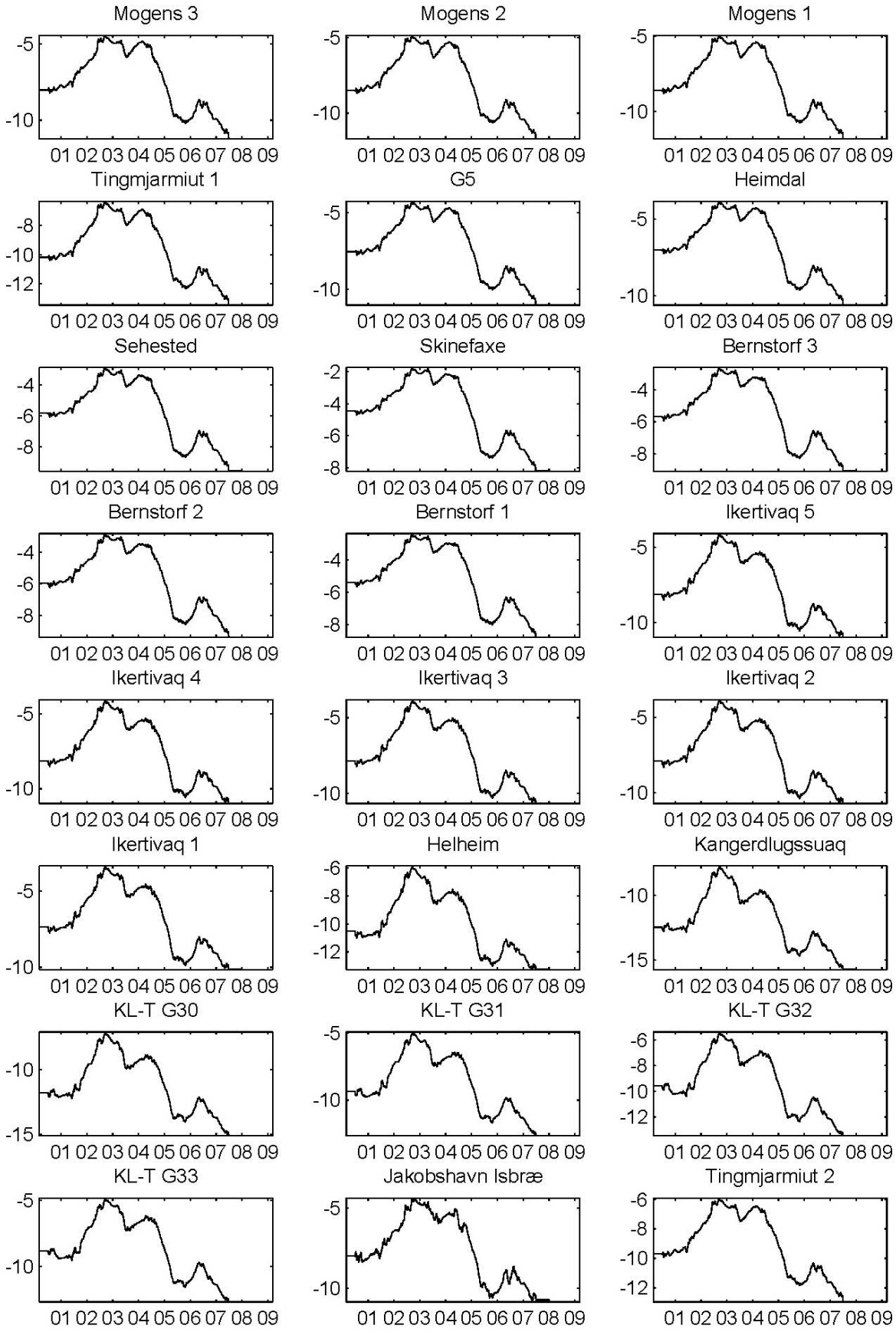

Figure 35 Surface air temperature levels (365 day centred moving averages) from ERA-Interim reanalysis data at the location of each glacier. x-axis is time (years starting), y-axis is SAT (° C). Some proximal glaciers have very similar data. The first and last 182 days of data is likely to be invalid due to insufficient data for a calculation of moving average.

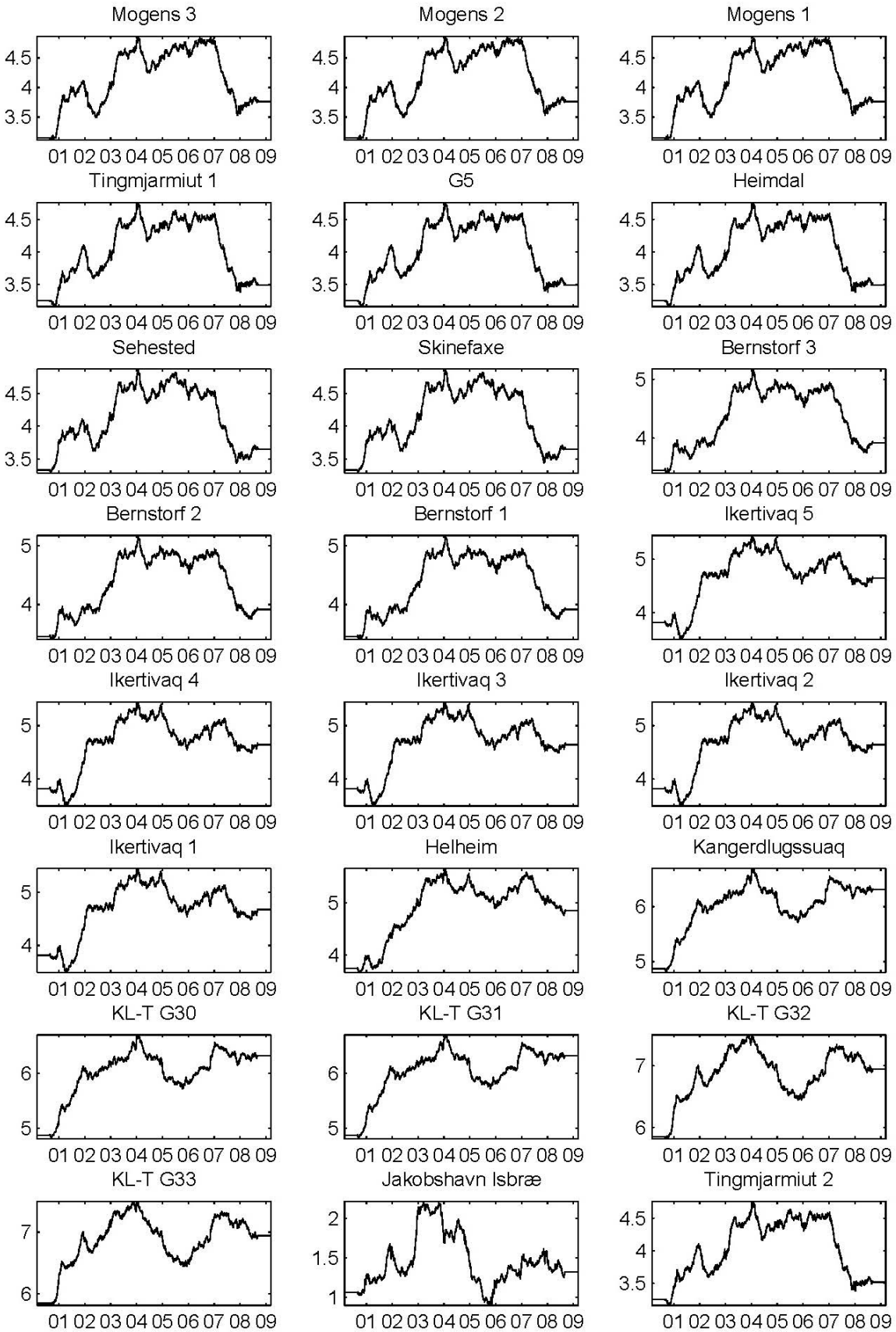

Figure 36 Sea surface temperature levels (365 day moving averages) from MODIS data, taken as an average from a box off the coast of each glacier (see **Figure 4** for box locations). Some glaciers have the same data as they are set around a single SST box. x-axis represents time with ticks showing the start of each year, y-axes represent temperature in ° C. The first and last 182 days do not have enough surrounding data to produce moving averages and are maintained at an artificial level.

Sea surface temperatures show increasing levels from 2001 to a peak at the start of 2004. The mean increase in temperature across all glaciers during this period was 1.6° C. After the rise to 2004 levels, high temperatures are maintained until the start of 2007 in the most southern study areas which includes the Mogens, Tingmjarmiut, Sehested, Skinefaxe and Bernstorf glaciers. Further north, temperature levels at Helheim, Kangerdlussaq and the KL-T glaciers reduce after 2004 by approximately 0.8° C, before recovering to similar levels by the start of 2007. By the start of 2008 the southern glaciers have experienced a sharp fall in SSTs to levels similar to those of 2001, whilst the SSTs surrounding the northern glaciers show only a slight decline in temperature.

3.4.1 SST/SAT forcing

To assess the potential forcing of calving margin position by sea and air surface temperatures, the level time series of the datasets were compared. Average time series were calculated across all south-eastern glaciers for SAT, SST and margin position. The relative influence of each glacier (its averaging weight) was determined proportionally by the glacier width, which was calculated by the mean distance across the fjord over the region of calving margin position variability. The rate of margin position level change was also calculated by differentiation of the margin position level. The results are shown in **Figure 37**. **Figure 37** A shows ERA-Interim reanalysis SAT levels over the observation period. SAT levels increase over mid 2001 to 2003, remaining high until late 2004. During this period glaciers show retreat (**Figure 37** C and D), ending approximately when SATs start to fall again, reaching a minima in late 2005. SATs then continue to stay lower than 2001 levels for the rest of the observation period, whilst on average glaciers experience a small degree of advance. SST levels (**Figure 37** B) start by following a similar trend to SAT levels by increasing over 2001 to the start of 2004. Unlike SAT levels, during a period of glacier stabilisation and small advance, they remain relatively high until the start of 2007, whereupon they experience only a small decline.

Using data averaged across all south-eastern glaciers, plots of rate of glacier margin position change versus SSTs and SATs were made, as for an average year of the sampling period (**Figure 38**). Both plots show a high degree of negative correlation, indicating that retreat generally occurs during times of raised temperatures. The relationship appears non-linear

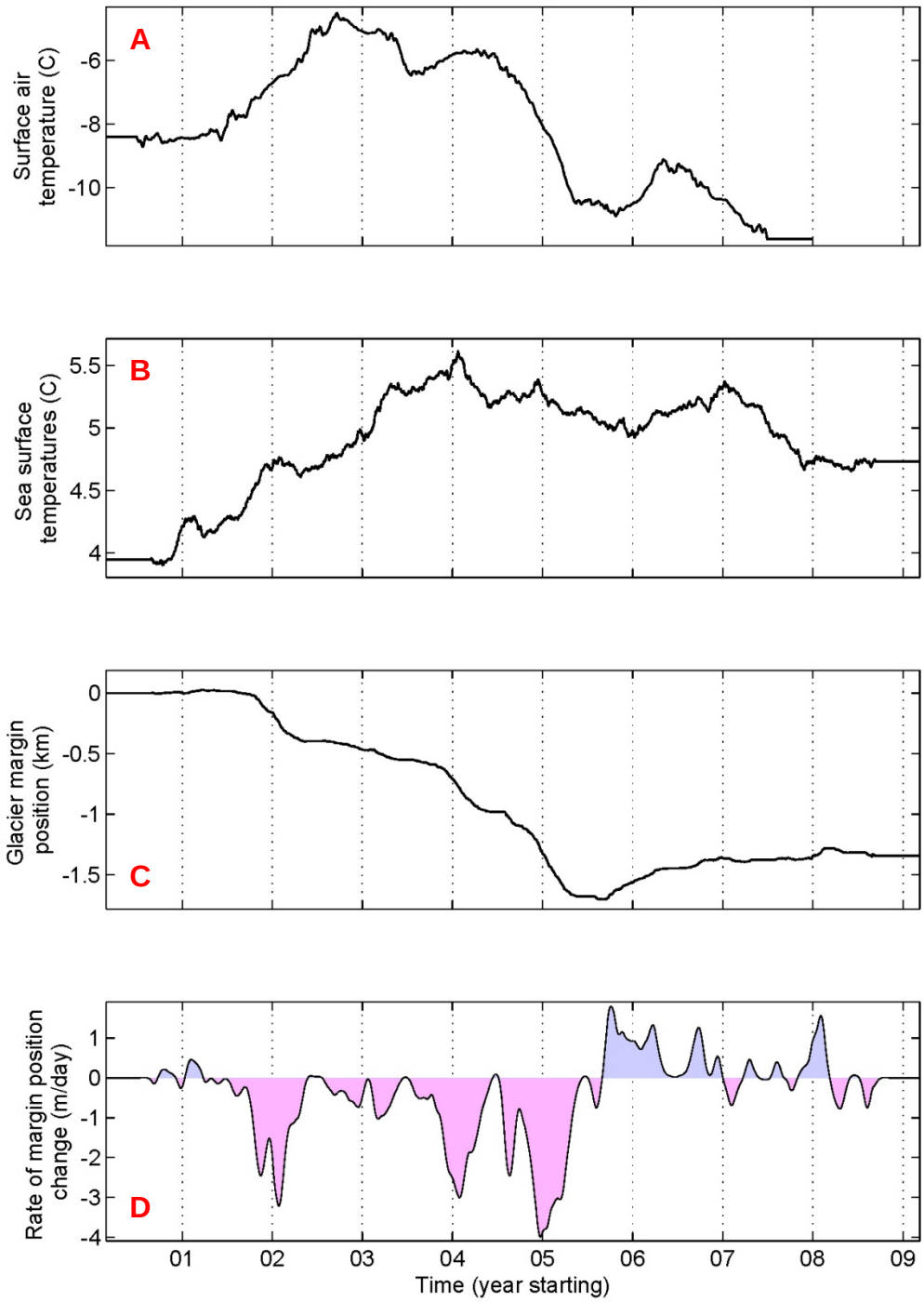

Figure 37 Mean level scale changes in SAT (A), SST (B) and glacier margin position (C) calculated using a 365-day centred moving average for the south-east. The derivative of margin position change is also shown (D), with retreat filled pink and advance filled blue. Glaciers were weighted by width during calculation of the mean. The first and last 182 days of data are likely to be invalid, due to the span of the moving average procedure.

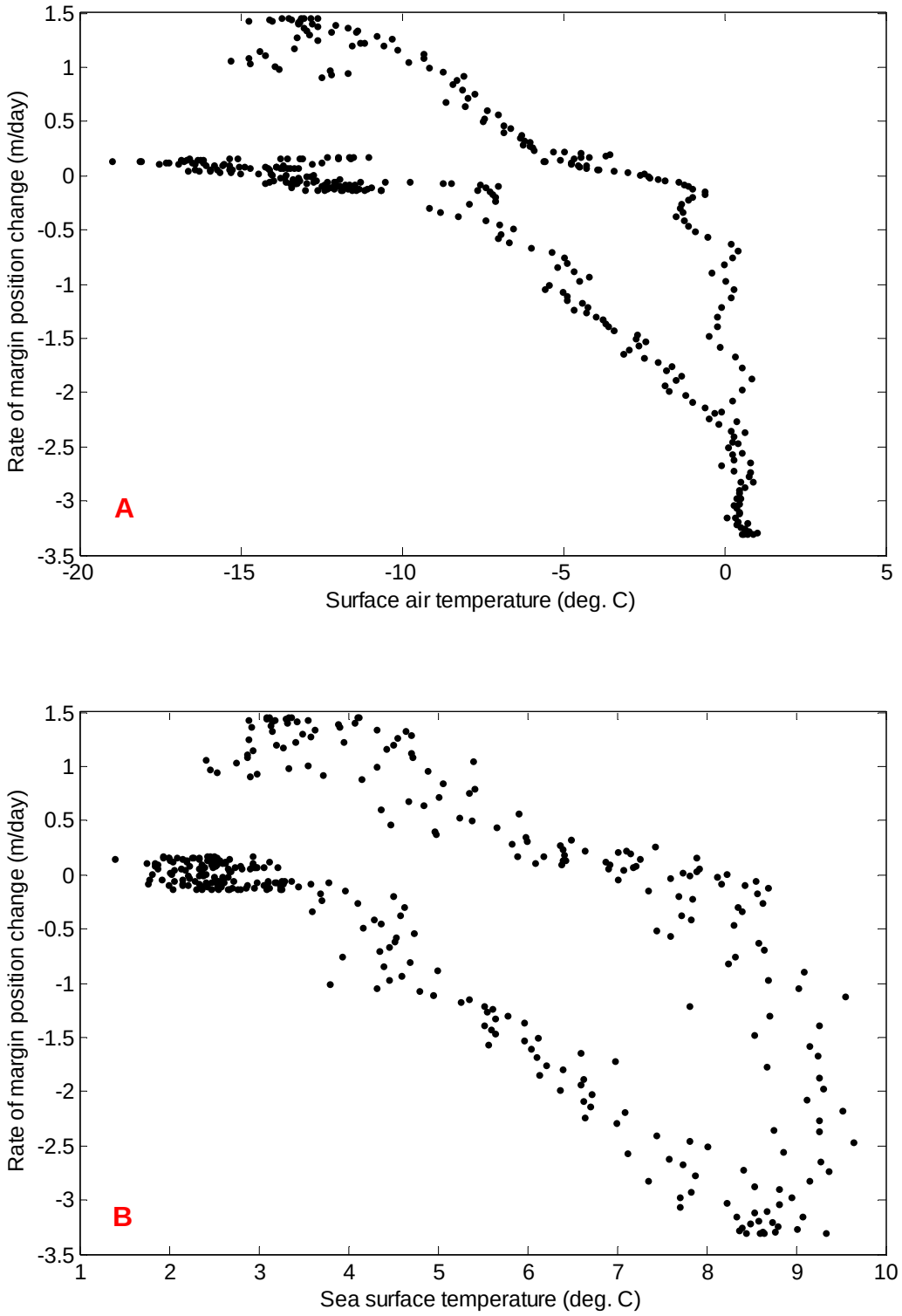

Figure 38 Annually averaged rate of margin position change plotted as a function of air (A) and sea (B) surface temperature, averaged for all south-eastern glaciers. Negative margin position change appears to occur when temperatures are lower.

for SATs, with retreat rapidly accelerating when SATs approach or exceed 0 °C, and approximately linear for SST. The points which make up this trend represent consecutive days and are therefore autocorrelated. Progression through the year may be followed in a coherent line clockwise on the figures, starting from the top left. To begin with, in winter, the rate of margin position change remains high, signifying advance. The rate then becomes negative as temperatures rise during the summer, before returning to positive values as temperatures drop with the approach of winter. By the end of the average year, the final margin position rate of change value reached is lower than the starting value, as over the course of the monitoring period the glaciers generally retreat (see 3.3 Margin position trends).

Inter-annual scale margin position changes may also be visualised by comparing the level components of the data. The responses of the glaciers vary, and are presented as a series of individual plots in **Figure 39** (SATs) and **Figure 40** (SSTs). Again, due to autocorrelation in the data, points may be tracked through time, starting from the top left of the plots and continuing clockwise. For both SATs and SSTs there are consistent response patterns across many of the glaciers. For SATs these responses involve increasing temperatures with little change in glacier position, until a point is reached, upon which rapid retreat occurs. This retreat appears to continue regardless of the following temperature change, which may remain high (for example, the case of Mogens 3) or decrease (as for Kangerdlugssuaq). Temperatures then remain low, which produces no change in margin position for some glaciers (e.g. Mogens 3), or small degrees of advance (e.g. Bernstorf 3, Helheim). The generalised shape is shown in **Figure 41**. Similar patterns are seen for SSTs as they follow a similar trend to SATs. However, retreats do not appear in quite such well defined steps. Instead raised SSTs appear to occur with a more proportional retreat in margin position (e.g. Mogens 3, Bernstorf 4).

3.4.2 Statistical testing

To enable detection of a margin position forcing by SSTs and SATs all three time series were separated into annual scale level, seasonal variability and short term variation components. The level component was extracted, as described above, and subtracted to give a detrended dataset consisting of seasonal variability and short term noise. The medium term seasonal

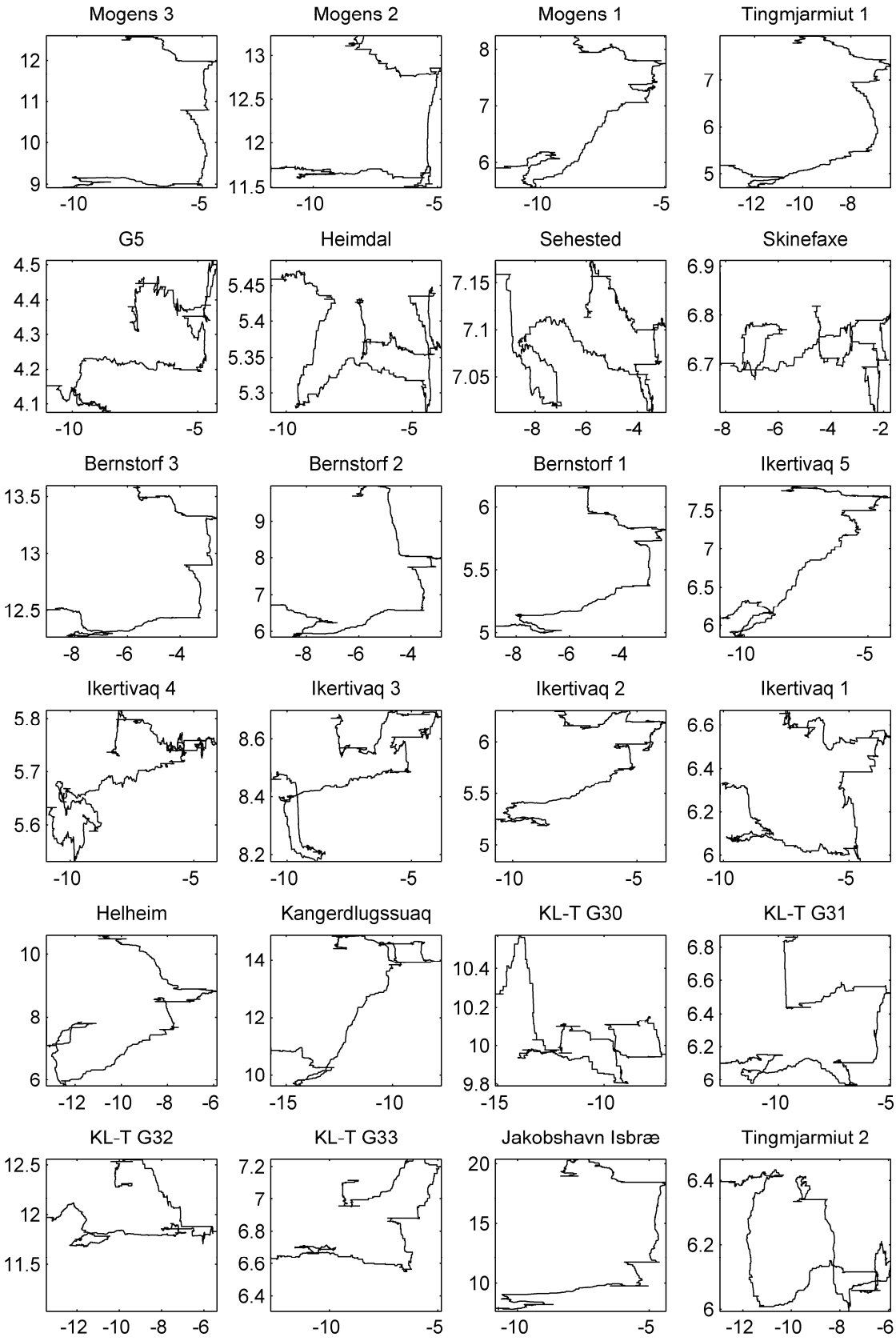

Figure 39 SAT levels (x-axes, °C) plotted against glacier margin position levels (y-axes, km) for all sampled glaciers.

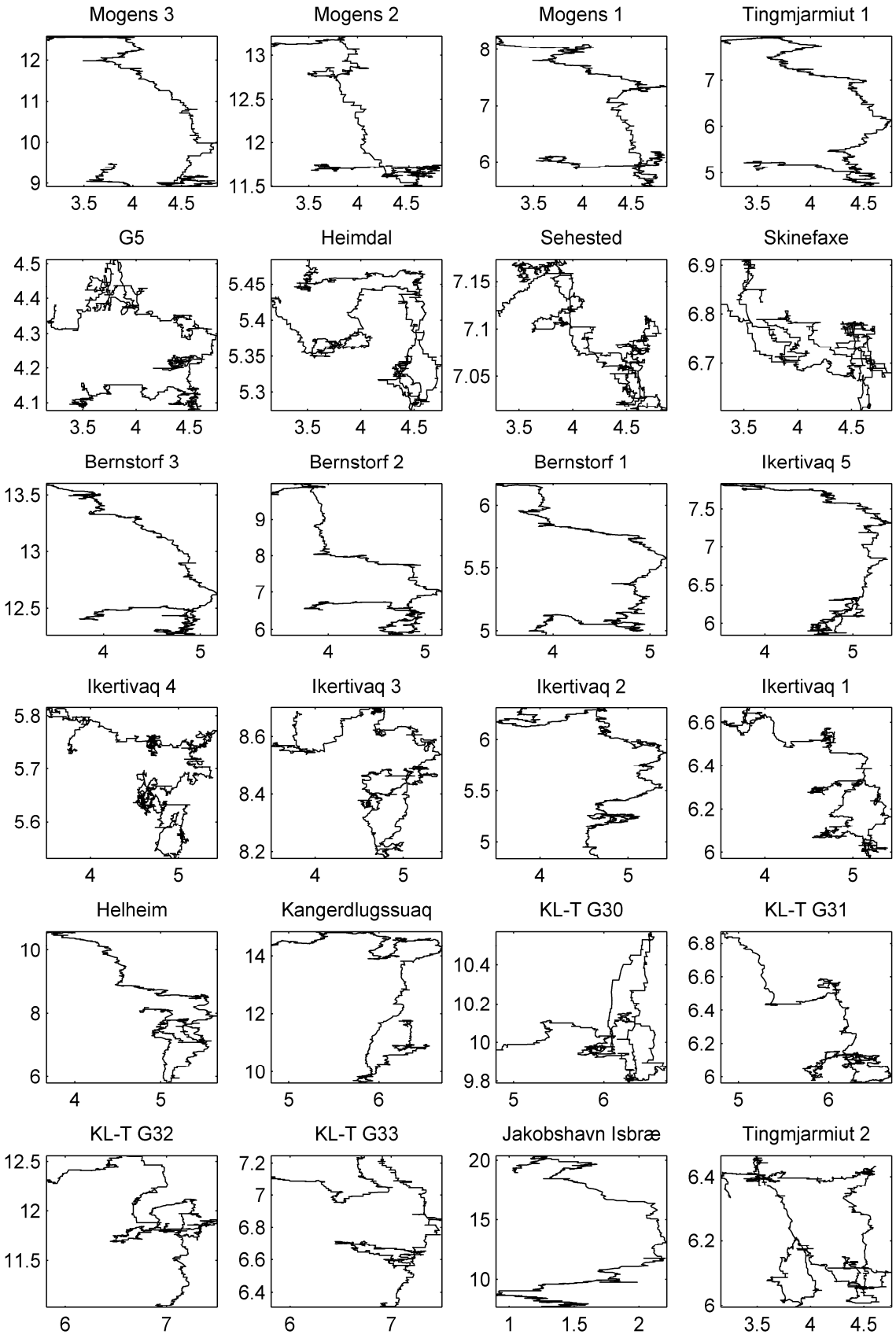

Figure 40 SST levels (x-axes, °C) plotted against glacier margin position levels (y-axes, km) for all sampled glaciers.

component was then isolated through the use of a smoothing function and also subtracted from the data to give a component consisting of short term (daily to weekly) changes and stochastic error.

To test for a possible forcing, correlations were performed between the first derivative of smoothed margin position change and both SAT and SST time series data. Correlations were also performed on the level, seasonal and short term variability components individually. The results are presented in **Table 2**. For many glaciers, correlations using time series data were statistically significant, likely due to the autocorrelation present in the data. For SATs against the derivative of calving margin position, correlation coefficients for most glaciers were very small, with only Bernstorf 2, Jakobshavn Isbræ and KL-T G31 showing weak degrees of negative correlation, having correlation coefficients of -0.65, -0.53 and -0.51 respectively. G5 showed an unexpected positive correlation between SAT and margin position levels with a coefficient of 0.50. The mean correlation coefficient for all glaciers (weighted by glacier width) was -0.20, showing advance occurred in times of lowered temperature, but signified a low degree of correlation. Similar correlations with SST data also had low magnitude coefficients. Those with greatest magnitude were Jakobshavn Isbræ, Bernstorf 2, KL-T G31 and Helheim with coefficients of -0.75, -0.64, -0.55 and -0.45 respectively. Again G5 showed the opposite trend with a coefficient of 0.64. The mean correlation coefficient across all glaciers was -0.19, similar to that of the SAT correlations. A histogram of the correlation coefficients may be seen in **Figure 42** where it is apparent that more glacier negative correlation coefficients are found for SAT as opposed to SST.

Conducting correlations using the level components of data also found small correlation coefficients for both SST and SAT. The weighted mean SAT coefficient was -0.22, whist weighted mean SST coefficient was -0.14. The histogram of correlation coefficients (**Figure 42**) shows more glaciers exhibiting a negative correlation for SAT than SST.

SAT correlations on seasonal order trends yielded some relatively high coefficients of 0.71 for Kangerdlugssuaq and Skinefaxe and 0.63 for G5 and KL-T G32, as well as some lower coefficients of -0.61, -0.54 and -0.53 for Sehested, Jakobshavn Isbræ and Tingmjarmiut 1 respectively. The same procedure using SSTs found the highest and lowest coefficients to

	Margin position rate of change vs SATs		Margin position rate of change vs SSTs		Margin position level rate of change vs SAT levels		Margin position level rate of change vs SST levels		Detrended margin position rate of change vs detrended SATs		Detrended margin position rate of change vs detrended SSTs		Margin position short term change vs SAT short term change		Margin position short term change vs SST short term change	
Glacier	**Coeff.**	**p-value**	**Coeff.**	**p-value**	**Coeff.**	**p-value**	**Coeff.**	**p-value**	**Coeff.**	**p-value**	**Coeff.**	**p-value**	**Coeff.**	**p-value**	**Coeff.**	**p-value**
Mogens 3	-0.05	0.01	-0.05	0.01	-0.50	0.00	-0.27	0.00	-0.13	0.00	-0.20	0.00	0.07	0.27	0.01	0.95
Mogens 2	-0.31	0.00	-0.22	0.00	-0.30	0.00	0.06	0.00	-0.35	0.00	-0.30	0.00	0.02	0.82	-0.04	0.63
Mogens 1	-0.13	0.00	-0.08	0.00	-0.25	0.00	-0.09	0.00	-0.22	0.00	-0.18	0.00	0.01	0.91	0.10	0.18
Tingmjarmiut1	-0.17	0.00	-0.20	0.00	-0.60	0.00	-0.30	0.00	-0.13	0.00	-0.27	0.00	-0.06	0.31	-0.02	0.83
G5	0.50	0.00	0.64	0.00	-0.03	0.13	-0.15	0.00	0.54	0.00	0.64	0.00	-0.06	0.23	-0.03	0.63
Heimdal	0.12	0.00	0.04	0.01	-0.11	0.00	0.03	0.07	0.12	0.00	0.07	0.00	0.05	0.33	0.07	0.26
Sehested	-0.22	0.00	-0.28	0.00	-0.19	0.00	-0.09	0.00	-0.19	0.00	-0.28	0.00	0.02	0.60	0.09	0.10
Skinefaxe	-0.06	0.00	0.03	0.13	-0.21	0.00	-0.05	0.01	-0.05	0.01	0.06	0.00	-0.02	0.73	-0.01	0.93
Bernstorf 3	-0.17	0.00	0.00	0.87	-0.45	0.00	-0.14	0.00	-0.25	0.00	-0.05	0.01	-0.03	0.46	0.01	0.88
Bernstorf 2	-0.65	0.00	-0.64	0.00	-0.35	0.00	-0.02	0.33	-0.65	0.00	-0.66	0.00	0.01	0.91	0.08	0.28
Bernstorf 1	-0.41	0.00	-0.22	0.00	-0.27	0.00	-0.16	0.00	-0.46	0.00	-0.34	0.00	-0.09	0.08	0.11	0.09
Ikertivaq 5	-0.04	0.02	-0.05	0.00	-0.06	0.00	-0.31	0.00	-0.09	0.00	-0.08	0.00	0.01	0.85	-0.06	0.33
Ikertivaq 4	-0.15	0.00	-0.11	0.00	-0.09	0.00	-0.06	0.00	-0.16	0.00	-0.11	0.00	-0.02	0.68	0.07	0.16
Ikertivaq 3	0.05	0.00	0.06	0.00	-0.03	0.09	0.01	0.57	0.06	0.00	0.06	0.00	-0.04	0.36	-0.04	0.45
Ikertivaq 2	-0.23	0.00	-0.21	0.00	-0.13	0.00	-0.16	0.00	-0.26	0.00	-0.23	0.00	-0.03	0.48	0.07	0.19
Ikertivaq 1	0.10	0.00	0.09	0.00	-0.30	0.00	-0.06	0.00	0.11	0.00	0.11	0.00	-0.06	0.20	0.03	0.56
Helheim	-0.34	0.00	-0.45	0.00	-0.37	0.00	-0.04	0.01	-0.38	0.00	-0.50	0.00	0.04	0.42	0.02	0.69
Kangerdlugssuaq	-0.35	0.00	-0.13	0.00	-0.09	0.00	-0.07	0.00	-0.40	0.00	-0.14	0.00	-0.08	0.04	0.11	0.03
KL-T G30	0.01	0.49	-0.03	0.13	0.06	0.00	-0.17	0.00	-0.04	0.04	0.00	1.00	0.02	0.75	-0.08	0.29
KL-T G31	-0.51	0.00	-0.55	0.00	-0.14	0.00	0.12	0.00	-0.59	0.00	-0.60	0.00	0.07	0.16	0.03	0.67
KL-T G32	-0.07	0.00	0.13	0.00	0.04	0.04	-0.18	0.00	-0.13	0.00	0.09	0.00	0.02	0.68	-0.06	0.32
KL-T G33	-0.17	0.00	-0.22	0.00	-0.20	0.00	-0.27	0.00	-0.19	0.00	-0.28	0.00	0.10	0.12	0.01	0.94
Jakobshavn Isbræ	-0.53	0.00	-0.75	0.00	-0.43	0.00	-0.48	0.00	-0.63	0.00	-0.84	0.00	-0.03	0.49	-0.02	0.70
Tingmjarmiut 2	-0.28	0.00	-0.14	0.00	-0.16	0.00	0.10	0.00	-0.29	0.00	-0.16	0.00	0.02	0.63	0.03	0.65
Weighted mean	**-0.2038**	**0.0118**	**-0.1933**	**0.0279**	**-0.2156**	**0.0116**	**-0.1439**	**0.0557**	**-0.2356**	**0.0011**	**-0.2288**	**0.021**	**-0.0093**	**0.4726**	**0.0224**	**0.4487**

Table 2 Results of correlations, showing coefficient achieved for each glacier and associated p-value. Table cells are shaded to allow for rapid interpretation of the data. Higher coefficients are coloured green and lower coefficients are coloured red. More significant p-values are coloured blue, whilst those less significant are coloured yellow. In general correlation coefficients were low for reasons described in section 4.4 SST/SAT forcing.

occur on a similar set of glaciers. The glaciers with higher magnitude coefficients in these seasonal scale tests were those which were noted to have higher degrees of seasonality (**Table 1**). The correlation coefficient histograms show a more similar distribution between air and sea surface temperatures than correlations using other orders of data. Correlations performed using short term variability data produced very low magnitude coefficients as well as insignificant p-values.

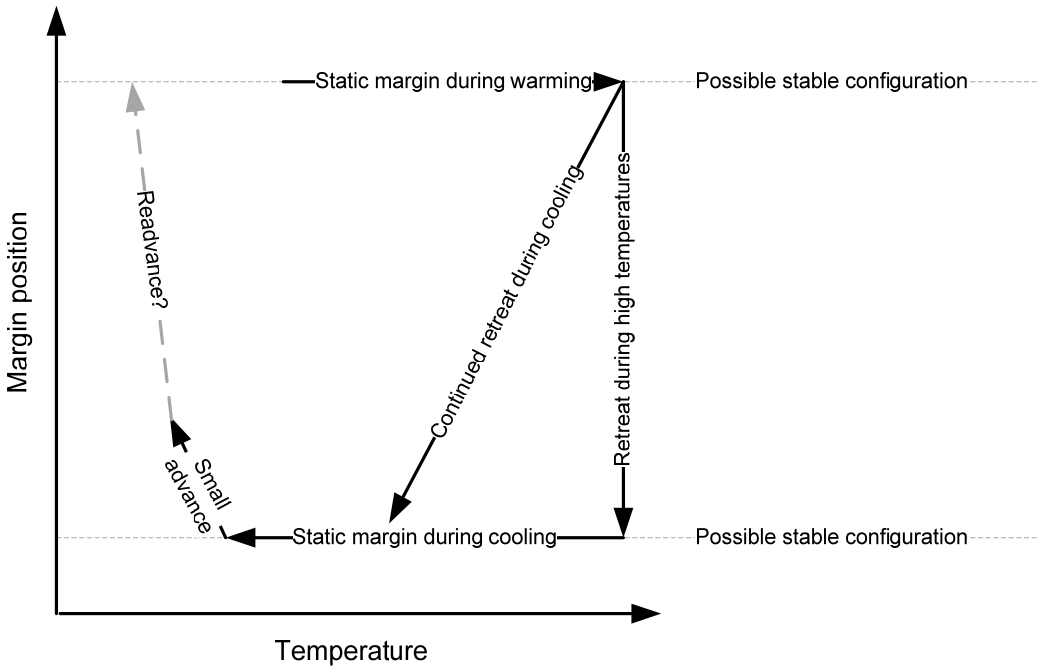

Figure 41 Generalised progression of margin positions with changes in sea or air surface temperatures. It is possible that re-advance may occur in a hysteresis cycle, or that a lower stable configuration may be reached in a further step change retreat.

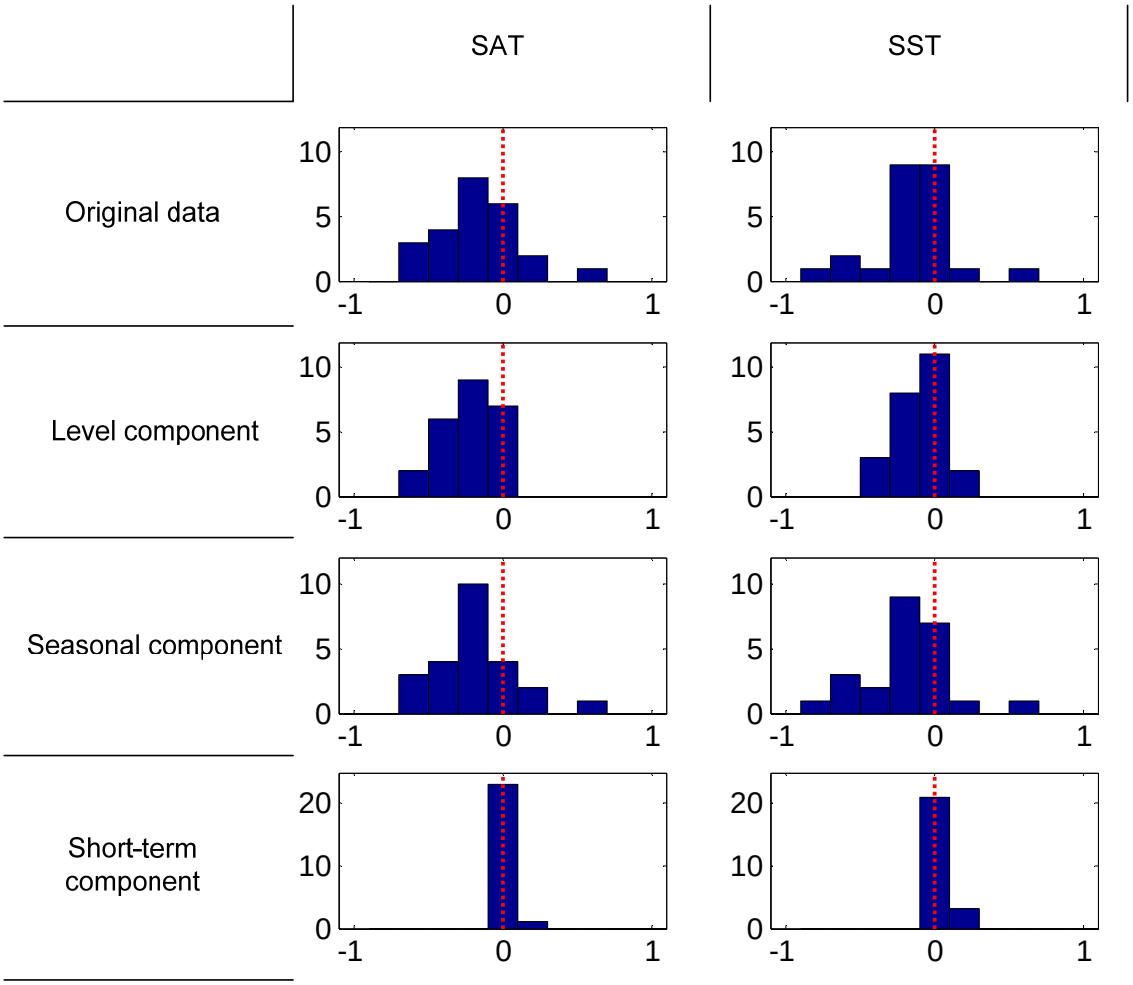

Figure 42 Histograms of correlation coefficients between rate of margin position change (top row) and SATs as well as SSTs. Also shown are histograms for similar correlations using margin position level, seasonal and short-term component data. Slightly more negative correlation coefficients are found for SATs than SSTs.

4 Analysis

4.1 Data quality

It is difficult to assess error within the data, as the use of an unchecked automatic algorithm could falsely detect a feature such as a shadow as the glacier margin, producing plausible but incorrect data. This limits confidence in the margin positions of individual glaciers, but is unlikely to significantly distort conclusions drawn about regional scale changes or forcing mechanisms. The automatically derived data fared well in the validation exercises, suggesting that such occurrences are rare and that the deductions of this analysis are less likely to be undermined. Due to data availability, validation was performed on two of the larger glaciers, which may not fully represent problems specific to smaller glaciers. For example, fjord wall shadows are more likely to produce false glacier margin positions on smaller glaciers than on larger ones, due to shadows stretching across the full width of the glacier causing a contrast change similar in extent to that of the calving margin. Weighting of glaciers in averages produced for the response of the south-east by width reduces the influence of such problems.

The short term noise levels present in the data (See section 2.1.15 Error) prevent the identification and analysis of individual calving events. Without being able to separate changes in margin position into short term changes in advance and retreat, changes in margin position must be taken as a conflated function of glacier velocity and calving rate. If velocity data were collected, decomposition may be possible. As margin position changes are the result of rate imbalances, an increase in calving rate with a simultaneous increase in velocity will fail to produce observable change. This is likely to be the case in the long term as research has shown that glacier velocity is controlled at least in part by the resistance to flow imposed at the calving boundary (see 1.3.2 Control at the calving margin). No estimate of mass balance can be made from the data. Changes in margin position may be interpreted as an imbalance of unknown magnitude between velocity and calving and are still an indicator of response to environmental forcing.

4.2 Seasonality

The patterns of seasonality found on many of the sampled glaciers show, with a high degree of confidence, that the position of the glacier front is forced by a mechanism which itself

contains a seasonal pattern. The large scale of seasonal changes, such as a 2.6 km range for Kangerlugssuaq and 1.8 km for Helheim, suggest that glaciers are highly sensitive to this forcing and that it is likely to have the ability to induce longer term sustained margin position changes (discussed in 4.3 Margin position trends). It also shows that the glacier front can change significantly over very short timescales and that dynamic change may occur rapidly. The response shows that the ice sheet is likely to be highly susceptible to climatic warming, as is predicted for the region (IPCC 2007).

4.3 Margin position trends

This study found that many glaciers in the south-east of the GrIS retreated over the period of early 2002 to mid 2005, with a weighted sample mean retreat of 1.69 km, consistent with the findings of Howat et al. (2008) and Moon and Joughin (2008). The recent re-advance has been limited both in terms of extent and magnitude, with a weighted average advance over the sampled glaciers of 0.36 km. Comments based upon limited observations, suggesting the glaciers in the region have fully re-advanced (Kerr 2009) appear incorrect. The observed retreat suggests that many south-eastern glaciers have been making contributions to sea level rise and could continue to do so if their response to environmental forcing continues in a similar manner. As retreats were found to be significant on many glaciers of all sizes, future research may benefit from considering a wider range of glaciers than the well studied three largest (Jakobshavn Isbræ, Kangerdlugssuaq and Helheim).

The stepped nature of changes observed on many of the glaciers suggests a progression through a number of tipping points to successive stable states. It is possible that these stable states represent equilibriums found between the grounding line and the bedrock and are thus determined by glacier bathymetry. This has been predicted by theory (Meier & Post 1987; Weertman 1974) and modelling (Vieli et al. 2001; Nick et al. 2009). Attempts to characterise glacier margin position variation within each stable configuration using principle component analysis could not extract strong signals, which may be due to the small sample of years. It is possible that seasonal changes represent variations in glacier floating tongues, whilst permanent step changes are the result of altered grounding line locations. Observations on Helheim glacier (Joughin et al. 2008b), where the bathymetry has been surveyed, show that persistent margin positions appear to coincide with locations of bedrock highs. The bathymetry is unknown for most GrIS outlet glaciers and the results of

this study suggest that such data would be useful in gaining a greater understanding of dynamic changes, and assist with the prediction of future change.

4.4 SST/SAT forcing

The increased SATs and SSTs during mid 2001 to 2005 correspond to a period of significant retreat in margin position. It would seem physically likely and intuitive to suggest that by some mechanism, one or both of these variables were somehow responsible the changes. The high degree of correspondence between SATs and SSTs with margin position change on an average annual basis further suggests they may be responsible for changes in margin position, but it is possible that the relationship is the result of comparing two datasets which simply contain repeated seasonal scale variation. The nonlinear response of margin position to SATs indicates that temperatures may act as a trigger for margin position retreats which, once initiated, are self maintained by positive feedback mechanisms, as previously described (1.3.2 Control at the calving margin).

The deviation of SATs and SSTs from each other on a level (inter-annual) scale allows for an assessment of their relative influence on margin position, which is not possible when they exhibit covariation. The lack of retreat and small re-advance seen over mid 2005 to 2008, whilst SATs are cooler, suggests they are a controlling mechanism. During this period some SSTs remain high, whilst others show a small decline. As the retreat appears to cease and even reverse during this time it appears that SATs may be the dominant control, at least in comparison with SSTs. There is also no categorical correspondence between the glaciers which show re-advance and locations which show continued high or diminished SSTs, further suggesting a limited influence of SSTs. It is possible that both SATs and SSTs force margin position, with elevated SSTs preventing re-advance. It should be noted that when making comparisons on level scales a larger number of years are probably required to draw confident conclusions than are available.

When comparing periods of advance and retreat to SATs and SSTs (**Figure 39** and **Figure 40**), there is a consistent response pattern across many glaciers, characterised in **Figure 41**. The step-change nature of the response further corroborates the theory which recognises multiple bathymetrically defined stable states. Transitions between states appear to be triggered by specific temperature levels, after which they show independence of

temperature change. Evidence for this comes from the consistency of response pattern across glaciers, the variation in temperature below a threshold without change in margin position, the short periods of time and lack of persistent margin positions between states and the stability of margin positions, regardless of temperature variation once in the second state.

Threshold temperatures may control retreat through modulation of sea ice levels (see 1.3.3 Calving modulation). It has been shown that the formation of sea ice is highly sensitive to air temperatures (McPhee 2008 chap. 6) and many sea ice models are indeed based upon air temperature levels (Chetyrbotskii 2008; McPhee 2008 chap. 7). There is some evidence in the data (**Figure 34**) that inter-annual retreat is caused by an extension of the calving season, as opposed to an increase in calving rate. The physical mechanism implied by this observation is consistent with the nonlinear threshold based relationship between SAT and margin position change.

One aim of this study was to use a high number of short term observations to statistically determine the triggers of individual calving events. This would have allowed an assessment of the relative roles of SAT and SST in controlling margin positions, as the data would not have exhibited the same degree of covariation and there would have been a large sample size of relatively independent observations. The noise present in the dataset prevented the identification of individual calving events and thus correlations at this scale showed no trend or significance. It is also possible that the modelled re-analysis temperatures also contained errors.

Statistical testing found low correlation coefficients in the expected direction (lowered temperatures corresponding to advance). Slightly stronger coefficients were found for SAT than SST, suggesting a potential dominance of control. As response to temperature change appeared to occur in geometrically defined step transitions instigated by the exceeding of thresholds, followed by independence of temperature during state change, there is no linear relationship between SATs or SSTs and the derivative of margin position. This may be why statistical testing failed to find high correlation coefficients. The highly significant p-values are likely to be the result of autocorrelation in the data, which violates the independent sampling assumption of the test. This is highlighted by the low p-values

calculated for detrended daily level data, which has a much lower degree autocorrelation. Vector autoregressive moving average modelling (V-ARMA), a technique more commonly applied to econometric time series data (Wei 2005, p.386; Peña et al. 2000, p.365), may have helped to alleviate this problem, although findings would still have been limited by the lack of proportional relationship between variables.

5 Conclusion

The development of an automated method allowed for the extraction of margin positions for 24 glaciers in the south-east of Greenland, as well as Jakobshavn Isbræ, although some data quality issues may be present for Ikertivaq glaciers and KL-T G33. For the tested glaciers, data fared well in validation exercises against manually checked data from an independent study (Joughin et al. 2008b). The method thus represents a less labour intensive means for calculating glacier margin position change. The efficiency of the method allowed 79,152 images of glacier fronts to be investigated and should mean future research is no longer limited to a small number of glaciers or low temporal resolution. This study serves as a pilot for future expansion of the method over the whole ice sheet, which would show periods of advance and retreat in unprecedentedly high spatio-temporal detail. The public release of such a dataset may be beneficial to further research seeking to understand dynamic change on the GrIS, as well as forming an input or validation dataset for the future generations of dynamic ice-sheet wide models currently under preparation.

Seasonality was found on many of the glaciers showing that they are forced by a mechanism which itself exhibits a seasonal cycle. The large range of seasonal change suggests that GrIS outlet glaciers may be very sensitive to the operational forcing mechanism and that it is likely to have the ability to cause large sustained retreats over short time periods. On inter-annual timescales retreat a weighted average retreat of 1.69 km was found to have occurred between July 2001 and July 2005, after which a small re-advance occurred on some glaciers, averaging 0.36 km by July 2008. The retreat is consistent with other research, whilst the re-advance appears to have been overstated by Kerr (2009). The finding of significant changes on small glaciers also highlights their potential importance in determining the mass balance of the ice sheet, particularly as much research has focused on the three largest GrIS outlet glaciers (Jakobshavn Isbræ, Kangerdlugssuaq or Helheim).

Studies which assess the mass balance (Slobbe et al. 2009; Cazenave et al. 2009) or velocity structure (Rignot & Kanagaratnam 2006) of the GrIS are often based upon comparisons of state between a number of years, typically 3 to 10 years apart. The rapid changes observed in under a year by this study suggest that the findings of such studies are highly sensitive to the choice of years used for comparison, and that their conclusions relating to mass balance may not be robust. Using high temporal resolution data, this research has been able to precisely locate periods of dynamic change within time and may be used to inform the choice of years such studies of elevation, velocity and gravity fields use for comparisons, particularly when the method has been applied to the whole ice sheet. It also highlights the possibility and benefits of using higher temporal resolution data, which is seldom done in studies of GrIS change. Many studies are based upon data from satellites with repeat pass frequencies higher than the sampling rate. This study provides an example of ways in which automation, albeit with some loss in accuracy and confidence in validity, can use all available data to produce more robust findings, accurately located in time.

Evidence was found for the existence of discrete stable grounding line states, between which tidewater glaciers are not in equilibrium and have rapidly changing margin positions. This shows the possible importance of bathymetry, which is largely unknown, in understanding the dynamic response of the ice sheet. It appears that changes in temperature may trigger retreats from stable positions, suggesting that the short to mid-term response of the GrIS to future climate change is likely to be nonlinear and subject to tipping points, at least until glaciers have retreated onto land. Combined with the observed sensitivity to seasonal cycles and large scale of changes observed to be possible within short time periods, this presents a concerning mechanism of potential response to predicted climate change.

Conclusive attribution of margin position changes to SATs or SSTs was not possible from this data due to high degrees of covariation over longer timescales and noise in the data over short timescales. However, a qualitative assessment of temperature and margin position time series indicates that SATs may have been more likely than SSTs to have caused the observed margin position changes. This is based upon the 2005 to 2008 response where SSTs remained high in some locations but SATs dropped, causing the cessation of retreat for most glaciers. Furthermore, no categorical difference was found between margin position

levels for glaciers that had experienced high or lowered SSTs. The use of statistical correlations could not establish causality, which could have been highly significant over short timescales, had there been less noise in the data. Tests were limited in their ability to explain the relationship between margin position change and temperature by its nonlinear step-change nature. Modulation of calving rates by the buttressing effect of sea ice formation, with season length controlled by surface air temperature, forms a plausible physical explanation for the data. Further evidence for this comes from the apparent cause of retreats being an increase in duration of calving season length, as opposed to an increase in intensity. Forcing could however be the result of multiple physical mechanisms. It is possible that a full understanding of margin position control may have to be gained through field work.

Future research will extend data collection across the whole ice sheet to gain a widespread high spatio-temporal resolution picture of margin position change, possibly for public release, and compare the timing of the sea ice season with periods of advance and retreat.

6 References

Abdalati, W. et al., 2001. Outlet glacier and margin elevation changes: Near-coastal thinning of the Greenland ice sheet. *Journal of Geophysical Research-Atmospheres*, 106(D24), 33729-33741.

Ahmad, S. et al., 2002. Highlights of MODIS products. In *Geoscience and Remote Sensing Symposium, 2002. IGARSS '02. 2002 IEEE International*. pp. 2299-2301 vol.4.

Alley, R.B. et al., 2005. Ice-Sheet and Sea-Level Changes. *Science*, 310(5747), 456-460.

Bamber, J.L., Alley, R.B. & Joughin, I., 2007. Rapid response of modern day ice sheets to external forcing. *Earth and Planetary Science Letters*, 257(1-2), 1-13.

van den Broeke, M., 2005. Strong surface melting preceded collapse of Antarctic Peninsula ice shelf. *Geophysical Research Letters*, 32(12), L12815.

Canny, J., 1986. A computational approach to edge-detection. *IEEE transactions on pattern analysis and machine intelligence*, 8(6), 679-698.

Cazenave, A. et al., 2009. Sea level budget over 2003-2008: A reevaluation from GRACE space gravimetry, satellite altimetry and Argo. *Global and Planetary Change*, 65(1-2), 83-88.

Chetyrbotskii, A., 2008. Modeling fast ice formation and destruction in the Sea of Japan. *Water Resources*, 35(4), 397-407.

Costa, L.D.F. & Cesar, J.R.M., 2000. *Shape Analysis and Classification: Theory and Practice* 1st ed., CRC Press.

Das, S.B. et al., 2008. Fracture propagation to the base of the Greenland Ice Sheet during supraglacial lake drainage. *Science*, 320(5877), 778-781.

Ekstrom, G., Nettles, M. & Abers, G.A., 2003. Glacial earthquakes. *Science*, 302(5645), 622-624.

Ekstrom, G., Nettles, M. & Tsai, V.C., 2006. Seasonality and increasing frequency of Greenland glacial earthquakes. *Science*, 311(5768), 1756-1758.

Hassan, M. et al., 2008. Evaluation of Sobel, Canny, Shen & Castan using sample line histogram method. In *International Symposium on Information Technology, 2008.* pp. 1-7.

Heath, M., 1997. A robust visual method for assessing the relative performance of edge-detection algorithms. *IEEE transactions on pattern analysis and machine intelligence*, 19(12), 1338-1359.

Holland, D., 2008. Acceleration of Jakobshavn Isbrae triggered by warm subsurface ocean waters. *Nature Geoscience*, 1, 659 - 664.

Howat, I.M., Joughin, I. & Scambos, T.A., 2007. Rapid changes in ice discharge from Greenland outlet glaciers. *Science*, 315(5818), 1559-1561.

Howat, I.M. et al., 2005. Rapid retreat and acceleration of Helheim Glacier, east Greenland. *Geophysical Research Letters*, 32(22), L22502.

Howat, I.M. et al., 2008. Synchronous retreat and acceleration of southeast Greenland outlet glaciers 200006: ice dynamics and coupling to climate. *Journal of Glaciology*, 54, 646-660.

IPCC, 2007. *Climate Change 2007: The Physical Science Basis. Contribution of Working Group I to the Fourth Assessment Report of the Intergovernmental Panel on Climate Change*, Cambridge, United Kingdom and New York, NY, USA: Cambridge University Press.

IPCC, 2001. *The Physical Science Basis. Contribution of Working Group I to the Third Assessment Report of the Intergovernmental Panel on Climate Change*, Cambridge, United Kingdom and New York, NY, USA: Cambridge University Press.

Joughin, I., Abdalati, W. & Fahnestock, M., 2004. Large fluctuations in speed on Greenland's Jakobshavn Isbrae glacier. *Nature*, 432(7017), 608-610.

Joughin, I. et al., 2008a. Seasonal speedup along the western flank of the Greenland Ice Sheet. *Science*, 320(5877), 781-783.

Joughin, I. et al., 2008b. Ice-front variation and tidewater behavior on Helheim and Kangerdlugssuaq Glaciers, Greenland. *Journal of Geophysical Research-Earth Surface*, 113(F1), F01004.

Joughin, I. et al., 1996. A mini-surge on the Ryder Glacier, Greenland, observed by satellite radar interferometry. *Science*, 274(5285), 228-230.

Kerr, R.A., 2009. Fall Meeting of the American Geophysical Union: Galloping Glaciers of Greenland Have Reined Themselves In. *Science*, 323(5913), 458a.

Klein, A., Hall, D. & Riggs, G., 1998. Global Snow Cover Monitoring Using MODIS. In Tromsø, Norway, pp. 363-366.

Krabill, W. et al., 2004. Greenland Ice Sheet: Increased coastal thinning. *Geophysical Research Letters*, 31(24), L24402.

Legresy, B. et al., 2004. Influence of tides and tidal current on Mertz Glacier, Antarctica. *Journal of Glaciology*, 50(170), 427-435.

Luckman, A. et al., 2006. Rapid and synchronous ice-dynamic changes in East Greenland. *Geophysical Research Letters*, 33(3).

Luckman, A. & Murray, T., 2005. Seasonal variation in velocity before retreat of Jakobshavn Isbræ, Greenland. *Geophysical Research Letters*, L08501.

McPhee, M., 2008. *Air-Ice-Ocean Interaction*, USA: Springer.

Meier, M.F. & Post, A., 1987. Fast Tidewater Glaciers. *Journal of Geophysical Research*, 92(B9), 9051-9058.

Moon, T. & Joughin, I., 2008. Changes in ice front position on Greenland's outlet glaciers from 1992 to 2007. *Journal of Geophysical Research-Earth Surface*, 113(F2), F02022.

Nettles, M. et al., 2008. Step-wise changes in glacier flow speed coincide with calving and glacial earthquakes at Helheim Glacier, Greenland. *Geophys. Res. Lett.*, 35, L24503.

Nick, F. et al., 2009. Large-scale changes in Greenland outlet glacier dynamics triggered at the terminus. *Nature Geoscience*, 2, 110-114.

Parkinson, C.L. & Greenstone, R., 2000. *EOS Data Products Handbook: Volume 2*, Greenbelt, Maryland: NASA/Goddard Space Flight Center.

Paterson, W., 1994. *The physics of glaciers (3rd Edition ed.)*, Oxford: Pergamon, Elsevier Science Ltd.

Peña, D., Tiao, G.C. & Tsay, R.S., 2000. *A Course in Time Series Analysis*, WileyBlackwell.

Pfeffer, W.T., 2007. A simple mechanism for irreversible tidewater glacier retreat. *Journal of Geophysical Research-Earth Surface*, 112(F3), F03S25.

Reeh, N. et al., 2001. Sea ice and the stability of north and northeast Greenland floating glaciers. *Annals of Glaciology, Vol 33*, 33, 474-480.

Riggs, G. & Hall, D., 2004. Snow Mapping with the MODIS Aqua Instrument. In Portland, Maine, USA.

Rignot, E. et al., 2008. Mass balance of the Greenland ice sheet from 1958 to 2007. *Geophysical Research Letters*, 35, L20502.

Rignot, E. et al., 2004. Rapid ice discharge from southeast Greenland glaciers. *Geophysical Research Letters*, 31(10).

Rignot, E. & Kanagaratnam, P., 2006. Changes in the velocity structure of the Greenland ice sheet. *Science*, 311(5763), 986-990.

Rojas, F., Schowengerdt, R.A. & Biggar, S.F., 2002. Early results on the characterization of the Terra MODIS spatial response. *Remote sensing of environment*, 83(1-2), 50-61.

Shepherd, A. et al., 2009. Greenland ice sheet motion coupled with daily melting in late summer. *Geophysical Research Letters*, 36, L01501.

Simmons, A.S., Uppala, D.D. & Kobayashi, S., 2007. *ERA-Interim: New ECMWF reanalysis products from 1989 onwards*, ECMWF.

Slobbe, D.C., Ditmar, P. & Lindenbergh, R.C., 2009. Estimating the rates of mass change, ice volume change and snow volume change in Greenland from ICESat and GRACE data. *Geophysical Journal International*, 176(1), 95-106.

Sohn, H.G., Jezek, K.C. & van der Veen, C.J., 1998. Jakobshavn Glacier, West Greenland: 30 years of spaceborne observations. *Geophysical Research Letters*, 25(14), 2699-2702.

Sole, A. et al., 2008. Testing hypotheses of the cause of peripheral thinning of the Greenland Ice Sheet: is land-terminating ice thinning at anomalously high rates? *The Cryosphere Discuss.*, 2(4), 673-710.

Thomas, R.H., 2004. Force-perturbation analysis of recent thinning and acceleration of Jakobshavn Isbræ, Greenland. *Journal of Glaciology*, 50(168), 57-66.

Uppala, S.M. et al., 2005. The ERA-40 re-analysis. *Quarterly Journal of the Royal Meteorological Society*, 131(612), 2961-3012.

Vermote, E. & Kotchenova, S., 2008. *MOD09 (Surface Reflectance) User's Guide Version 1.1*, MODIS Land Surface Reflectance Science Computing Facility.

Vieli, A., Funk, M. & Blatter, H., 2001. Flow dynamics of tidewater glaciers: a numerical modelling approach. *Journal of Glaciology*, 47(159), 595-606.

van de Wal, R.S.W. et al., 2008. Large and rapid melt-induced velocity changes in the ablation zone of the Greenland Ice Sheet. *Science*, 321(5885), 111-113.

Weertman, J., 1974. Stability of the junction of an ice sheet and an ice shelf. *Journal of Glaciology*, 3, 3-11.

Wei, W.W., 2005. *Time Series Analysis: Univariate and Multivariate Methods* 2nd ed., Addison Wesley.

Zunfeng, H., Hongshe, D. & Xiaorui, L., 2008. A novel fast subpixel edge location method based on Sobel-OFMM. In *Automation and Logistics, 2008. ICAL 2008. IEEE International Conference on*. pp. 828-832.

Zwally, H.J. et al., 2002. Surface melt-induced acceleration of Greenland ice-sheet flow. *Science*, 297(5579), 218-222.

7 Supplementary animations

Supplementary animations may be found on the accompanying CD-ROM. They are provided in AVI format, compressed using the Cinepak codec, which is bundled with most versions of Microsoft Windows. Recommended viewing is with Windows Media Player on a computer with minimum specifications of 500 MHz CPU, 256 MB RAM and Microsoft Windows version 98 or above. Captions for the animations are provided below.

Supplementary Animation S1 Animation showing MODIS imagery and edge detection for Kangerdlugssuaq glacier. Left hand plot shows band 1 surface reflectance of Kangerdlugssuaq and the surrounding area for each cloud free day, which forms a single frame of the animation; axis units are km. Central top figure shows surface reflectance of the 'active region', the area within which edge detection takes place; axis units are km. Second central figure down shows detected edge pixels (white) over the active region using the Sobel method; axis units are km. Third central figure down shows frequency of detected edge pixels (y-axis) using the Sobel method along the length of the glacier (x-axis, km). High frequencies signify likely calving margin positions. Central bottom figure shows gradient (y-axis) of across-glacier averaged surface reflectance along the length of the glacier (x-axis, km), used as part of the brightness profiling method of calculating margin position. High brightness gradient locations signify likely calving margin locations. Right hand plot shows detected margin positions after consolidation of the two detection methods and noise removal procedures; x-axis is relative margin position in km, y-axis is time in years beginning. A horizontal line travels down the plot to signify animation location within time.

Supplementary Animation S2 Plots are the same as in Supplementary Animation S1, but for Helheim Glacier. Plot details are described in the caption for S1.